Distribution Agreement

In presenting this thesis or dissertation as a partial fulfillment of the requirements for an advanced degree from Emory University, I hereby grant to Emory University and its agents the non-exclusive license to archive, make accessible, and display my thesis or dissertation in whole or in part in all forms of media, now or hereafter known, including display on the world wide web. I understand that I may select some access restrictions as part of the online submission of this thesis or dissertation. I retain all ownership rights to the copyright of the thesis or dissertation. I also retain the right to use in future works (such as articles or books) all or part of this thesis or dissertation.

Signature:

_____ _____

Amanda Leanne Gill Date

CD8 T Cell Differentiation during Viral Infection

By

Amanda Leanne Gill

Doctor of Philosophy
Graduate Division of Biological and Biomedical Sciences
Immunology and Molecular Pathogenesis

_____
Rafi Ahmed, Ph.D.
Advisor

_____
Rama Amara, Ph.D.
Committee Member

_____
Kavita Dhodapkar, M.D.
Committee Member

_____
Jacob Kohlmeier, Ph.D.
Committee Member

_____
Edmund Waller, M.D., Ph.D.
Committee Member

Accepted:

_____
Kimberly Jacob Arriola, Ph.D., M.P.H.
Dean of the James T. Laney School of Graduate Studies

_____
Date

CD8 T Cell Differentiation during Viral Infection

By

Amanda Leanne Gill
B.A., Bryn Mawr College

Advisor: Rafi Ahmed, Ph.D.

An abstract of
a dissertation submitted to the Faculty of the
James T. Laney School of Graduate Studies of Emory University
in partial fulfillment of the requirements for the degree of
Doctor of Philosophy
in Graduate Division of Biological and Biomedical Sciences
Immunology and Molecular Pathogenesis
2023

Abstract

CD8 T Cell Differentiation during Viral Infection

By Amanda Leanne Gill

CD8 T cells play a crucial role in antiviral immunity. In order to develop better vaccines and T cell-based therapies, we need to understand how CD8 T cells differentiate in different viral contexts, and what mechanisms regulate their fate and functional capacity. We now have a better understanding of which processes favor effective memory responses during acute infection, as well as which factors lead to sustained antiviral responses during chronic infection.

We examined memory CD8 T cell differentiation using the acute lymphocytic choriomeningitis virus (LCMV) infection model. Through these studies, we were able to define a late-memory phenotype and use this to guide our analyses of the fate decisions occurring within the first few days after infection. We determined that long-lived memory CD8 T cells localized to the splenic white pulp and expressed TCF-1, IL-7Ra, CD62L, CXCR3, and CD28. This phenotype may be of interest as a target for functional immunity following vaccination or infection. We next sought to examine how these cells were generated, so we analyzed CD8 T cell differentiation in the earliest phase of the acute response—before the first division of an activated CD8 T cell, as well as in the first few days following infection. Remarkably, these studies showed heterogeneity emerging in the antigen-specific population within 24 hours. At this time, at least two distinct populations of cells were identified—one population that was more effector-like, and one that appeared to have a memory precursor "precursor" phenotype. This finding suggests that memory fate determining decisions may occur substantially earlier than previously thought, and that interventions to improve memory responses may need to occur concomitantly early.

One of the earliest proteins to be expressed on CD8 T cells following infection is CD69, which is now widely used as a marker of cellular activation and tissue-residency. We investigated which mechanisms might enable such rapid expression. We found that both TCR and type I interferon signaling could upregulate CD69 on antigen-specific CD8 T cells as early as 1 day after infection. Type I interferon also regulated the expression of CD69 on naïve, non-specific CD8 T cells within the same time frame. Surprisingly, we found that naïve CD8 T cells actually harbored high levels of *Cd69* message and pre-formed protein. We hypothesize that these intracellular stores enable rapid recruitment of CD8 T cells following an immune insult.

Finally, we investigated the basic mechanisms of immune dysfunction during chronic infection, when antigen is never cleared and classical memory CD8 T cells do not develop. In this case, PD-1^{+}TCF-1^{+} stem-like CD8 T cells act as critical resource cells that sustain the antiviral response. They also provide the proliferative burst of effector CD8 T cells after PD-1 directed immunotherapy. We sought to determine what happens to the number of these progenitor cells in the setting of increased effector differentiation. Not only were stem-like CD8 T cells maintained following PD-1 blockade, but they actually increased their self-renewal in an mTOR-dependent manner, indicating that the PD-1 inhibitory pathway also regulates this process. At the same time, the stem-cell like transcriptional signature and *in vivo* functionality remained intact. These findings have broad implications for the improvement of immunotherapy in humans.

CD8 T Cell Differentiation during Viral Infection

By

Amanda Leanne Gill
B.A., Bryn Mawr College

Advisor: Rafi Ahmed, Ph.D.

A dissertation submitted to the Faculty of the
James T. Laney School of Graduate Studies of Emory University
in partial fulfillment of the requirements for the degree of
Doctor of Philosophy
in Graduate Division of Biological and Biomedical Sciences
Immunology and Molecular Pathogenesis
2023

Table of Contents

Abstract
Table of contents
List of figures

Chapter 1: Introduction 13
I. CD8 T cell responses during viral infection 13
II. CD8 T cell differentiation during acute infection 13
1. Early activation and expansion 13
2. Contraction 15
3. Memory precursor differentiation 15
4. Generation of long-lived memory 17
5. Memory subsets 19
5.1 Effector memory vs. central memory 19
5.2 Tissue-resident memory cells 20
6. Location and cellular fate 22
7. Earliest activation and differentiation 24
III. CD8 T cell differentiation during chronic infection 26
1. CD8 T cell exhaustion 26
2. Stem-like CD8 T cells 28
3. Transitory effectors and terminal differentiation 29
4. Role of the PD-1 pathway in CD8 T cell exhaustion 30
5. PD-1 pathway blockade 32
6. Mechanisms of reinvigoration following PD-1 pathway blockade 33

Chapter 2: Longitudinal analysis of the phenotype, transcriptional profile, and anatomic location of memory CD8 T cell subsets after acute viral infection 37
I. Summary 37
II. Introduction 38
III. Results 40
IV. Discussion 47
V. Materials and Methods 49

Chapter 3: Early fate decisions and the generation of early memory precursor CD8 T cells 60
I. Summary 60

II. Introduction 60
III. Results 62
IV. Discussion 66
V. Materials and Methods 67

Chapter 4: Intracellular stores facilitate rapid expression of CD69 on antigen-specific and non-specific CD8 T cells following TCR or cytokine stimulation 79
I. Summary 79
II. Introduction 79
III. Results 82
IV. Discussion 86
V. Materials and Methods 88

Chapter 5: PD-1 blockade not only promotes effector cell differentiation, but also increases the self-renewal of stem-like CD8 T cells to maintain the number of progenitor cells 104
I. Summary 104
II. Introduction 104
III. Results 105
IV. Discussion 110
V. Materials and Methods 111

Chapter 6: Discussion 129
I. Evidence of early memory precursor "precursors" 129
II. Functional role of CD69 in orchestrating the early immune response 130
III. PD-1 regulates stem-like CD8 T cells' self-renewal 131
IV. PD-1 blockade does not functionally or transcriptionally alter stem-like CD8 T cells 133

References 134

List of Figures

Chapter 1

Figure 1. Characterization of markers, functional qualities, and homing patterns of CD8 T cells during differentiation and memory formation 35

Figure 2. CD8 T cell differentiation during chronic infection..... 36

List of Figures

Chapter 2

Figure 1. Characterization of LCMV-specific memory CD8 T cell subsets after acute infection 52

Figure 2. Phenotypic profile of KLRG1/IL-7Rα subsets among $GP33^{+}$ CD8 T cells after acute infection 53

Figure 3. CD28 expression correlates with a memory phenotype 54

Figure 4. Transcriptional profile of three KLRG1/IL-7Rα CD8 T cell subsets after acute infection 55

Figure 5. Expression of key memory markers among three KLRG1/IL-7Rα CD8 T cell subsets after acute infection..... 56

Figure 6. IV-labeling reveals the location of $GP33^{+}$ CD8 T cells in the spleen after acute infection 57

Figure 7. MPs localize to the splenic white pulp as early as one to two weeks after acute infection 58

Figure 8. Summary of the anatomical distribution of memory CD8 T cell subsets over time 59

List of Figures

Chapter 3

Figure 1. Long-lived GP33^{+} memory CD8 T cells express TCF-1, CD62L, CD28, & CXCR3.. 70

Figure 2. Surface phenotype of antigen-specific CD8 T cells early following infection 71

Figure 3. Early heterogeneity in surface marker expression among CD8 T cells 72

Figure 4. Transcriptional profiling reveals distinct gene expression programming on each day following infection..... 73

Figure 5. Single cell analysis reveals transcriptional heterogeneity at each timepoint 74

Figure 6. Transcriptional findings are consistent with surface expression profiles..... 75

Figure 7. Summary of putative sub-populations at each timepoint based on transcriptional analyses..... 76

Figure 8. Heterogeneity in the naïve precursor population is not responsible for the heterogeneity observed post-infection..... 77

Figure 9. Expression of key markers is consistent between “dirty” and “pure naïve” precursor population 78

List of Figures

Chapter 4

Figure 1. CD69 is upregulated on both antigen-specific and non-specific CD8 T cells early following cognate antigen stimulation 93

Figure 2. CD69 is upregulated on antigen-specific CD8 T cells prior to the first division 94

Figure 3. CD69 is upregulated on both CD44hi and CD44lo CD8 T cells 95

Figure 4. Both TCR and interferon can upregulate CD69 *in vitro* 96

Figure 5. Both TCR and interferon can upregulate CD69 on antigen-specific CD8 T cells *in vivo* 97

Figure 6. Interferon can upregulate CD69 on non-specific CD8 T cells *in vivo* 98

Figure 7. CD69 expression on non-specific CD8 T cells is interferon-dependent 99

Figure 8. CD69 is upregulated in many other systemic viral infections 100

Figure 9. Naïve CD8 T cells express high levels of *Cd69* mRNA 101

Figure 10. Naïve CD8 T cells actively translate *Cd69* mRNA and consequently have large intracellular stores of CD69 protein 102

Figure 11. Summary of CD69 transcription and translation within naïve and activated CD8 T cells 103

List of Figures

Chapter 5

Figure 1. PD-1 blockade promotes effector cell differentiation 116

Figure 2. PD-1 blockade decreases the frequency of stem-like CD8 T cells but their numbers increase 117

Figure 3. Quantitation of stem-like CD8 T cells after PD-1 blockade 118

Figure 4. Quantitation of stem-like CD8 T cells after PD-1 blockade in chronic LCMV infection without transient CD4 depletion 119

Figure 5. Stem-like CD8 T cells are maintained up to 8 weeks following initial PD-1 blockade 120

Figure 6. Increased proliferation and self-renewal of stem-like CD8 T cells after PD-1 blockade 121

Figure 7. mTOR mediates expansion of stem-like CD8 T cells following PD-1 blockade..... 122

Figure 8. mTOR mediates proliferation of stem-like CD8 T cells following PD-1 blockade.... 123

Figure 9. Stem-like CD8 T cells that have received cycle 1 PD-1 therapy can robustly proliferate in response to viral challenge..... 125

Figure 10. The transcriptional program of stem-like CD8 T cells is conserved after PD-1 blockade 124

Figure 11. Stem-like CD8 T cells that have received cycle 1 PD-1 therapy can respond to an additional cycle 126

Figure 12. Cycle 1-treated and untreated mice respond equally well to two week PD-1 therapy 127

Figure 13. CD8 T cell differentiation during chronic infection and after PD-1 blockade..... 128

Chapter 1: Introduction

I. CD8 T cell responses during viral infection

CD8 T cells respond to intracellular pathogens. As adaptive immune cells, they constitute the second wave of an immune response, following innate immune cells' immediate and generalized defenses. They possess exquisitely specific receptors which precisely target infected cells and trigger a cascade of events that ultimately leads to their destruction. In this way, CD8 T cells are crucial for mediating viral control. If the virus is cleared, CD8 T cells possess a unique capacity to "remember" the offending pathogen and are able to respond more quickly and more robustly upon a secondary insult. If the virus is not cleared, CD8 T cells must instead adapt to the chronic antigen load in a specialized way, and this mechanism ensures that they can sustain an ongoing immune response for an extended period of time.

II. CD8 T cell differentiation during acute infection

1. Early activation and expansion

Following viral infection, antigen is taken up by antigen-presenting cells (APCs) and presented to naïve antigen-specific CD8 T cells via major histocompatibility class (MHC) I molecules. It is estimated that a mouse contains between 50-200 naïve precursor CD8 T cells specific for any one particular viral epitope (1). This makes cognate antigen recognition a considerably rare event, but it takes place within highly specialized anatomic compartments in the spleen (the white pulp) and in lymph nodes (the paracortex), where naïve CD8 T cells come in close proximity to incoming APCs and antigen (2).

To reach the activation threshold, naïve CD8 T cells require three signals: 1) Antigen recognition, 2) co-stimulation, and 3) activating cytokines (3). Co-stimulation mainly occurs through binding of the CD28 receptor on T cells to CD80 and CD86 on APCs—both upregulated in inflammatory contexts (4, 5). Other co-stimulatory receptors include OX40, 41BB, ICOS, CD27, CD40L, and many others (6–8). Activating cytokines include IL-12 or type I interferons (IFNα/β) (9).

Upon receiving all three signals, an activated CD8 T cell undergoes dramatic reprogramming. Chiefly, activation triggers rapid clonal expansion and differentiation. The magnitude of this initial clonal burst—typically between 10^4 and 10^5 fold—is critical to long-term immunity as it determines the number of memory CD8 T cells (10–13). Division occurs as rapidly as every 6 to 8 hours, and cells acquire progressive changes in gene expression that enable effector functions, migration, and cell cycling—all features required for the control of the infection (14–16). We and many others have extensively profiled the precise changes in gene expression that accompany effector differentiation during acute viral clearance, as well as the gradual changes that ensue, following clearance, as the residual population acquires memory qualities.

Upon antigenic stimulation, expanded CD8 T cells rapidly produce effector molecules such as granzymes, perforin, and other antiviral cytokines, including interferon-γ (IFNγ) and tumor necrosis factor-α (TNFα), which aid in pathogen elimination (16–19). As well, they gain the ability to enter nonlymphoid tissues where they carry out their cytolytic activity (20, 21). Specific mechanisms of chemokine-driven trafficking and activation are discussed in Section 6: Location and cellular fate.

Direct killing occurs when CD8 T cells encounter target cells expressing specific MHC class I-peptide complexes. Experiments using perforin gene knockout mice, which lack the

capacity for granule exocytosis (necessary for cytolysis), revealed that perforin was critical in the clearance of lymphocytic choriomeningitis virus (LCMV), a nonlytic virus that is eliminated in a CD8 T cell-dependent manner (22). Perforin has been shown to facilitate the delivery of granzymes into target cells; granzyme B can subsequently activate the caspase cascade, inducing apoptosis associated with rapid DNA fragmentation (23, 24).

2. Contraction

Following viral clearance and the peak of CD8 T cell expansion, the majority of activated virus-specific CD8 T cells die by apoptosis. There are two main mechanisms that precipitate this massive contraction: passive cell death (PCD) and activation induced cell-death (AICD) (3). In PCD, T cells die due to withdrawal from survival-associated cytokines, such as IL-2. In AICD, death is mediated by death-inducing factors that are upregulated upon antigenic stimulation, including Fas ligand (FasL) and TNFα (25).

After this death phase of the response, the remaining fraction of CD8 T cells (typically 5-20%) survives, seeding a population of long-lived memory cells (12, 26–28). Importantly, this smaller fraction is not derived from a subset of preformed memory CD8 T cells, but rather from the pool of activated effector cells themselves, which undergo additional differentiation (27–29). This population constitutes the memory precursor pool and is detailed in the next section.

3. Memory precursor differentiation

The memory T cell pool slowly develops from an effector T cell population that is rich in cellular and functional heterogeneity (28). In the last two decades, extensive research has teased out discrete patterns of phenotypical changes among this effector pool. The goal in discerning

these patterns has been to better understand which cells among the effectors go on to survive and become long-loved memory cells. With this, we can gain insight into long-term protective immunity at a much earlier point in the immune response.

Kaech et al. first characterized the quintessential "memory precursor" (30). These studies demonstrated that expression of IL-7Rα could distinguish memory fate (30, 31). IL-7Rα was expressed more highly on a small subset of effector CD8 T cells at the peak of the response, and this subset of cells was the fraction that ultimately survived post-contraction (30). Adoptive transfer of sorted IL-7Rα^{hi} or IL-7Rα^{lo} effector CD8 T cells into naïve mice showed that IL-7Rα^{hi} cells preferentially survived and differentiated into functional long-lived memory cells (30, 31). When challenged, the IL-7Rα^{hi} cells showed robust expansion, superior cytokine production, and were capable of more rapid pathogen clearance, as compared to IL-7Rα^{lo} cells (30, 31). Further, studies in IL-7-deficient mice demonstrated that IL-7Rα is functionally required for memory precursor survival (30).

Investigations have since been conducted to elaborate upon the memory precursor phenotype—aiming to fully characterize which precise cellular decisions drive memory fate. Sarkar et al. and Kalia et al. established which earlier populations gave rise to the IL-7Rα^{hi} memory precursor population (32, 33). Sarkar et al. found that IL-7Rα was uniformly down-regulated on effector cells and regained by a fraction around day 7 post-infection (30, 32). This suggested that differential programming had already been established. Analysis at day 4.5 demonstrated a striking heterogeneity in the expression of killer cell lectin-like receptor G1 (KLRG1) among IL-7Rα^{lo} cells (32). Ultimately, KLRG1^{int} cells preferentially differentiated into fully functional memory cells (as compared to KLRG1^{hi} cells)—re-expressing IL-7Rα and CD62L (L-selectin), localizing

to lymph nodes, and proliferating rapidly in response to secondary challenge (32). IL-2 production was also exclusively limited to KLRG1^{int} memory precursor population.

Kalia et al. established CD25 (IL-2Rα) as an even earlier marker of effector cell heterogeneity and memory precursor fate (33, 34). CD25 is rapidly and uniformly upregulated by antigen-specific CD8 T cells after TCR stimulation (33). Approximately 3.5 days post-infection, a subset was shown to selectively downregulate CD25, such that two distinct populations (CD25^{lo} and CD25^{hi}) became apparent (33). Ultimately, CD25^{lo} cells, which are relatively less sensitive to IL-2, were shown to preferentially give rise to memory precursors. In contrast, CD25^{hi} cells were more terminally differentiated: they perceived more robust IL-2 signaling, proliferated more rapidly, differentiated into effectors more readily, and underwent apoptosis more frequently (33).

Thus, our understanding of the heterogeneity among effector CD8 T cells and their capacity to give rise to long-lived memory cells has drastically advanced in recent years. CD25^{lo} effectors are the earliest definitive memory precursors and they can be distinguished by day 3.5. These CD25^{lo} cells become KLRG1^{int} by day 4.5, re-express IL-7Rα by day 7, and eventually give rise to highly functional memory cells following viral clearance. Earlier delineations of memory precursor fate are now being studied and are described in Section 7: Earliest activation and differentiation.

4. Generation of long-lived memory

The resulting population of long-lived memory cells is endowed with a capacity for multipotency, self-renewal, and robust proliferation (27, 35). Long-term, these memory cells persist in the absence of antigen, but slowly divide in a cytokine-dependent manner—namely via IL-7 and IL-15 signaling (27, 36). Upon reinfection, memory CD8 T cells almost immediately

spring into action—producing effector molecules, clonally expanding, and undergoing differentiation into secondary effectors. Collectively, this amounts to faster control of a secondary infection compared to a primary response.

Long-lived memory CD8 T cells have a naïve-like phenotype which complements their effector-like genomic landscape (37). In both humans and mice, memory CD8 T cells have been extensively characterized. The memory phenotype is defined by high surface expression of CD44, CD62L, IL-7Rα, and CCR7 and low expression of CD25, CD43, KLRG1, and granzyme B (16, 30, 38, 37, 32). A more complete characterization of the memory phenotype is provided in **Fig. 1**. Functionally, CD62L and CCR7 are key lymphoid homing molecules, targeting memory cells to T cells zones within secondary lymphoid organs (SLOs), while IL-7Rα enables homeostatic maintenance via IL-7 signaling (30, 38). Importantly, this expression pattern largely resembles that of a naïve cell.

On the other hand, memory CD8 T cells are also poised for effector function via discrete epigenetic modifications at key effector genes (39, 40). Specifically, Youngblood et al. demonstrated that differentiation of naïve CD8 T cells into effectors is accompanied by demethylation of effector genes (*Gzmb* and *Prf1*) and repression of naïve-associated genes (*Sell* and *Tcf7*), while these changes are reversed as effector cells develop into long-lived memory cells (37, 39). These epigenetic modifications enable rapid memory recall responses—a hallmark feature of memory CD8 T cells (32, 41–43). Their epigenetic landscape permits rapid production of effector molecules, including granzyme B, perforin, IFNγ, and TNFα, in response to antigenic re-stimulation (37, 43, 44). These molecules are cytotoxic and serve to rapidly induce death of virus-infected cells and aid in pathogen clearance, as detailed previously.

Long-term maintenance in the absence of antigen is another hallmark of memory CD8 T cells. Many studies have demonstrated that memory CD8 T cells can be maintained for decades following infection or immunization (37, 45, 46). Akondy et al. examined the human long-lived memory pool (37). In these studies, *in vivo* deuterium labelling was used to mark human CD8 T cells responding to the live yellow fever virus (YFV) vaccine. Analysis of the labelled cells over time demonstrated that the memory CD8 T cell pool originated from cells that had divided extensively early on in the infection, and the pool was then maintained by quiescent cells that divided less than once per year (37). This is the mechanism by which long-lived memory CD8 T cells are homeostatically maintained for long periods of time.

5. Memory subsets

Long-lived memory CD8 T cells slowly acquire unique functional characteristics. Key distinctions between the classical effector memory (Tem), central memory (Tcm), and tissue-resident memory (Trm) subsets are discussed below.

5.1 Effector memory vs. central memory

Originally, the Tem/Tcm subdivision was based on tissue-homing properties. $CD62L^{hi}CCR7^{hi}$ memory cells were found in the spleen, blood, and lymph nodes, whereas $CD62L^{lo}CCR7^{lo}$ cells were also found in the spleen and blood, but not in lymph nodes (47, 48). Instead, the $CD62L^{lo}CCR7^{lo}$ memory cells were found to be enriched in nonlymphoid tissues (49, 50). $CD62L^{hi}CCR7^{hi}$ memory cells had the capacity to synthesize IL-2, while $CD62L^{lo}CCR7^{lo}$ cells could not, but were instead more efficient producers of IFNγ and TNFα. $CD62L^{hi}CCR7^{hi}$ memory cells were designated Tcm, while the more effector-like $CD62L^{lo}CCR7^{lo}$ memory cells

were designated Tem (48). Tem are situated at peripheral sites, poised to initiate first-line pathogen defense, while Tcm are situated in lymphoid tissues poised to rapidly proliferate and provide a second wave of effectors (27, 28, 48, 51). A summary of the distinguishing features between these two subsets (surface markers, transcription factors, homing patterns, and functional capacities) is shown in **Fig. 1**.

In addition to understanding the phenotypic and functional characteristics of different types of memory cells, it has also been of considerable interest to determine the lineage relationship between them. Based on the initial observation that the memory pool gradually converted from a $CD62L^{lo}CCR7^{lo}$ phenotype to a $CD62L^{hi}CCR7^{hi}$ phenotype, Wherry et al. determined whether this was due to gradual death of one subset and outgrowth of another, or due to the direct conversion of one cell type to another (28, 29, 52). Using a series of adoptive transfer experiments involving sorted $CD62L^{hi}$ or $CD62L^{lo}$ memory CD8 T cell populations, Wherry et al. demonstrated that $CD62L^{lo}$ Tem gradually converted to $CD62L^{hi}$ Tcm in the absence of antigen (29). Of course, these studies also provided validation that functional changes arising in the memory pool (such as protective and recall capacity) are a direct consequence of $CD62L^{lo}$ Tem converting to $CD62L^{hi}$ Tcm (29). The ultimate result of this linear Tem to Tcm conversion is that the memory pool is populated with cells that are capable of rapid recall and proliferation, as well as antigen-independent long-term self-renewal (28).

5.2 Tissue-resident memory cells

Trm cells were characterized more recently, originally borne from discrepancies among Tem cells in circulation versus within non-lymphoid tissues (NLTs) (50, 53, 54). Trm cells are defined by their permanent residence within NLTs and their lack of recirculation (50). This is in

contrast to Tcm and Tem cells, which constitutively recirculate. Early on, this migratory behavior was evaluated by a number of groups, but studies involving NLT grafts and parabiotic surgery ultimately demonstrated that memory T cells within NLTs could not equilibrate between graft and host or between parabionts (55–57). These studies demonstrated that memory T cells within NLTs do not circulate. More recent intravascular staining strategies have corroborated these findings (58, 59).

Trm entry into and establishment within NLTs is a highly regulated process. At resting state, naïve CD8 T cells traffic throughout blood and SLOs. Upon antigen recognition, they proliferate and, once productively primed in an SLO, they give rise to effectors that migrate throughout the host (54, 60). Most likely, Trm cells arise from these migrated effector cells and they become permanently established in situ (50, 61, 62).

Migration of effector CD8 T cells from SLOs into the blood is mediated by upregulation of the transcription factor kruppel-like factor 2 (KLF2), which positively regulates sphingosine-1 phosphate receptor 1 (S1PR1) (54, 63, 64). S1PR1 induces chemotaxis towards S1P in the efferent lymph and blood (64). Following this, signals for tissue entry are relatively tissue-specific, for example α4β7 integrin facilitates migration into the small intestine (57, 65). After migration, α4β7 is rapidly downregulated, while in situ upregulation of CD69 and αeβ7 (CD103) also occurs (57, 66).

CD69 and CD103 are the canonical Trm markers. Functionally, αeβ7 binds E-cadherin and enables epithelial adherence, but may also promote CD8 T cell survival (67–69). Studies have shown that αeβ7 KO CD8 T cells are able to migrate to the small intestine epithelium, brain, and skin epidermis, but are not retained (70, 71). CD69 antagonizes S1PR1 and so prevents S1PR1-mediated tissue egress (64, 66, 69)s. In support of this are studies in which CD69 KO CD8 T cells

were not maintained in skin epidermis or lungs (69, 72). It must be noted, however, that expression of CD69 and CD103 may be restricted to certain subsets of Trm or to certain tissue compartments, so their utility as markers of tissue-residency is limited. Otherwise, Trm cells, like Tem cells, are $CD62L^{lo}$, $CCR7^{lo}$, and IL-$7R\alpha^{lo}$ (54, 63).

After their establishment, Trm cells remain in and survey NLTs long after antigen clearance, positioned to provide highly effective frontline defense against viral infections (50, 73). Given their effector-like origin, it follows that they are poised for rapid execution of effector functions (rather than for proliferation). First, Trm cells display increased motility during inflammatory conditions via upregulated integrin ($\alpha v\beta 1$ and $\beta 1$) and chemokine (CXCL10) expression (74). They are also able to adopt "dendritic-like" cell morphologies which facilitate host cell scanning (75). Once pathogen recognition has occurred, they primarily mediate ex vivo cytotoxicity via constitutively high levels of expression of granzyme B (54, 66). The complete phenotypic, migratory, and functional profile of Trm cells is outlined in **Fig. 1**.

6. Location and cellular fate

Understanding the interplay between cellular localization and immune fate has been of considerable recent interest. These studies have focused on the spleen, in particular.

Structurally, the spleen can be divided into red pulp (RP) and white pulp (WP), each of which carries out a unique set of functions. The RP is the main site of red blood cell (RBC) opsonization and recycling, while the WP is the primary immunologic region, functioning essentially as a lymph node for the circulatory system (2, 76). The WP and RP are separated by a marginal zone (MZ) consisting mainly of macrophages. The WP can be further divided into B cell zones (BCZ) and T cell zones (TCZ), also called periarteriolar lymphatic sheathes (PALS) because

they form around central arterioles (2). Naïve and Tcm cells, as well as conventional dendritic cells (cDC1s), are found within the TCZ, where they are activated and primed in response to cognate antigen delivered by the central arteriole (2). B cells sit in follicles within the BCZ, forming germinal centers and producing antibody upon antigen recognition (2). Finally, bridging channels (BC) exist between the WP and RP and are widely believed to form conduits that are traversed by naïve and activated lymphocytes as they migrate through the MZ, into the RP, and back into circulation (76).

As discussed previously, naïve CD8 T cells continuously circulate between blood, SLOs, and lymph (77). To enter a lymph node, CD62L on T cells binds peripheral node addressin (PNAd) on HEVs, which enables CCR7 on T cells to recognize CCL21 on HEVs (77, 78). Following several intermediate steps, transmigration into the TCZ occurs (79). CCL21 is abundantly expressed by fibroblastic reticular cells (FRCs) and acts to direct T cells throughout the TCZ and the interfollicular zone, where this network terminates (2, 80, 81). Importantly, both CD62L and CCR7 are required for initial splenic entry, and loss of CCR7 results in scattering of T cells throughout the spleen (76, 82). Recently emigrated naïve T cells pause briefly to scan the TCZ before S1P-mediated egress and subsequent return to lymph and/or blood (83–85)

During inflammation, inflammatory signals (such a CCL2, CCL5, and TNFα) induce changes in lymph node architecture and homing requirements (86–90). Reactive lymph nodes induce CCR5 expression on naïve CD8 T cells, which draws them along local CCL3 and CCL4 gradients towards DC/CD4 T cell interactions (91, 92). HEVs of reactive lymph nodes also increase CXCL9 expression, which increases $CXCR3^{+}$ T cell recruitment (93, 94). In the rare event that a T cell encounters its cognate antigen within the lymph node, CD69 is transiently upregulated, which antagonizes S1PR1 and increases dwell time to enable appropriate co-stimulatory and

cytokine signals (95). After a few days, much of the expanded population has left the lymph node altogether, as effectors ready to initiate an antiviral response (77).

Localization of distinct CD8 T cell subsets within the spleen is now being uncovered, and a clear link has emerged between location and memory fate. In particular, location appears to correlate with the degree of memory differentiation: more terminally-differentiated Tem cells are enriched in the splenic RP and more fate-permissive Tcm cells are enriched in the splenic WP (96, 97). One study using irreversibly YFP-tagged effector CD8 T cells showed that, following acute LCMV infection, TCZ were disrupted and YFP^+ effector CD8 T cells trafficked to the RP via BC, but upon resolution, YFP^+ memory CD8 T cells localized to the WP (98, 99).

While we understand some of the dynamics of splenic CD8 T cell localization during activation and contraction, we still lack knowledge of the precise signals which guide cells to these locations, and whether these signals may influence long-term memory survival.

7. Earliest activation and differentiation

More recently, early CD8 T cell differentiation has been a topic of intense investigation. Understanding which early signals shape CD8 T cell fate may hold the key to understanding a great many other immune phenomena. For example, uncovering the earliest basis of memory T cell development would perhaps enable us to formulate better T cell-targeted vaccines and T cell-based therapies. Our investigations into this area are greatly informed by the comprehensive analyses of memory CD8 T cell fate and phenotype outlined above.

In order to evaluate differentiation at earlier time points, a transfer model of viral infection must be employed. This is because the endogenous frequency of virus-specific CD8 T cells is typically too low to detect this early. In the case of LCMV, CD8 T cells from P14 transgenic mice

are transferred into B6 mice prior to infection in order to increase the $GP33^+$ precursor frequency. Transgenic P14 mice have a clonal, $GP33^+$ CD8 T cell repertoire (100, 101). P14 chimeras are infected with high-dose LCMV (2x10^6 pfu, i.v.) and P14 ($GP33^+$) CD8 T cells can be detected using their congenic marker. In this model, LCMV-specific responses can be monitored as early as 1 day post-infection. Naïve CD8 T cells upregulate a great number of surface proteins upon activation, and this model has been used to characterize these *in vivo*.

Classical surface markers for "early activation" are upregulated within 24 hours and include: CD25, CD43, CD44, CD69, and programmed cell death-1 (PD-1) (102, 103). Concurrently, several surface markers are known to be immediately down-regulated upon activation, these include CD62L, CCR7, and IL-7Ra. One goal in recent studies has been to elucidate a more complete picture of the earliest possible memory precursor phenotype. To date, the earliest definitive memory precursor was delineated on day 3.5 post-infection, as detailed above (33).

Recently, T cell factor-1 (TCF-1) has become recognized as a master regulator of early memory fate in CD8 T cells. TCF-1 is a transcription factor downstream of the canonical Wnt pathway and is proposed to drive a stem cell-like self-renewal program (104–108). TCF-1 is highly expressed in naïve CD8 T cells but downregulated during effector differentiation by systemic inflammation (105). Studies by Zhou et al. and others have demonstrated that TCF-1 deficiency leads to limited proliferation of effector CD8 T cells as well as impaired Tcm differentiation (108). This was due to diminished IL-15 driven proliferation and reduced expression of Eomes, IL-2Rβ (CD122) and anti-apoptotic Bcl-2 (108). Further studies have also shown that TCF-1 downregulation requires cell cycling and is responsible for Tcm cell fate determination during asymmetric division (105, 106).

Several studies have attempted to make sense of early cell fate decisions using high-throughput transcriptomics (109). Molecular heterogeneity among splenic CD8 T cells has been demonstrated as early as after the first division following activation (110, 111). In this case, division 1 cells were isolated on the basis of their dilution of CFSE, a division-tracking dye. One subpopulation of division 1 cells appeared to be most similar to effector cells that were isolated from days 4 and 7 post-infection ($Div1_{TE}$), while the other subpopulation was more similar to Tcm and naïve cells ($Div1_{MEM}$). $Div1_{MEM}$ had higher expression of *Il7r, S1pr1*, and *Klf2*, while $Div1_{TE}$ had higher expression of *Eomes, Id3,* and *Foxo1*. Surprisingly, both populations expressed similar levels of several memory-associated genes, including *Lef1, Bach2,* and *Tcf7*.

Early heterogeneity in CD8 T cell responses suggests that these cells make memory decisions remarkably quickly—perhaps before they even divide for the first time. This highlights the importance of initial TCR signal strength, co-stimulation, and cytokine signaling in shaping the formation of memory in the long-term.

III. CD8 T cell differentiation during chronic infection

1. CD8 T cell exhaustion

When a viral infection is not cleared, severe defects develop within the CD8 T cell compartment, to the point that memory differentiation fails to occur (112). In this case, CD8 T cells undergo "exhaustion." T cell exhaustion likely evolved as an adaptation to prevent host immunopathology, but in the case of chronic infection, it severely limits control of the virus.

CD8 T cell exhaustion has now been extensively characterized, but it was first elucidated by Zajac et al. (113). In these studies, virus-specific CD8 T cells were shown to persist during

chronic LCMV infection, but they lacked effector function. Further investigation of CD8 T cells from chronic infection showed that they do initially develop the ability to perform effector functions, however, these functions are subsequently lost in a hierarchical manner (114). Production of IL-2 and cytotoxic capacity were the first functions to be compromised during persistent antigenic stimulation, followed by a gradual loss in cytokine production—TNFα next, then IFNγ production became impaired in severe stages of exhaustion. Eventually, CD8 T cells fully lacking effector functions can be found, and in extreme situations virus-specific CD8 T cells can be physically deleted (115, 116). Importantly, this deletion occurred in response to epitopes that were presented at the highest levels, while functional exhaustion was induced in CD8 T cells that saw lower levels of antigen presentation (114).

We now have a more complete understanding of T cell exhaustion. Exhausted cells have unique transcriptional and epigenetic signatures—distinct from naïve, effector, or memory CD8 T cells. The exhausted signature includes alterations in metabolic fitness, dysregulation of cytokine signaling, and, most importantly, overexpression of inhibitory receptors, including PD-1, CTLA-4, LAG-3, TIM-3, TIGIT (117–122).

These findings have now been documented in numerous other viral settings, including in other mouse models (polyoma virus, adenovirus, mouse hepatitis virus), non-human primate models (SIV), and in human chronic infections (human immunodeficiency virus [HIV], hepatitis B virus [HBV], and hepatitis C virus [HCV]) (123). Of course, this functional exhaustion is also hallmark of tumor-specific CD8 T cells during cancer.

2. Stem-like CD8 T cells

We now have a deeper understanding of CD8 T cell differentiation in settings of chronic antigen stimulation. The pool of exhausted CD8 T cells actually represents a remarkably heterogeneous population (124). Paley et al. were the first to demonstrate this—uncovering at least two subpopulations: a T-bet^{hi}PD-1^{int} progenitor subset and their terminally-differentiated Eomes^{hi}PD-1^{hi} progeny (125). The Eomes^{hi}PD-1^{hi} population did not replicate and expressed higher levels of inhibitory receptors. Following this, multiple studies examined this heterogeneity more closely. TCF-1 was identified as a crucial transcription factor that conferred memory/stem-cell like features on a subset of virus-specific CD8 T cells (107, 126–128). This subset of TCF-1^{+} "stem-like" CD8 T cells had the capacity for self-renewal and gave rise to terminally-differentiated effector cells (129, 130).

Stem-like cells express PD-1 and are also CXCR5^{+} and TIM-3^{-}, while the more terminally differentiated TCF-1^{-} subset expresses higher levels of PD-1 and is CXCR5^{-} and TIM-3^{+}. Although both subsets express PD-1, stem-like CD8 T cells have low or no expression of any other inhibitory receptor (131). Stem-like cells also express Ly108 (SLAMF6), CD73, survival-associated transcription factors (Id3, Lef-1, and Bcl-6), costimulatory receptors (CD28 and ICOS), and low levels of CD127 and CD62L (129, 132). Epigenetically, the regulatory regions of *Tcf7* and *Id3* are more accessible in stem-like CD8 T cells than in exhausted cells (133).

Beyond their unique gene expression profiles, stem-like and terminally differentiated subsets are also distributed in distinct spatial compartments (129, 134). Stem-like CD8 T cells are sequestered within SLOs—particularly within the TCZ and the splenic WP. In these spaces, there is relatively low antigen burden and viral replication. On the other hand, terminally-differentiated CD8 T cells are found at sites with high antigen burden—in peripheral tissues and in the splenic

RP. Recently, Dähling et al. demonstrated that cDC1s in the TCZ may actually serve to maintain the stem-like CD8 T cell population, creating a niche that protects them from high levels of antigen (135).

Stem-like CD8 T cells serve as a crucial resource population during chronic infection. They sustain the pool of virus-specific CD8 T cells and enable prolonged effector responses. Importantly, our lab recently discovered that this particular subset of cells also provides the proliferative burst seen after PD-1 blockade (129). Concerning the use of PD-1-directed immunotherapy in the clinic, this finding demonstrated a potential mechanistic basis for patient outcome. Many studies have since further investigated this mechanism and are detailed in Section 5: PD-1 pathway blockade.

3. Transitory effectors and terminal differentiation

Stem-like CD8 T cells are critical for the maintenance of virus-specific responses during chronic infection. As stem-like CD8 T cells differentiate, they gradually lose expression of TCF-1, and this coincides with the progressive upregulation of canonical inhibitory receptors and loss of effector function (129, 132, 136). In this process, stem-like CD8 T cells gain expression of TIM-3 and can then be subsetted according to a number of different schemes. Our lab and others recently identified a transitory effector population that consists of newly-generated stem-like progeny (137–139). This population of CD8 T cells is characterized by an effector-like transcriptional signature, including expression of the chemokine receptor CX3CR1, granzyme B, and multiple pro-inflammatory cytokines (137). Hudson et al. demonstrated that this transitory population was highly functional—they could proliferate *in vivo* and they were critical for viral control (137, 139).

Beltra et al. have also proposed a "four-cell-stage" developmental framework for differentiation. In this case, Ly108 and CD69 define four hierarchical subsets of exhausted CD8 T cells (136). Stem-like CD8 T cells are classified as Ly108^{+}CD69^{+}; their progeny lose CD69 expression and enter circulation. These Ly108^{+}CD69^{-} cells then further differentiate, gain cytotoxic functionality, and lose Ly108 expression. Eventually, terminally-exhausted CD8 T cells enter peripheral tissues and remain resident within them, becoming Ly108-CD69^{+}.

Terminal-differentiation or terminal-exhaustion, as described previously, indicates the gradual loss of all functional capacity. CD101 has recently emerged as a surface marker that can further distinguish the terminally-differentiated CD8 T cell population (137). Transitory effector-like CD8 T cells are PD-1^{+}Tim-3^{+}CX3CR1^{+}CD101-, while terminally-differentiated CD8 T cells are PD-1^{++}Tim-3^{+}CX3CR1-CD101^{+}. Importantly, CD101 expression beautifully distinguishes three transcriptionally distinct virus-specific CD8 T cell populations: stem-like, transitory, and terminally-differentiated (137). *Cx3cr1*, *Klrg1*, and *Tbx21* (encoding T-bet) were preferentially expressed in the transitory subset, while surface inhibitory receptors were particularly enriched in the terminally-differentiated subset. A summary of the characteristic features delineating each of these three CD8 T cell subsets is provided in **Fig. 2.**

4. Role of the PD-1 pathway in CD8 T cell exhaustion

Given that CD8 T cells are crucial for mediating both viral and tumor control, uncovering the mechanisms underlying their dysfunction in chronic settings is of great importance. The inhibitory receptor PD-1 is a key regulator of CD8 T cell function and plays a central role in regulating CD8 T cell exhaustion. Sustained expression of PD-1 is a cardinal feature of CD8 T cells in chronic infection and cancer.

PD-1 is a transmembrane receptor of the CD28 family (140). PD-1 signaling plays a major role in the direct negative regulation of TCR signaling following T cell activation (141). This is achieved through engagement of its ligands, PD-L1 or PD-L2, and subsequent phosphorylation of tyrosines within its immunoreceptor tyrosine-based inhibitory motif (ITIM) and immunoreceptor tyrosine-based switch motif (ITSM) (140, 142). Phosphorylated PD-1 recruits the SH2-domain-containing tyrosine phosphatase (SHP-2), which in turn dephosphorylates early mediators of T cell activation, including the initial stimulatory and costimulatory signaling molecules such as CD28 (141, 143, 144). This results in higher net dephosphorylation of CD28 and TCR signaling components and attenuated T cell activation (143, 145).

PD-L1 and PD-L2 are both members of the B7 family and are constitutively expressed by many hematopoietic and nonhematopoietic cell types, particularly APCs (140, 142). Importantly, PD-L1 expression can be induced by type I and type II IFNs, as well as many other cytokines (146). Importantly, PD-L1 is expressed in the tumor microenvironment and is associated with poor prognosis; in this case, tumor cells exploit the PD-1 signaling axis in order to enhance their survival (147).

Downstream PD-1 signaling affects many aspects of T cell function. PD-1 ligand engagement results in decreased metabolic fitness through a reduction in Akt activation, mTOR inhibition, and repression of the transcriptional coactivator PGC-1α (peroxisome proliferator-activated receptor γ coactivator 1α), among many other mechanisms (122, 148).

Studies involving the manipulation of PD-1 expression (through blockade or genetic ablation) have greatly informed our understanding of the role of PD-1 in CD8 T cell differentiation—in both acute and chronic settings. PD-1 deficient mice experience multiple autoimmune features due to breakdown of peripheral tolerance, and acute infection induces lethal

immunopathology (149). More specifically, PD-1 functions as an inhibitory receptor during the early stages of CD8 T cell activation and PD-1 blockade during this time has been shown to enhance effector function and result in faster clearance of acute infection (103). During chronic infection, genetic absence of PD-1 has been shown to result in the accumulation of more cytotoxic CD8 T cells, but these cells were also more terminally-differentiated and exhausted (150).

5. PD-1 pathway blockade

Therapeutic blockade of the PD-1 pathway therefore reinvigorates the CD8 T cell response. This occurs through a dramatic reversal PD-1-driven anergy and exhaustion. PD-1 blockade reprograms metabolism, promotes proliferation, and drives increased expression of effector molecules, such as perforin, granzymes, and cytokines. In the original studies from Barber et al. PD-1 blockade was performed through the *in vivo* administration of antibodies that blocked the PD-1/PD-L1 (151). This treatment enhanced CD8 T cells' ability to kill virally-infected cells and ultimately led to a significant reduction in the viral load (151). These experiments were performed in the chronic "CD4-unhelped" LCMV model system (the most stringent model of CD8 T cell exhaustion).

Since then, PD-1 blockade has been examined in countless settings of chronic infection and cancer, in both mice and humans. PD-1-targeted therapy has shown successes in many cases. In non-human primates, PD-1 blockade enhanced SIV-specific T and B cell responses to ultimately increase control of the virus (152). In HCV, T cell responses were similarly enhanced—with a 100-fold suppression of viremia during treatment (153). In humans, dramatic progress has occurred since the approval of the first αPD-1 blocking antibody by the US Food and Drug Administration (FDA) in 2014. Now, PD-1-directed immunotherapy is a cornerstone of treatment

for numerous cancers: advanced melanoma, small-cell lung cancer, non-small cell lung cancer, cervical cancer, urothelial cancer, gastric cancer, triple-negative breast cancer, renal cell carcinoma, head and neck squamous cell carcinoma, hepatocellular carcinoma, Hodgkin lymphoma (154). Use of PD-1-directed therapeutics for chronic viral infection in humans is an emerging interest. Patients with chronic HCV infection who received αPD-1 therapy were able to achieve a 4-log reduction in viral load after treatment (155). Clinical uses of αPD-1 therapy for HIV are promising, but remain uncertain (156–159).

Resistance to immunotherapy is a primary concern, however. Resistance can occur due to inadequate T cell infiltration into the tumor. This can be caused by alterations in PD-L1 expression, high mutational burden or increased neoantigen expression, disrupted antigen presentation, or localized immunosuppression (160). Resistance can also occur following prolonged therapy, when patients who previously responded to therapy are no longer responsive (160). Understanding this mechanism of acquired resistance has been far more elusive.

6. Mechanisms of reinvigoration following PD-1 pathway blockade

Current investigations have shifted to focus on the mechanisms by which PD-1 blockade reinvigorates the CD8 T cell response, so we can learn to circumvent the shortcomings of this therapy in the clinic. From our lab and others, now know that PD-1 blockade acts specifically on the stem-like subset of CD8 T cells, as discussed previously (129). PD-1-directed therapy induces proliferation and differentiation of stem-like CD8 T cells into highly function effectors. In humans, this proliferative burst can be observed as an increase in Ki-67^{+} PD-1^{+} CD8 T cells following therapy, mostly during the first or second cycles of treatment (161).

The emerging effector CD8 T cells will go to sites of infection or tumor and carry out target cell killing. This accumulation of effector cells and lysis of infected or cancerous cells ultimately leads to enhanced viral control and tumor burden (151). In addition to PD-1 blockade acting within the lymphoid tissues, ligation of PD-1 on antigen-specific effectors with PD-L1 or PD-L2 at the target sites enables further effector capacity and better killing of these target cells.

PD-1 blockade also acts in a CD28-dependent manner (162). This is consistent with findings related to the localization of stem-like CD8 T cells: they are in close proximity to $B7^+$ DCs in the TCZ of lymphoid organs. Kamphorst et al. performed studies in which CD28 was conditionally knocked-down during chronic infection, and showed that expansion following PD-1 blockade was restricted to CD28-expressing cells (162). CD28 was also required for effective αPD-1 therapy in tumor-bearing mice. Most importantly, these findings have been reflected in the clinic. Proliferating CD8 T cells are predominantly $CD28^+$ in the peripheral blood from cancer patients receiving PD-1-directed therapy, and unresponsive tumor-infiltrating CD8 T cells (TILs) are marked by loss of CD28 expression (162, 163).

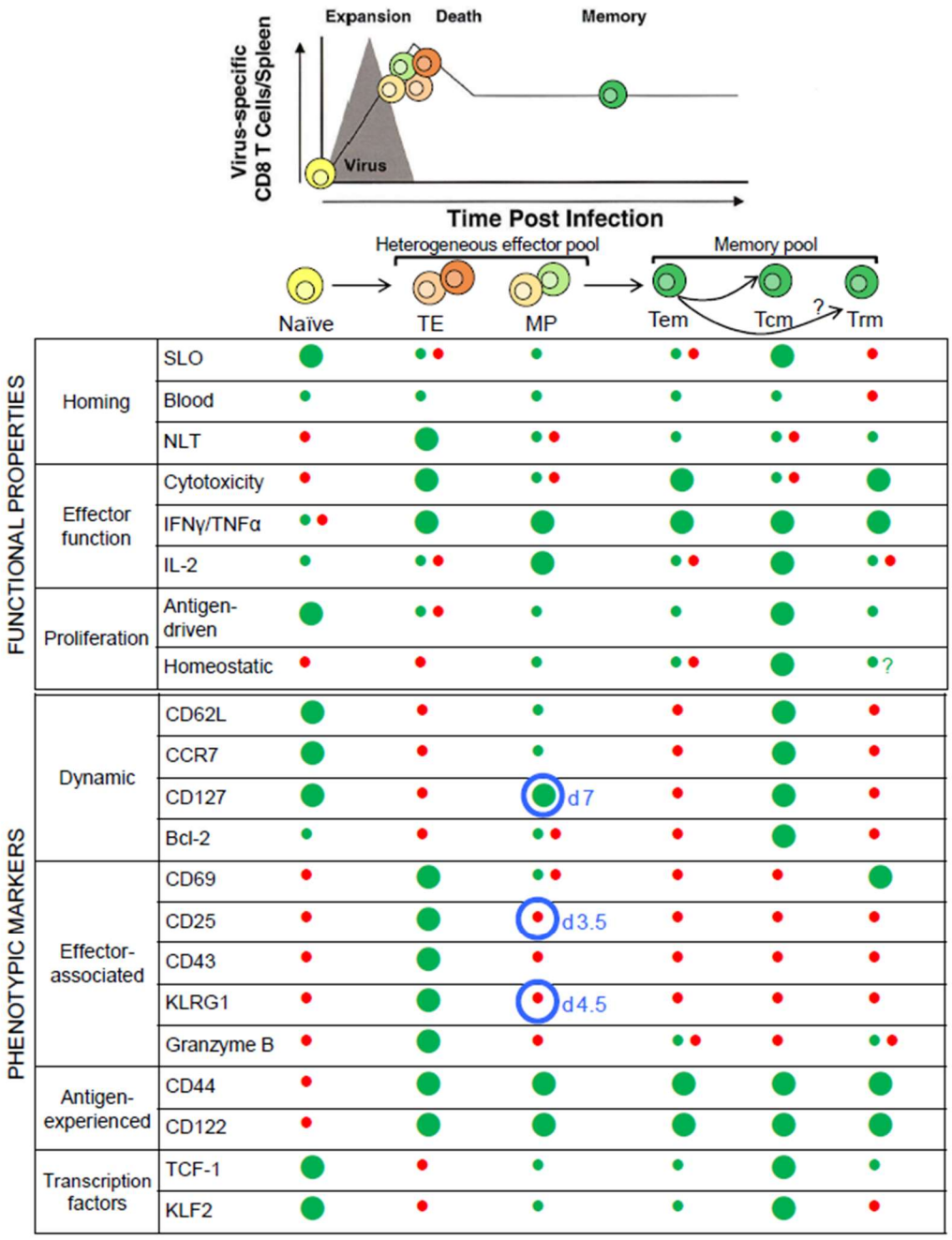

Figure 1. Characterization of markers, functional qualities, and homing patterns of CD8 T cells during differentiation and memory formation. Size of the dot corresponds to magnitude of expression of the marker or degree of functional capacity, and color corresponds to upregulation (green) or downregulation (red). Blue circles indicate early memory precursor markers and the days at which they can distinguish MP vs. TE cells. CD103 is often expressed in concert with CD69, but Trm cells in many locations are also $CD103^{-}$. Abbreviations: TE, terminal effector. MP, memory precursor. Tem, effector memory. Tcm, central memory. Trm, resident memory. SLO, secondary lymphoid organ. NLT, non-lymphoid tissue. Adapted from *Wherry, EJ & Ahmed, R. Memory CD8 T-Cell Differentiation during Viral Infection. J Virol, 2004*.

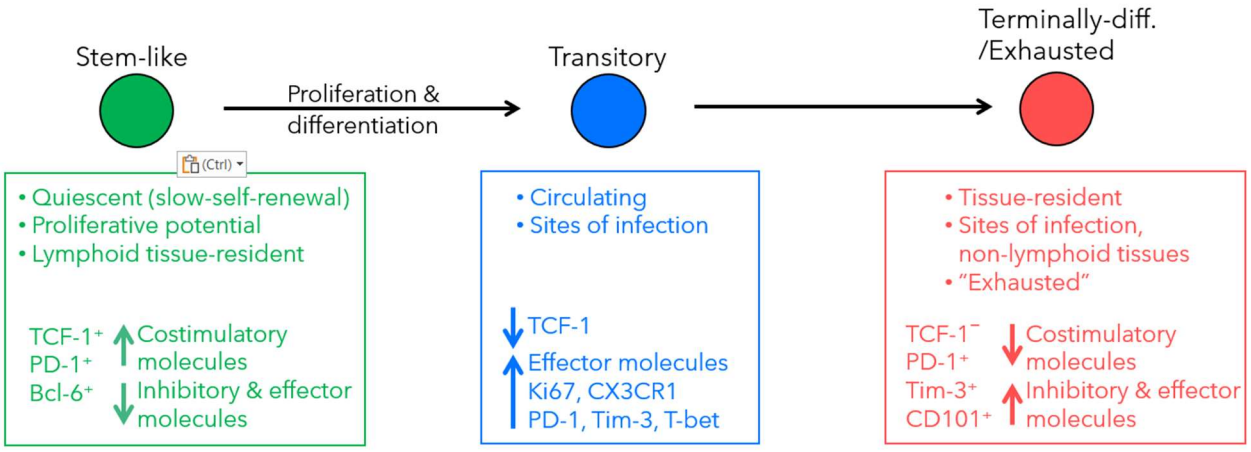

Figure 2. CD8 T cell differentiation during chronic infection. Three key populations of CD8 T cells emerge during chronic infection. Their hierarchical relationship is shown with arrows. The key functional features of each cell type are also listed in boxes at the bottom, along with the key surface markers and transcription factors that define them.

Chapter 2: Longitudinal analysis of the phenotype, transcriptional profile, and anatomic location of memory CD8 T cell subsets after acute viral infection

Gill AL, Hudson WH, Valanparambil RM, Ahn E, McGuire DJ, Wieland A, McManus DT, Kissick HT, Akondy RS, and Ahmed R. (2022). Longitudinal analysis of the phenotype, transcriptional profile, and anatomic location of memory CD8 T cell subsets after acute viral infection. *Journal of Virology*. 97 (1), e01556-01522.

I. Summary

Increased demand for novel, highly effective vaccination strategies necessitates a better understanding of long-lived memory CD8 T cell differentiation. To achieve this understanding, we used the mouse model of acute lymphocytic choriomeningitis virus (LCMV) infection. We reexamined classical memory CD8 T cell subsets and performed in-depth, longitudinal analysis of their phenotype, transcriptional programming, and anatomic location within the spleen. All analyses were performed at multiple time points from 8 days to 1 year post-infection. Memory subsets are conventionally defined by their expression of KLRG1 and IL-7Rα, as follows: KLRG1^{+}IL-7Rα^{-} terminal effectors (TEs) and KLRG1^{-}IL-7Rα^{+} memory precursors (MPs). But we also characterized a third KLRG1^{+}IL-7Rα^{+} subset which we refer to as KLRG1^{+} MPs. In these analyses, we defined a comprehensive memory phenotype that is associated with higher levels of CD28 expression. We also demonstrated that MPs, KLRG1^{+} MPs, and TEs have distinct localization programs within the spleen. We found that MPs became preferentially enriched in the white pulp as early as 1 to 2 weeks post-infection, and their predominance in the white pulp was maintained throughout the course of a year. On the other hand, KLRG1^{+} MPs and TEs localized to the red pulp just as early, and they consistently localized to the red pulp thereafter. These findings indicate that location may be crucial for memory formation and that white pulp-derived signals may contribute to long-term memory survival. Achieving robust memory responses

following vaccination may require more deliberate consideration of which memory phenotypes are induced, as well as where they traffic, as these factors could impact their longevity.

Importance

CD8 T cells play a critical role in viral immunity and it is important to understand how memory cells are formed and what processes lead to their long-term maintenance. Here, we use a mouse model of acute infection to perform an in-depth, longitudinal analysis of memory CD8 T cell differentiation, examining the phenotype and location of memory cells out to 1 year post-infection.

II. Introduction

Development of CD8 T cell memory following vaccination is of great importance, as these cells are crucial in providing durable protection again secondary infection (16, 19). Memory CD8 T cells are able to undergo long-term self-renewal, yet they remain poised to rapidly recall effector functions upon antigen re-encounter (37, 39).

Following primary infection, naïve antigen-specific CD8 T cells encounter antigen and become activated—undergoing proliferation and acquiring effector functions that enable them to kill virally-infected cells (16, 19, 164, 165). This activated population is heterogeneous. The majority of cells which are KLRG1^{+}IL-7Rα^{-} are destined to die through apoptosis following clearance of the infection and are called “terminal effectors” (TEs) (166). A small subset (5-10%) survives—these “memory precursors” (MPs) express higher levels of IL-7Rα and lower levels of KLRG1 and seed the long-lived memory pool (29, 30, 32). These subsets are also referred to as short-lived effector cells and memory precursor effector cells (SLECs and MPECs), respectively (27). Importantly, IL-7Rα is critical for the survival of long-lived memory CD8 T cells (30).

The memory pool arising from KLRG1^{-}IL-7Rα^{+} MPs can be subdivided based on cellular function and localization. Classically, memory CD8 T cells are divided into two populations based on their expression of the homing markers CD62L (L-selectin) and CCR7 (48). CD62L^{lo}CCR7^{lo} cells are "effector memory" (T_{em}) and localize to inflamed tissues, while CD62L^{hi}CCR7^{hi} cells are "central memory" (T_{cm}) and preferentially home to secondary lymphoid organs (27, 48, 167). Both T_{em} and T_{cm} will recirculate through the blood to complete their respective surveillance cycles. An additional "tissue-resident" memory subset (T_{rm}) does not circulate and provides protection exclusively from non-lymphoid compartments (60, 66, 67, 168).

Memory CD8 T cells also have highly specialized localization programs within tissues—particularly within secondary lymphoid organs (98, 99, 169). Intrasplenic localization, for example, has been shown to correlate with memory phenotype. In some studies, T_{em} seem to be enriched in the red pulp (RP), while Tcm are enriched in the white pulp (WP) (96, 97, 169). T_{rm} also have distinct expression profiles which enable their migration to and within specific tissue compartments (73, 170). Beyond homing capacity, these subsets are also distinguished by core functional properties. T_{em} and T_{rm} are more terminally-differentiated and cytotoxic, while T_{cm} are more fate-permissive and have high proliferative and recall potential (27, 167, 171, 172).

Characteristics of these memory programs have been continually refined as new markers of function emerge. Recently, TCF-1 has become one of the most important markers of long-lived memory—a key transcription factor that drives self-renewal via Wnt signaling (107, 108, 173–176). CD28 is also of interest, as TCR signal strength has been shown to correlate with memory formation (171, 177, 178). Importantly, CD28 is expressed at high levels on long-lived memory CD8 T cells in humans (37, 44). Chemokine receptors (including CXCR3 and CX3CR1) have

additionally been implicated in memory formation, as spatial organization has been shown to mediate survival and recall potential (179–183).

In this study, we provide a comprehensive, longitudinal analysis of the expression of established and putative memory markers across both time and space. We evaluated the expression of KLRG1 and IL-7Rα up to 1 year after acute LCMV infection and we performed phenotypic and transcriptional analyses of the subsets defined by these markers. We also performed spatial characterization of memory CD8 T cells within the spleen, tracking them in the RP and WP using intravenous (i.v.) anti-CD8α labeling (59). We were able to match phenotype and location in order to better characterize the functional compartmentalization of the spleen. We found that location may be an important determinant of long-lived memory. Taken together, our studies provide a deeper understanding of how memory CD8 T cells differentiate and survive following acute infection. Knowing which processes facilitate memory formation and dictate their longevity will be crucial in the development of novel therapeutic and vaccination strategies.

III. Results

Longitudinal characterization of KLRG1/IL-7Rα subsets of CD8 T cells following acute infection

In this study, we investigated the longitudinal responses of CD8 T cells following acute LCMV infection. We saw robust proliferation of virus-specific CD8 T cells that peaked on day 8, and then we monitored responses for 1 year by frequency (**Fig. 1a**) and absolute number (**Fig. 1b)**. As shown previously, CD8 T cell responses against three LCMV epitopes varied according to their immunodominance, with NP396 eliciting the most robust response, followed by GP33 and GP276 (12, 184–186).

At day 8, the vast majority (~70%) of $GP33^+$ CD8 T cells were TEs (**Fig. 1c** and **d**), while MPs constituted <10% of the total population. At this timepoint, roughly 10% of $GP33^+$ CD8 T

cells expressed both KLRG1 and IL-7Rα, which we refer to as "KLRG1$^+$ MPs," and 10% of GP33$^+$ CD8 T cells expressed neither marker, which we refer to as "double-negatives" (DNs). By absolute number, the TEs exceeded KLRG1$^+$ MPs and MPs by >10-fold. DNs constituted <10% of total GP33+ CD8 T cells after day 8, so we removed them from our analysis after this timepoint. Between days 8 and 60 post-infection, the relative dominance of TEs, KLRG1$^+$ MPs, and MPs underwent a dramatic shift; after day 60, the populations grew more stable. On day 15, the proportion of TEs dropped to ~50% of the total GP33$^+$ population and their numbers contracted by ~10-fold. The proportion of KLRG1$^+$ MPs increased to ~15%, while their numbers decreased by ~2 to 3-fold. The proportion of MPs doubled from day 8 to ~20% and their numbers remained roughly the same. By day 30, MPs could also be broken down and referred to as T_{em} and T_{cm}, but we will continue to refer to them as a bulk MP population for simplicity. At day 30, there were roughly equivalent proportions and absolute numbers of TEs, KLRG1$^+$ MPs, and MPs, but by day 60 we observed a clear dominance of the MP population. MPs began to constitute >50% of the total GP33$^+$ population, while their numbers still remained roughly constant. TEs and KLRG1$^+$ MPs continued to contract by absolute number—by ~10-fold and ~2-fold respectively. From day 60 to 1 year post-infection, these trends continued but at a slower rate. At 1 year, MPs (now largely T_{cm}) reached >80% of the total GP33$^+$ CD8 T cell population, while TEs had completely disappeared. Interestingly, KLRG1$^+$ MPs still constituted ~10-15% of the population and, by absolute number, were present at ~5-fold lower levels than MPs. Altogether, following acute infection, TEs underwent a rapid period of contraction, by both number and frequency of total GP33$^+$ CD8 T cells, while KLRG1$^+$ MPs underwent a slower, more gradual contraction. MPs remained constant in numbers, achieving dominance in their proportion by 60 days post-infection. Their proportion among total GP33$^+$ CD8 T cells continued to rise as time went on and the other

populations diminished. These trends in the differentiation of memory GP33^{+} CD8 T cells were also observed for GP276^{+} and NP396^{+} CD8 T cells (**Fig. 1e** and **f**).

We next conducted a more in-depth analysis of IL-7Rα and KLRG1 expression within MPs, KLRG1^{+} MPs, TEs, and DNs (**Fig. 2**). Of course, IL-7Rα was expressed at highest levels within MPs, followed by KLRG1^{+} MPs, TEs, and DNs. Notably, as early as day 15 post-infection, MPs expressed higher levels of IL-7Rα than even naïve cells. On the other hand, KLRG1 was always expressed most highly on TEs. Much like IL-7Rα, expression of CD62L was highest on MPs, but exhibited bimodal distribution between days 30 and 60 post-infection. This presumably corresponded to the emergence of a heterogenous population of T_{em} and T_{cm} by day 30, and the eventual dominance of T_{cm} by 1 year post-infection.

We also evaluated the expression of other memory markers. TCF-1 signaling has been shown to promote the generation of long-lived memory CD8 T cells and enable recall potential (108, 175). In accordance, we found that TCF-1 levels were consistently highest in MPs and lowest in TEs. TCF-1 levels in MPs were consistently equivalent to those of naïve CD8 T cells.

We also investigated the expression of two chemokine receptors: CXCR3 and CX3CR1. We found that naïve CD8 T cells did not express CXCR3, while it was upregulated on day 8 in all four subsets and most highly within MPs. Following this, expression remained consistently highest among MPs, followed by KLRG1^{+} MPs and TEs. These findings are consistent with prior studies, which suggest that CXCR3 may directly impact memory formation as it controls the positioning of CD8 T cells relative to antigen in the spleen (93, 117, 180). Our studies also suggest that CX3CR1 is associated with a more effector-like phenotype. From day 8 onwards, CX3CR1 was expressed most highly on TEs, followed by KLRG1^{+} MPs, while MPs express much lower levels, and naïve cells were uniformly CX3CR1^{-}.

Finally, we examined the expression of two classic "exhaustion markers." Surprisingly, we found that both Tim-3 and PD-1 were expressed by some memory subsets early after acute infection. On day 8, Tim-3 was expressed most highly in the DN population, followed by TEs, KLRG1$^+$ MPs, and MPs. On the other hand, PD-1 was expressed most highly in the KLRG1$^-$ populations (DNs and MPs), followed by KLRG1$^+$ MPs and TEs. This finding is consistent with previous work which suggests that PD-1 also plays an inhibitory role during naïve-to-effector CD8 T cell transitions (103). By day 60, TEs expressed the highest levels of Tim-3, followed by KLRG1$^+$ MPs and MPs, but all populations became Tim-3$^-$ after 1 year. All memory subsets were PD-1$^-$ by day 60 and remained PD-1$^-$ out to 1 year post-infection.

Altogether, we found that IL-7Rα-expressing classical MPs expressed high levels of CD62L, TCF-1, and CXCR3, while KLRG1-expressing classical TEs expressed high levels of CX3CR1. KLRG1$^+$ MPs appeared to express intermediate levels of all the markers. Only early after acute infection were MPs expressing PD-1 and TEs expressing Tim-3.

CD28 expression correlates with a memory phenotype

We next analyzed CD28 expression. We found that CD28 was uniformly upregulated in all GP33$^+$ CD8 T cells by day 8—and to levels higher than even naïve CD8 T cells (**Fig. 3a**). Following day 8, all GP33$^+$ CD8 T cells continued to express higher levels of CD28 than naïve cells, but CD28 was clearly expressed most highly on MPs, followed by KLRG1$^+$ MPs and TEs. We next wondered whether CD28 expression specifically correlated with the expression of other memory-associated markers. Indeed, we found that CD28 could distinguish a classical MP phenotype (**Fig. 3b**). CD62L, TCF-1, and CXCR3 were all expressed at consistently higher levels within a distinct CD28hi population, while CX3CR1 was expressed at higher levels within a

distinct CD28lo population. These findings were highly significant at multiple timepoints from 8 days to 1 year post-infection (**Fig. 3c**).

Transcriptional profiling of three KLRG1/IL-7Rα subsets following acute infection

Having examined the surface-level phenotypes of MPs, KLRG1$^+$ MPs, and TEs, we next sought to gain more insight into their fates and functions through transcriptomic analyses. We performed RNA-seq on the three sorted populations (among GP33$^+$ CD8 T cells) on day 50 post-infection (**Fig. 4a**). We also sorted CD44^{lo}CD62L^{hi} CD8 T cells from naïve mice to analyze as controls.

We first performed principal component analysis (PCA) to broadly compare the three subsets and naïve cells (**Fig. 4b**). Two principal components were identified that were responsible for 91% of variance in gene expression among the samples. The first principal component (PC1) explained 74% of the variance and showed that the three subsets were much more similar to each other than to naïve cells. On the other hand, PC2 explained 17% of the total variance and revealed that the three subsets were also distinct from one another.

Naïve CD8 T cells expressed the highest levels of *Lef1*, *Id3*, *Ccr7*, and *Sell* (**Fig. 4c**). Following LCMV infection, MPs and KLRG1$^+$ MPs were distinct but expressed many markers in parallel, while TEs expressed more subset-specific genes. MPs and KLRG1$^+$ MPs both expressed higher levels of *Il7r*, *Bcl2*, and *Eomes* as compared to naïve, as well as higher levels of some proliferation-associated proteins (*Syne2*, *Ufl1*, and *Ehd3*) and some effector molecules (*Tnf*, *Traf1*, and *Carmil2*). As for unique genes, MPs had the highest levels of *Cxcr3, Xcl1, Reck, Tnfsf8,* and *Cd28,* while KLRG1$^+$ MPs had the highest levels of *S1pr1, Ccr2, Lilr4b, Entpd1,* and *Il2ra.* The expression profile of TEs was dominated by effector-like genes (*Klrg1, Prf, Gzma, Gzmb, Il18rap,*

and *Ifng*), effector-programming transcription factors (*Zeb2*, *Tbx1*), inhibitory receptors (*Havcr2*), and multiple chemokine and trafficking molecules (*Cx3cr1, Ccl3, Ccl4, Ccl5, Ccl6, Ccl9,* and *S1pr5*). Notably, KLRG1$^+$ MPs also expressed intermediate levels of these genes.

Among antigen-specific CD8 T cells, MPs and TEs had the highest number of differentially expressed genes (DEGs) between them (2,002) (**Fig. 5a**), while KLRG1$^+$ MPs differentially expressed 291 and 1,237 genes as compared to MPs and TEs, respectively (**Fig. 5b** and **c**). Importantly, transcriptional levels of key memory markers (**Fig. 5d**) matched the surface expression profiling in Figures 2 and 3.

Taken together, MPs and TEs were highly transcriptionally distinct—MPs had proliferative and stem-like capacity, while TEs were terminally-differentiated. In contrast, KLRG1$^+$ MPs had a transcriptional profile which was roughly intermediate between those of MPs and TEs.

Longitudinal anatomic location of three KLRG1/IL-7Rα subsets within the spleen

We next sought to investigate how KLRG1 and IL-7Rα expression may be specifically tied to anatomic location and how the location of memory CD8 T cell subsets may ultimately determine their fate. We examined these questions out to 1 year post-infection, specifically within the spleen.

To evaluate localization within the spleen, we performed i.v. injection of fluorescently-conjugated anti-CD8α three minutes prior to euthanasia of the mouse (59) (**Fig 6a**). The injected antibody enters circulation and does not penetrate beyond the vasculature, so this technique enables the discrimination of blood-borne cells and tissue-localized cells (58). As such, CD8 T cells within the PBMC stained nearly 100% i.v.$^+$ (**Fig. 6b**). In the spleen, the RP is highly vascularized, while the WP is not. Instead, the WP is comprised of lymphoid aggregates:

periarteriolar lymphatic sheaths (PALS) surrounded by T cell zones and B cell zones. The RP is thus accessible to the injected antibody and stains largely i.v.$^{+}$, while the WP is not accessible to the antibody and stains largely i.v.$^{-}$ (59). As is well-known, naïve CD44^{lo} CD8 T cells specifically home to T cell zones within the WP and we found that they were, in fact, highly protected from i.v. labeling, staining >70% i.v.$^{-}$ (**Fig. 6c**). Naive CD8 T cells within infected mice also remained embedded at this proportion within the WP, and this population was used to determine the placement of the gates between the RP and WP for all experiments.

On day 8 post-infection, GP33^{+} CD8 T cells were roughly equally distributed throughout the RP and WP of the spleen, with a slight majority in the WP, although there was some variability among the samples (**Fig. 6d** and **e**). By day 15, there was a highly significant preference in localization of the GP33^{+} CD8 T cells to the RP: ~70 to 90% of GP33^{+} CD8 T cells stained i.v.$^{+}$ at this timepoint. At day 30, a similar frequency of GP33^{+} CD8 T cells was observed in the RP. This preference continued until at least day 90, gradually becoming less dramatic with only ~50 to 70% of GP33^{+} CD8 T cells in the RP on days 60 and 90. By 6 months post-infection, GP33^{+} CD8 T cells had undergone complete reorganization. A significant majority (~50-80%) now appeared in the WP. At 1 year post-infection, the GP33^{+} CD8 T cells ultimately lost this WP preference, becoming more widely dispersed between the RP and WP once again, with no significant majority in either compartment. These patterns of localization were consistent among GP276^{+} and NP396^{+} CD8 T cells.

Finally, we investigated the heterogeneity of tetramer^{+} CD8 T cells undergoing these localization programs. We assessed the location of each KLRG1/IL-7Rα subset from 8 days to 1 year post-infection, hypothesizing that IL-7Rα and KLRG1 expression might delineate WP versus RP-associated cells, as has been suggested previously (96). Thus, we examined IL-7Rα and

KLRG1 expression on GP33$^+$ CD8 T cells using i.v.-labeling (**Fig 7a** and **b**). We found that MPs were skewed towards the WP as early as one week post-infection, with a significant majority persisting in the WP over the course of 1 year.

On day 8 post-infection, at the peak of the CD8 T cell response, the majority of GP33$^+$ CD8 T cells were TEs, and these TEs were in the RP in a slight majority. At day 15, MPs and KLRG1$^+$ MPs were increasing in their overall proportion of the GP33$^+$ population. Among GP33$^+$ CD8 T cells in the WP, ~40% of were MPs, while this frequency was halved in the RP. Also at day 15, a slight majority of KLRG1$^+$ MPs were in the RP, and a significant majority of TEs were in the RP. From 30 days to 6 months post-infection, stark differences emerged in the compartmentalization of each memory subset. In the WP, MPs were consistently found at nearly twice the frequency as in the RP. On the other hand, KLRG1$^+$ MPs and TEs were consistently found at nearly twice the frequency in the RP versus the WP. By 1 year post-infection, the majority of GP33$^+$ CD8 T cells were MPs and KLRG1$^+$ MPs, and there was still a modestly higher frequency of MPs in the WP and KLRG1$^+$ MPs in the RP.

IV. Discussion

It is well-established that KLRG1 and IL-7Rα together define the populations of CD8 T cells which persist or die following infection. TEs contract, while MPs survive and seed the long-lived memory pool. During this period of contraction and differentiation, we observed a third KLRG1$^+$ MP population which actually accounted for ~5-40% of memory CD8 T cells at any given time. Our results show that KLRG1$^+$ MPs possess a unique phenotype and functional program. This population has a surface expression profile which is intermediate between that of MPs and TEs, but their transcriptional program suggests they are more similar to MPs than to TEs. In contrast, KLRG1$^+$ MPs appear to localize within the spleen in manner most similar to TEs—

within the RP. We speculate that TEs could actually give rise to KLRG1$^+$ MPs, which may in turn give rise to MPs. That is, a subset of TEs with higher expression of IL-7Rα could selectively survive and seed the KLRG1$^+$ MP pool, and KLRG1$^+$ MPs could subsequently down-regulate KLRG1 to become MPs. It is also possible that KLRG1$^+$ MPs simply die, as do TEs, and the MP population dominates by default.

Our results show that CD28 is expressed by long-lived memory CD8 T cells out to 1 year post-acute infection. This finding is consistent with others' studies in both mice and humans (37, 44, 187–190). We found that CD28 expression correlated with the expression of other memory-associated markers, including IL-7Rα, CD62L, TCF-1 and CXCR3, and inversely correlated with the expression of effector-associated markers, including KLRG1 and CX3CR1.

We also investigated the patterns of memory CD8 T cell localization following clearance of an acute viral infection. We examined their location within the spleen using i.v. labeling and characterized their location-specific phenotypes; these findings are summarized in **Fig. 8**. We found that bulk LCMV-specific CD8 T cells, although equally distributed on day 8, displayed a "preference" for the RP until day 90. We posit that this i.v.$^+$ population is actually comprised of memory CD8 T cells (T_{em} and T_{cm}) which are in the midst of their canonical circulation, between the vasculature and secondary lymphoid organs.

As early as one week post infection, we observed preferential localization of MPs to the WP and TEs/KLRG1$^+$ MPs to the RP. This is consistent with previous studies from Jung et al. and Seo et al. (96, 97). But we continued our investigation significantly longer than in these studies—out to 1 year post-infection—because we sought to track the precise longitudinal relationship between memory phenotype and location. Remarkably, the anatomic preferences established on day 8 post-infection held steady for ~1 year following infection. This suggests that there are

specific signals which regulate early localization following infection and that early homing may be crucial in driving the long-lived memory program. In particular, positioning within the T cell zones of the WP may regulate exposure to antigen as well as co-stimulatory signaling. Of course, it will also be necessary to determine whether these localization kinetics change in different contexts of acute infection, such as after respiratory, enteric, or epidermal infection.

Together, these data reexamine the relationship between memory CD8 T cell phenotype and location. We have uncovered novel characteristics of memory CD8 T cell subsets, and we have comprehensively tracked their localization within the spleen over an extended period of time. Our findings suggest that memory CD8 T cell function may be inextricably tied to their location. Designing vaccines with highly effective memory responses may require more thorough consideration of the phenotype of memory CD8 T cells elicited and how these cells traffic within the spleen.

V. Materials and Methods

Mice and viruses. All animal experiments were performed in accordance with Emory University Institutional Animal Care and Use Committee. C57BL/6J female mice were purchased from Jackson Laboratory. Mice were infected with the LCMV Armstrong strain (2×10^5 pfu, intraperitoneally [i.p.]).

Cell isolation. Once isolated from mice, spleens were smashed through 70μm nylon cell strainers to remove clumps. Cells were spun down at 2,000 RPM for 10 minutes, and the supernatant was removed. After resuspending the pellet, cells were incubated at room temperature with 2 ml of Ack lysis buffer for 2 minutes in order to lyse the RBCs. After incubation, an additional 35 ml of RPMI + 5% fetal bovine serum (FBS) was added to dilute the Ack lysis buffer, and the cells were

spun down at 2,000 RPM for 10 minutes. The resulting cell pellet was resuspended in phosphate-buffered saline (PBS) + 2% FBS + 0.5mM EDTA and cells were transferred to a 96-well round-bottom plate for staining.

Intravascular labeling. Intravascular labeling was performed as previously described (59). Anti-CD8α conjugated to PE or Alexa Fluor 647 was prepared for injection (3µg of antibody in 300 µl of PBS) and 300µl of the antibody dilution was injected i.v. into each mouse via the tail vein. After three minutes, mice were bled via heparinized capillary tubes and then sacrificed using isoflurane. Spleens were collected in RPMI + 5% FBS and immediately smashed through 70µm nylon cell strainers to remove clumps.

Flow cytometry. Surface staining was performed by incubating cells with fluorochrome-conjugated antibodies against CD8, CD4, CD19, PD-1, CD44, IL-7Rα, KLRG1, CD62L, CD28, CXCR3, and CX3CR1 (BD Bioscience, eBioscience, and Biolegend). Cells were incubated on ice for 30 minutes in PBS + 2% FBS + 0.5mM EDTA. The transcription factor TCF-1 was stained intracellularly with the eBioscience Foxp3/Transcription Factor Fixation/Permeabilization Kit (Thermofisher). For detecting LCMV-specific CD8 T cell responses, peptides bound to major histocompatibility complex (pMHC) tetramers were prepared against LCMV-GP33, LCMV-GP276, and LCMV-NP396 proteins, as described previously (12, 191). Cell viability was determined with the Live/Dead fixable aqua or near IR dead cell stain kit (Invitrogen). Samples were acquired on an LSR II or Symphony flow cytometer (BD Biosciences) and data were analyzed with FlowJo software (TreeStar).

Bulk RNA-sequencing and analysis. Samples were stained with extracellular antibodies for 30 minutes, washed with PBS + 2% FBS and sorted on a FACSAria II (BD Biosciences). Three populations of GP33^{+} CD8 T cells were sorted in triplicate: IL-7Rα^{+}KLRG1^{-}, IL-7Rα^{+}KLRG1^{+}, and IL-7Rα^{-}KLRG1^{+}. RNA was then isolated from each sample using the All-Prep DNA/RNA Micro Kit (Qiagen) and then submitted to the Emory Yerkes Nonhuman Primate Genomics Core. Reads from RNA-seq were aligned to the mm10 genome [accessed through Ensembl (192)] with STAR version 2.7. A cut-off of >3,000 counts per gene was applied to all samples.

Statistical analysis. All experiments were analyzed using Prism 9 (GraphPad Software). Statistical differences were assessed using paired two-tailed t tests or two-way ANOVA with Sidak's test for multiple comparisons. All summary plots indicate means ± standard error of the mean (SEM). In all cases *, $P \leq 0.05$; **, $P \leq 0.01$; ***, $P \leq 0.001$; ****, $P \leq 0.0001$. The number of mice analyzed at each timepoint ranged from 3 to 22. The sample size for individual experiments is denoted in the figure legend.

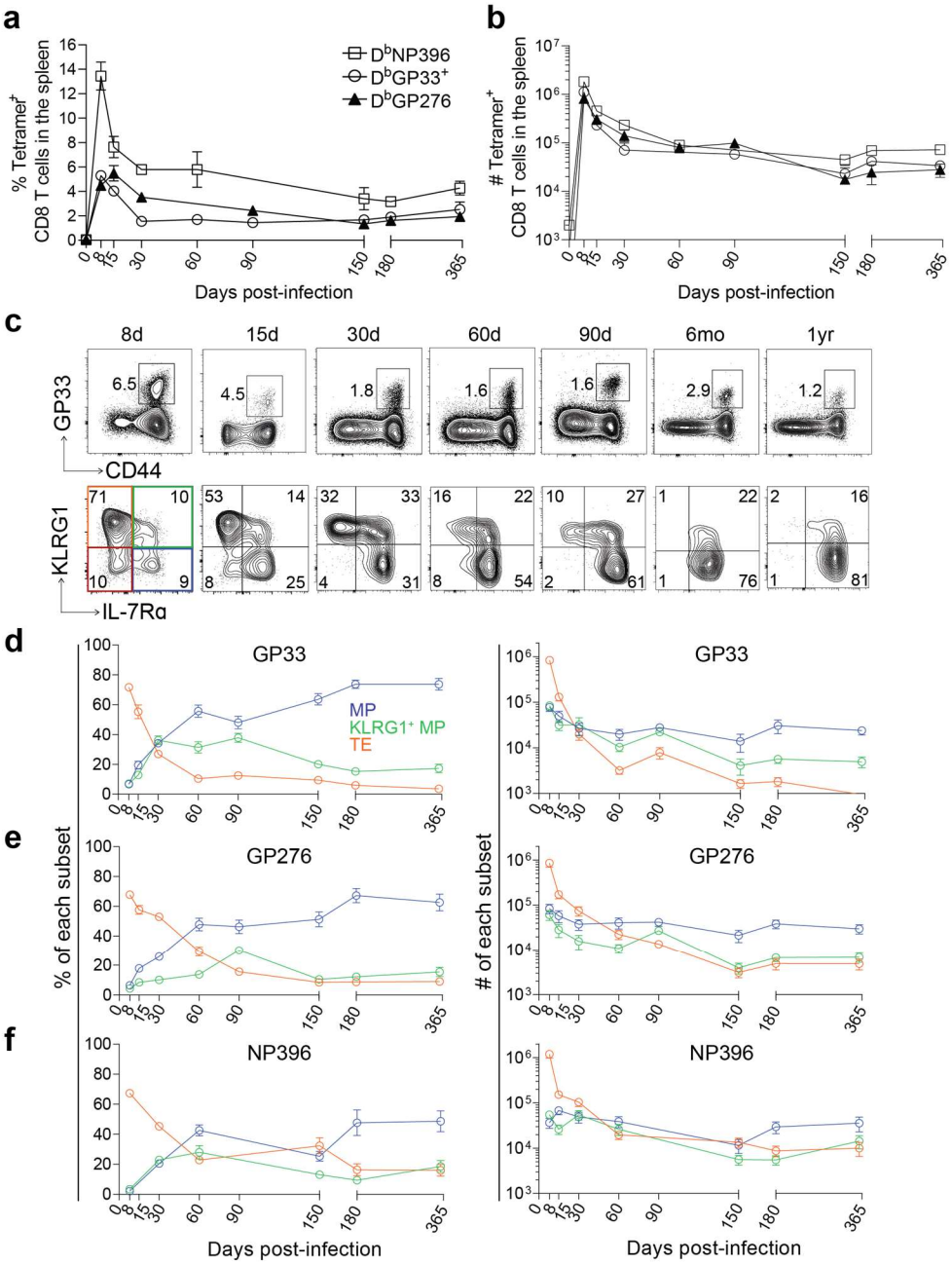

Figure 1. Characterization of LCMV-specific memory CD8 T cell subsets after acute infection. (**a**) Frequency and absolute number (**b**) of tetramer$^+$ CD8 T cells in the spleen after LCMV Armstrong infection of B6 mice (2×10^5 pfu, i.p.). D^{b}GP33-, D^{b}GP276-, and D^{b}NP396-specific responses are shown; Mean ± SEM. (**c**) Representative flow plots showing frequency of GP33$^+$ CD8 T cells and the expression of KLRG1 and IL-7Rα within them from 8 days to 1 year post-infection. (**d-f**) Summary of the frequency and absolute number of the indicated sub-populations within GP33$^+$, GP276$^+$ or NP396$^+$ CD8 T cells. IL-7Rα$^+$KLRG1$^-$ memory precursors (MPs, blue), IL-7Rα$^+$KLRG1$^+$ cells (KLRG1$^+$ MPs, green), IL-7Rα$^-$KLRG1$^+$ terminal effectors (TEs, orange), IL-7Rα$^-$KLRG1$^-$ double negative cells (DNs, red). Shown are the mean and standard error of the mean (SEM); n=5-12 mice per timepoint.

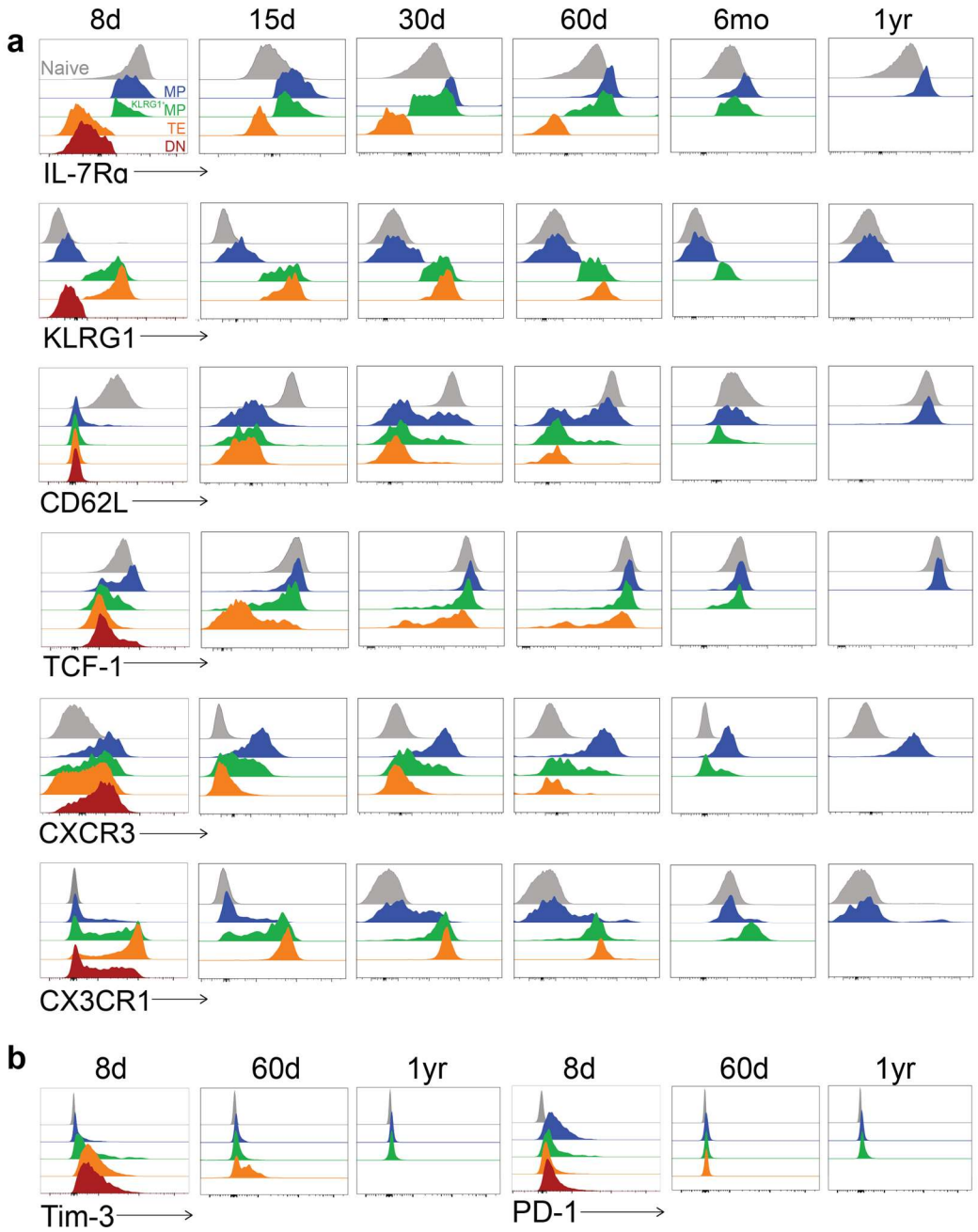

Figure 2. Phenotypic profile of KLRG1/IL-7Rα subsets among GP33^{+} CD8 T cells after acute infection. (**a**) Flow cytometry staining of memory markers within each of the four indicated subsets from 8 days to 1 year post-infection. All subsets are gated on GP33^{+} CD8 T cells. Naïve CD44^{lo} CD8 T cells are shown as gray histograms at the top of each plot. The DN subset quickly diminished after infection and so is not shown after day 8; the TE and KLRG1^{+} MP subsets also diminished after day 60 and so are not shown after that timepoint. Representative flow plots are shown; n=5-12 mice per timepoint. (**b**) Flow cytometry staining of exhaustion markers within each of the four indicated subsets as in (a). Representative flow plots are shown; n=3-8 mice per timepoint.

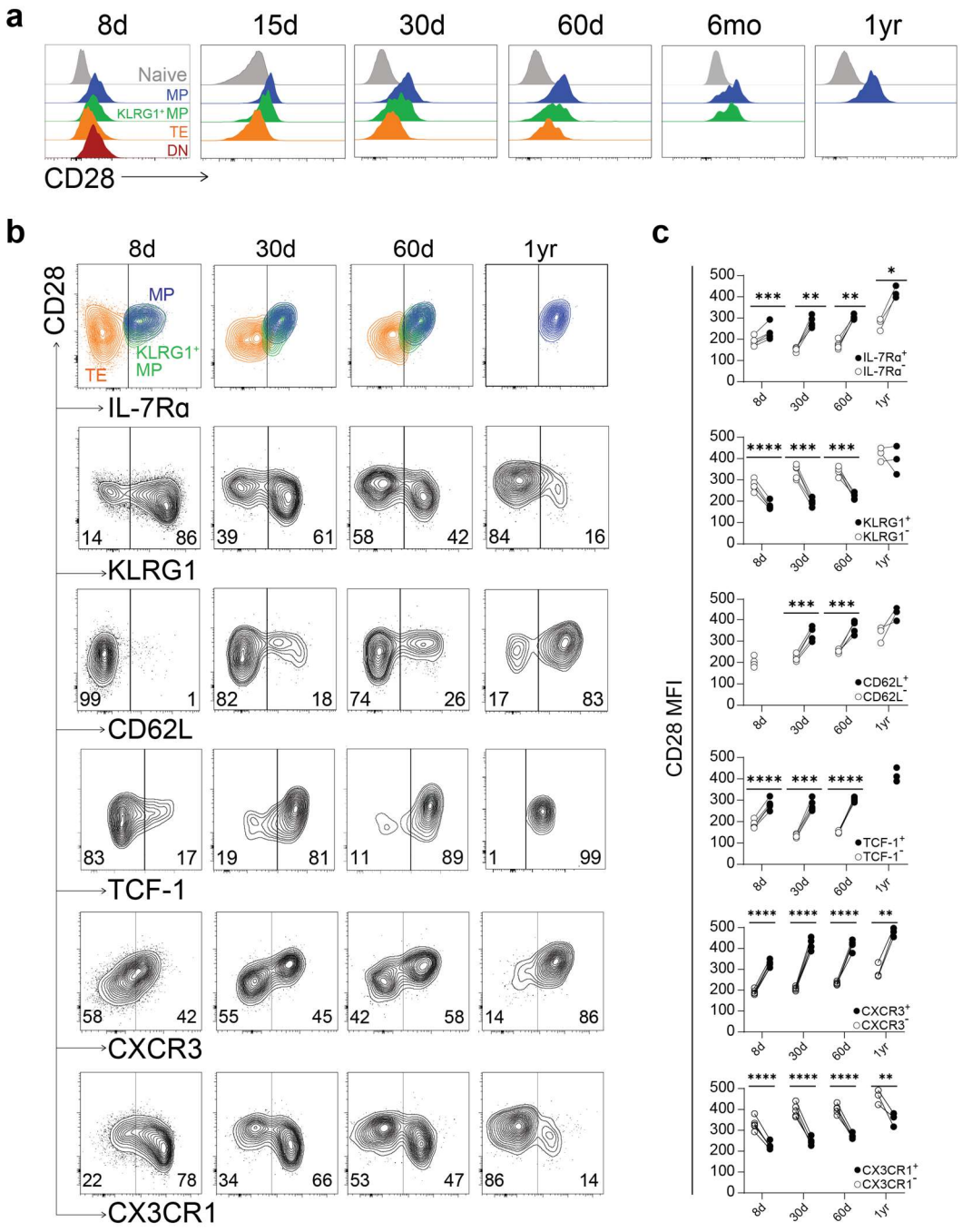

Figure 3. CD28 expression correlates with a memory phenotype. (**a**) Flow cytometry staining of CD28 within each of the four indicated subsets from 8 days to 1 year post-infection. All subsets are gated on GP33^{+} CD8 T cells. Naïve CD44^{lo} CD8 T cells are shown as gray histograms at the top of each plot. (**b**) Representative flow plots showing co-expression of IL-7Rα, KLRG1, CD62L, TCF-1, CXCR3, and CX3CR1 with CD28 on GP33^{+} CD8 T cells. (**c**) Quantification of CD28 MFI from (b) among marker^{+} and marker^{-} GP33^{+} CD8 T cells. Values are from one representative experiment with 3-4 mice per timepoint. *, $P \leq 0.05$; **, $P \leq 0.01$; ***, $P \leq 0.001$; ****, $P \leq 0.0001$ (all determined using paired two-tailed t tests).

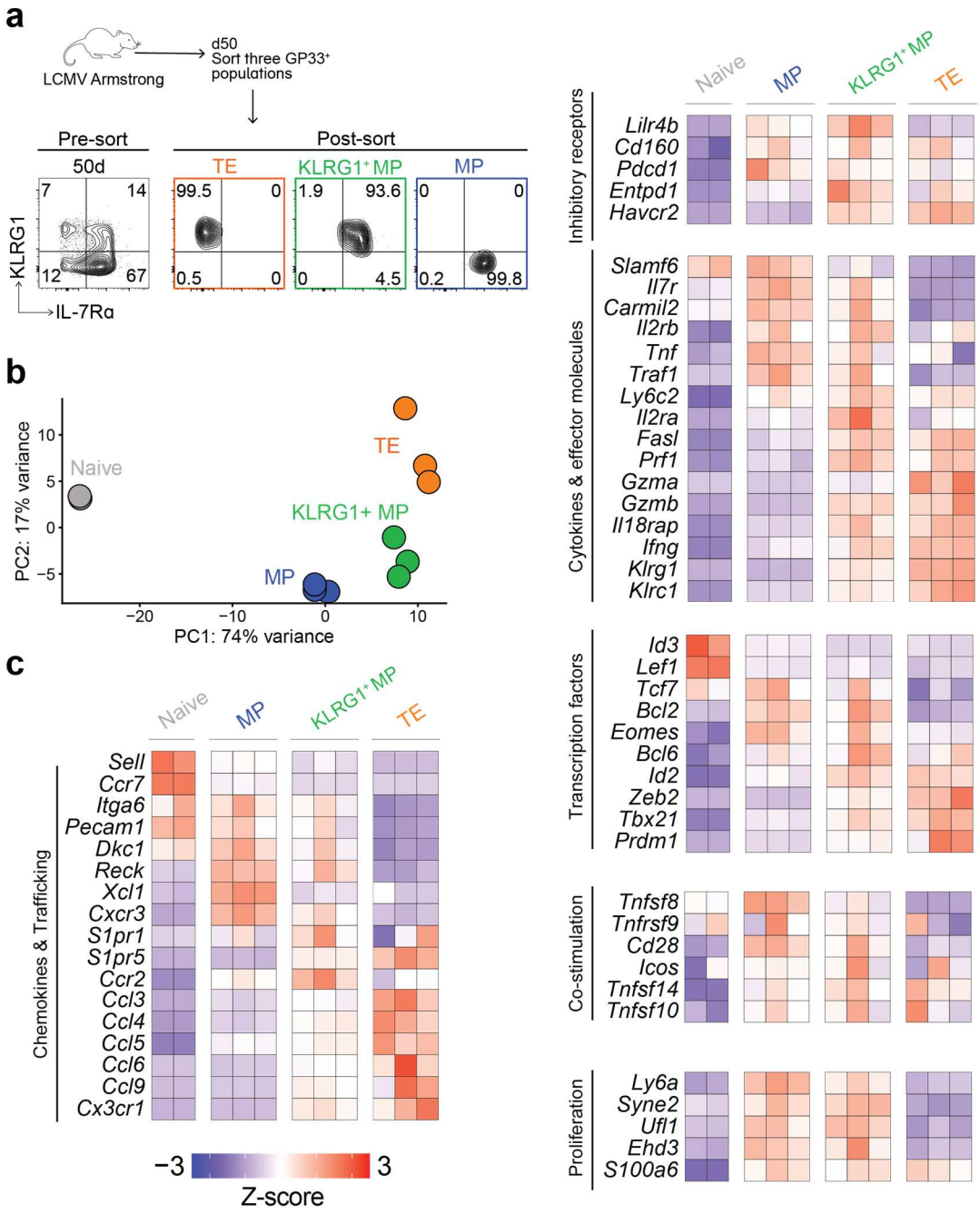

Figure 4. Transcriptional profile of three KLRG1/IL-7Rα CD8 T cell subsets after acute infection. (**a**) RNA was isolated from three sorted subsets (MPs, KLRG1$^+$ MPs, and TEs) and submitted for RNA-seq. Representative flow plots showing purity (>93%) of the three subsets before and after sorting. Each subset was sorted from bulk GP33$^+$ CD8 T cells at day 50 post-infection. Three sets of three mice were pooled, and then the three subsets were isolated from each pooled sample. (**b**) Principal component analysis (PCA) identified two principal components that explained 91% of variance between the samples. Each sample is plotted on these two components. (**c**) Heatmap showing Z-scores of top DEGs and other genes of interest across the three memory subsets.

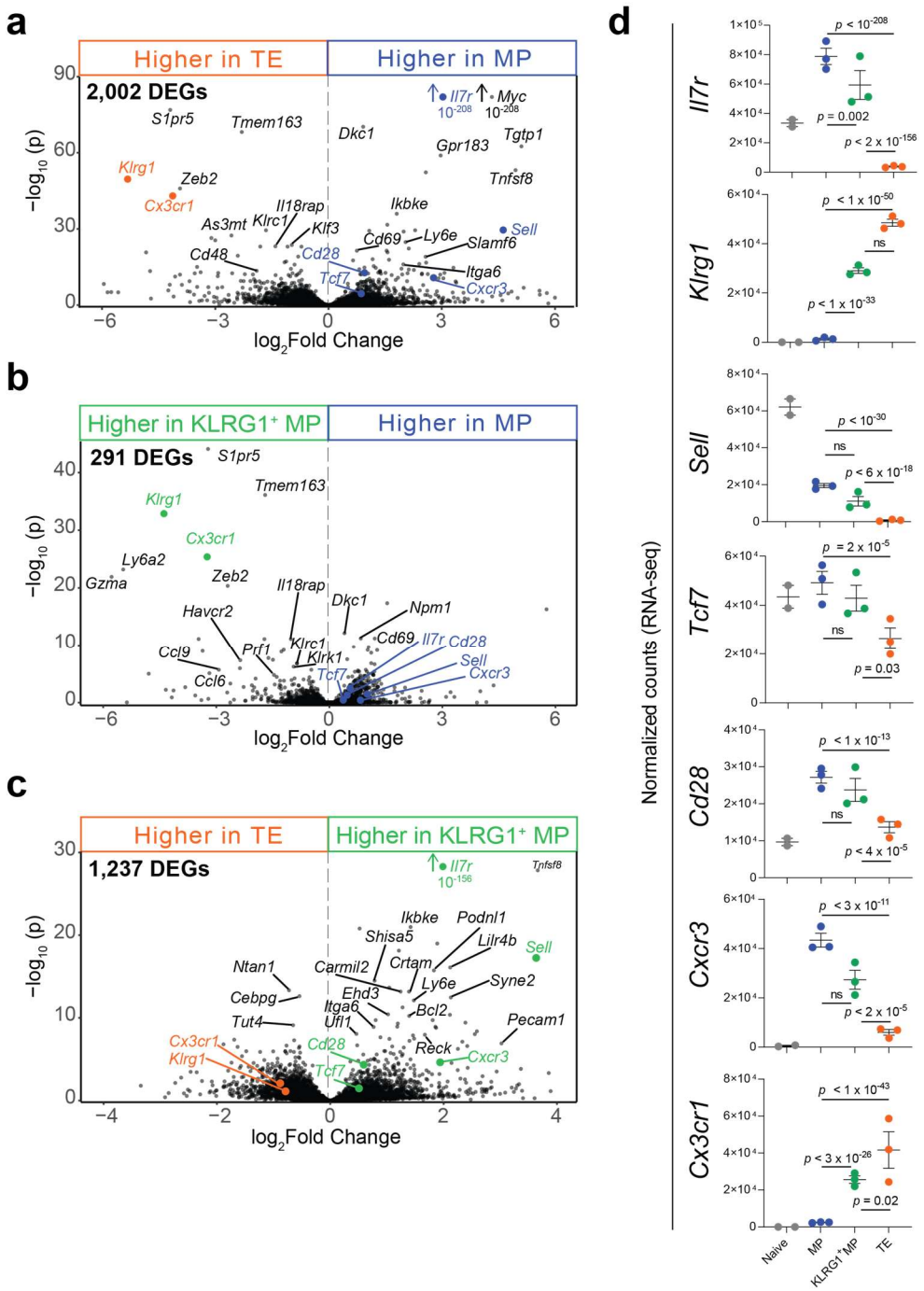

Figure 5. Expression of key memory markers among three KLRG1/IL-7Rα CD8 T cell subsets after acute infection. RNA was isolated from MPs, KLRG1$^+$ MPs, and TEs (among GP33$^+$ CD8 T cells) and submitted for RNA-seq, as in Figure 4. (**a-c**) Volcano plots showing DEGs between each of the three memory subsets ($p < 0.05$ was used as a cut-off). Compared subsets are shown at the top of each plot. Numbers of DEGs are shown in the top left corner of each plot. (**d**) Normalized counts of key memory markers (p values are from Wald's test, performed by "DESeq2" in R).

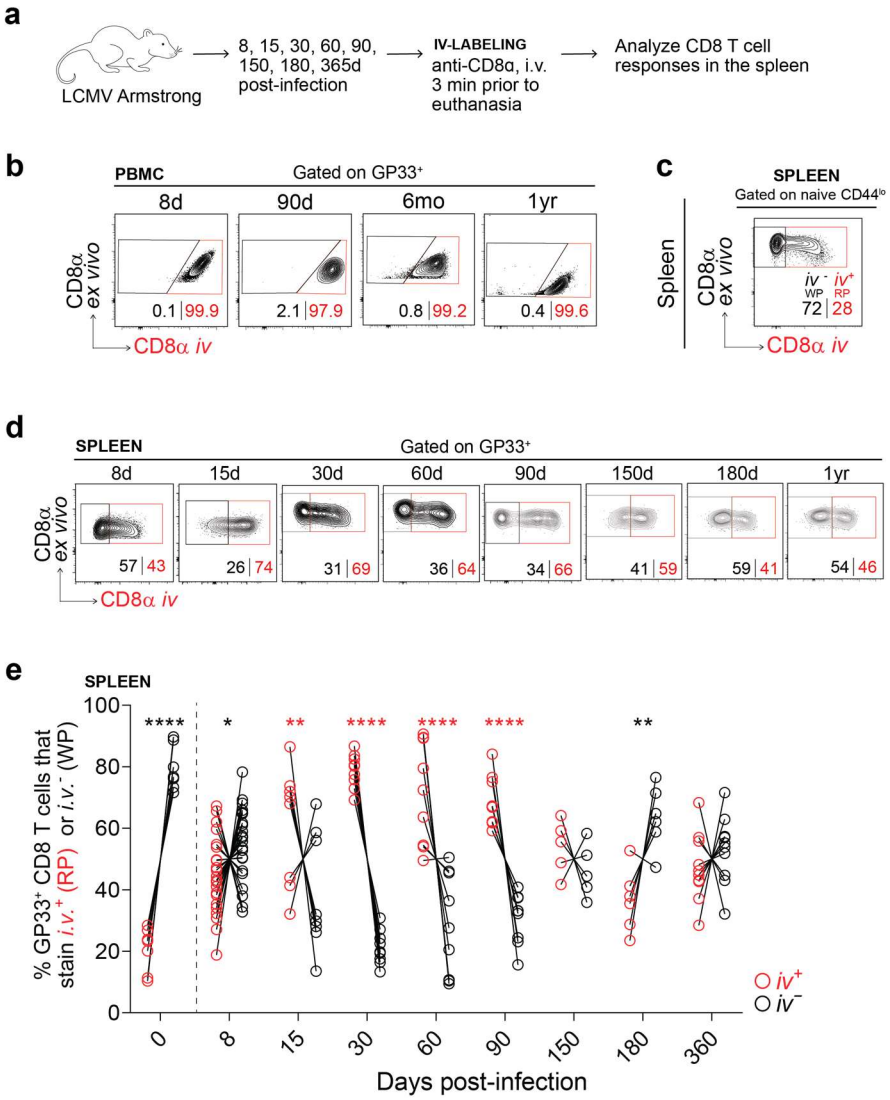

Figure 6. IV-labeling reveals the location of GP33$^+$ CD8 T cells in the spleen after acute infection. Experimental scheme. IV labeling was performed as previously described (59). Mice were infected with 2×10^5 pfu of LCMV Armstrong and sacrificed at multiple timepoints from 8 days to 1 year post-infection. Three minutes prior to sacrifice, mice received 3µg i.v. of anti-CD8α conjugated to a fluorophore, which labeled all CD8 T cells in circulation and in the splenic RP. CD8 T cells in the tissues and the splenic WP were inaccessible. (**b**) GP33$^+$ CD8 T cells within the PBMC, gated on i.v.-labeling. If >95% of PBMCs were i.v.$^+$, i.v. labeling was considered to be successful. (**c**) Naïve CD44^{lo} CD8 T cells within the spleen, gated on i.v.-labeling. CD8 T cells were presumed to be in the RP if they stained i.v.$^+$, or in the WP if they stained i.v.$^-$. Naïve CD44^{lo} CD8 T cells were always used to establish the gates between i.v.$^+$ and i.v.$^-$ tetramer$^+$ CD8 T cells in the spleen. (**d-e**) Analysis of the location of GP33$^+$ CD8 T cells in the spleen from 8 days to 1 year post-infection: representative flow plots (d) and summary plot (e) of the frequency of GP33$^+$ CD8 T cells within the RP or WP. Individual mice are shown; n=5-22 per timepoint. *, $P \leq 0.05$; **, $P \leq 0.01$; ***, $P \leq 0.001$; ****, $P \leq 0.0001$ (all determined using two-way ANOVA with Sidak's test for multiple comparisons).

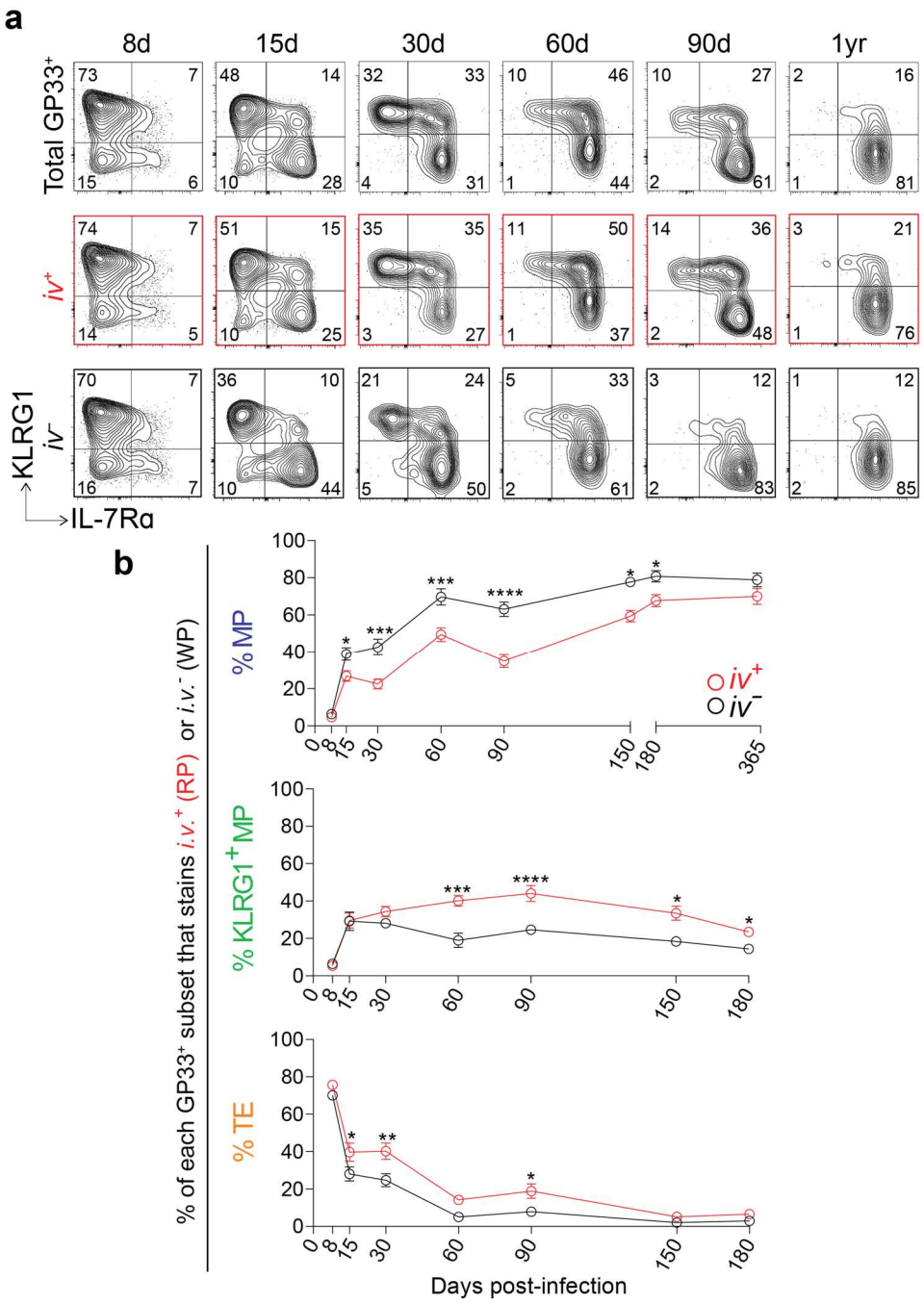

Figure 7. MPs localize to the splenic white pulp as early as one to two weeks after acute infection. (**a**) Representative flow plots showing KLRG1 and IL-7Rα expression on total GP33$^+$ CD8 T cells in the spleen (top row). Below, GP33$^+$ CD8 T cells are further gated by i.v. labeling, either i.v.$^+$ (RP) (middle row) or i.v.$^-$ (WP) (bottom row). Expression of KLRG1 and IL-7Rα within these populations is shown. (**b**) Summary of the frequency of each memory subset within GP33$^+$ CD8 T cells in the RP or WP. Shown are the mean and standard error of the mean (SEM); n=5-9 mice per timepoint. *, $P \leq 0.05$; **, $P \leq 0.01$; ***, $P \leq 0.001$; ****, $P \leq 0.0001$ (all determined using two-way ANOVA with Sidak's test for multiple comparisons).

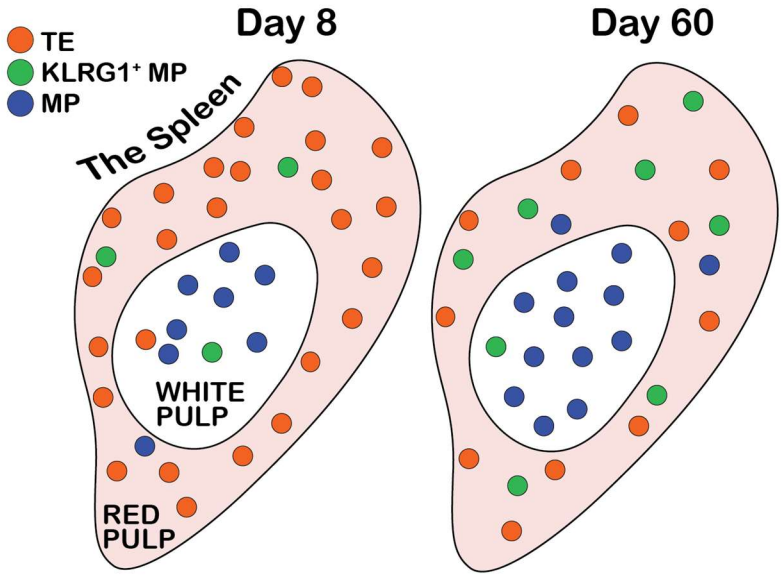

Figure 8. Summary of the anatomical distribution of memory CD8 T cell subsets over time. On day 8 following acute infection, the majority of antigen-specific CD8 T cells are TEs and these are primarily localized within the RP. Following this, TEs begin to contract, while KLRG1$^+$ MPs and MPs increase in their proportion. MPs quickly dominate within the WP—as early as 1-2 weeks following infection. KLRG1$^+$ MPs also become enriched within the RP. By day 60, the majority of antigen-specific CD8 T cells are MPs and these are primarily localized within the WP. TEs and KLRG1$^+$ MPs are significantly enriched within the RP.

Chapter 3: Early fate decisions and the generation of early memory precursor CD8 T cells

Gill AL, Hudson WH, Ahn E, McGuire DJ, Wieland A, Valanparambil RM, and Ahmed R. (2023). Early fate decisions and the generation of early memory precursor CD8 T cells. *Nature Immunology*. **(**In preparation).

I. Summary

As part of the acute antiviral response, CD8 T cells undergo robust proliferation and differentiation, producing heterogeneous progeny that coordinate viral clearance and seed long-lasting memory. The earliest fate decisions following initial activation of CD8 T cells remain poorly understood. Here, we utilized multiple high throughput sequencing analyses, including bulk and single cell RNA-sequencing, to examine the earliest programming of CD8 T cells in the first few days after infection. Our analyses revealed previously unknown heterogeneity in the early pool of antigen-specific CD8 T cells. At least two distinct populations of cells were identified just 1 day post-infection—one population that was more effector-like, and one that appeared to have a memory precursor "precursor" phenotype. Furthermore, we demonstrated that this heterogeneity could be elicited following infection of a purified pool of naïve precursors with a uniformly CD44loCXCR3lo phenotype. This indicated that naïve CD8 T cells may have the intrinsic capacity to divide and give rise to functionally distinct progeny. Together, these findings may help in the development of novel strategies to optimize CD8 T cell responses following infection, vaccination, and cancer.

II. Introduction

During acute viral infection, antigen-specific CD8 T cells proliferate and give rise to effector cells that clear the virus. The effector pool is heterogeneous and a small subset persists following infection, differentiating into memory cells, which provide protection against secondary

infection for the lifetime of the organism. Much effort has gone into understanding the basis of long-lived memory CD8 T cells—how effector cells dedifferentiate and gain memory features, which factors determine the quality of a memory response, and what phenotypical characteristics define highly functional memory cells. Early differentiation of memory CD8 T cells, however, remains largely unexplored. This is in part due to the inherent difficulties of visualizing antigen-specific CD8 T cells so early in the response (prior to their massive proliferation), without disturbing the antigen load and viral kinetics. In particular, we do not understand which early decisions determine the fate of an activated, antigen-specific CD8 T cell—especially during its first few divisions. Clarifying these early fate decisions will enable us to predict and shape better memory responses, by modifying vaccines or therapeutic interventions to target specific mechanisms that induce higher quality, longer-lived memory cells.

Several recent studies have emerged, examining early CD8 T cell differentiation in a P14 transfer model of LCMV Armstrong infection (109). These studies use high-throughput single cell and transcriptomic analyses to make sense of the enormously complex and dynamic changes in gene expression during this time. These include analyses of CD8 T cells isolated after 1 division (on the basis of CFSE or CTV tracking dyes), as well as days 4, and 7 post-infection (110, 111, 193). Results of these studies have shown that some degree of heterogeneity exists in the activated CD8 T cell pool as early as the first division following activation. But the timepoints lack continuity and the infection models are sometimes non-physiological.

Here, we sought to establish a comprehensive analysis of early CD8 T cell activation and differentiation following acute LCMV infection in order to better understand the generation of long-lived memory CD8 T cells. We generated P14 chimeric mice and analyzed the phenotype and transcriptional profiles of P14 CD8 T cells on days 1, 2, 3, and 8 post-infection, as well without

infection. We performed flow cytometry on splenocytes, as well as both single cell and bulk RNA-seq analysis on sorted P14 CD8 T cells from all samples. Our results demonstrate considerable heterogeneity in the P14 cells at each day post-infection. Importantly, two clusters of cells were identified on day 1 post-infection, one of which resembled a memory precursor (MP)-like phenotype and clustered more closely to the naïve group. These cells expressed higher levels naïve-associated genes (*Sell, Tcf7,* and *Il7r*) and lower levels of activation and co-stimulatory receptors (*Il2ra, Cd200, Tnfrsf9,* and *Tnfrsf4*). On day 8, MP and terminal effector (TE) clusters were also readily apparent. Moreover, we validated our transcriptomic analyses with surface protein and CITE-seq analyses. Finally, we show that the heterogeneity observed on day 1 post-infection arises independently of any heterogeneity innately present within the naïve donor population of P14 cells. This suggests that differentiation following activation is truly a dynamic and multifaceted process that requires continued investigation.

III. Results

Elucidation of the long-lived memory CD8 T cell phenotype has enabled us to understand some of the key features of highly-functional memory. The phenotype of memory CD8 T cells can vary and evolves over time, but a number of key markers have been shown to endow crucial memory functions, these include, TCF-1, CD62L, CD28, and CXCR3 (**Fig. 1**). All of these markers become enriched in the $GP33^{+}$ CD8 T cell population that survives out to 1 year post-Armstrong infection. On the contrary, CX3CR1 is associated with a more effector-like phenotype and CX3CR1 expression in the memory population appears to diminish over time. Understanding the phenotype and survival mechanisms of memory CD8 T cells means that we can also evaluate these features earlier on in infection, as possible predictors of long-lived memory fate.

We investigated questions surrounding early differentiation of CD8 T cells using a P14 chimeric system, followed by LCMV Armstrong infection (**Fig. 2A**). Transgenic P14 mice have a clonal, $GP33^+$ CD8 T cell repertoire and CD8 T cells from these mice were transferred into B6 mice prior to infection in order to increase their $GP33^+$ precursor frequency. Prior to transfer, P14 cells were also labeled with CTV tracking dye in order to enable visualization of discrete populations of divided cells. P14 chimeric mice were then infected with high-dose LCMV Armstrong (2x10^6 pfu, i.v.) and P14 ($GP33^+$) CD8 T cells were analyzed on days 1, 2, 3, and 8 using a congenic marker. We also analyzed P14 cells from mice that were uninfected as a control. Flow cytometry analyses showed rapid changes in the surface expression of many proteins following infection—even prior to the first division (**Fig. 2B-D**). CD62L expression was lost before the first division, at day 1, and cells remained $CD62L^-$ from then on (**Fig. 2B**). Ki67 was upregulated by day 2 and remained upregulated from then on. CD69 and Granzyme B were highly upregulated before the first division, while CD25 and PD-1 did not reach peak expression until day 2. Importantly, on day 1 post-infection, there was heterogeneous expression of CD25 and PD-1 within the P14 population. Most importantly, we examined the kinetics of TCF-1 expression in our model system, as mounting evidence supports the crucial role of TCF-1 in driving memory fate. Naïve P14 cells were uniformly $TCF\text{-}1^+$, as expected (**Fig. 2C**). However, at 1 day post-infection and before division, we observed heterogeneous down-regulation of TCF-1—about half of the population lost TCF-1 expression, but the other half retained it. A clear $TCF\text{-}1^+$ population was maintained through day 3. Importantly, TCF-1 was co-expressed with CD69 and CD25 in a subset of P14 cells on days 1 and 2, and co-expressed with CD62L, PD-1, Granzyme B, and Ki67 on days 1 through 3 (**Fig. 2D**). This suggested that memory precursor CD8 T cells may undergo

transient, early activation, and that the TCF-1-associated memory program may be highly dynamic at this early phase of the response.

Next, we pooled this flow cytometry data and performed hierarchical clustering analysis using the FlowSOM algorithm. From this analysis, we obtained a UMAP projection and identified multiple clusters within days 1, 2, and 3 post-infection (**Fig. 3A**). First, there was a clear relationship between the CTV signal intensity and the number of divided cells, with naïve and day 1 samples showing the highest intensity followed by day 2, day 3, and day 8. As shown in Figure 2, TCF-1 was expressed heterogeneously at each timepoint (**Fig. 3B**). Clusters with higher TCF-1 expression were all situated in closer proximity to the naïve population. These TCF-1hi clusters also had higher levels of CD127 (IL-7Ra), CD62L, and CXCR3, and lower levels of CD69, CD25, and CX3CR1.

Bulk RNA-seq analysis of sorted P14 CD8 T cells from days 1, 2, 3, and 8 post-infection reflected the trends observed in flow cytometry. Primarily, this bulk analysis enabled us to obtain a more general sense of the transcriptional relationship between the timepoints. We found substantial differences in the transcriptional programming of P14 cells at each timepoint (**Fig. 4A**). Principal component analysis (PCA) identified two principal components that explained 76% of the variance between the samples, and each set of samples clustered distinctly along PC1. Transcriptional kinetics of key genes aligned closely with the surface expression data (**Fig. 4B-C**). Notably, levels of *Tcf7* dropped substantially following infection but following this, transcription remained steady. Overall, the gene expression program in naïve P14 cells was characterized by high expression of *Ccr7, Sell, Il7r*, *Bcl6* and, of course, *Tcf7*. On day 1, *Xcl1* and *Cxcl10* were upregulated, and surprisingly, they were immediately downregulated. On day 2, *Batf3* and *Gzmb* reached their peak expression. *Ctla4* was highly expressed on day 3, but not on any other day.

Finally, classic MP and TE markers were upregulated on day 8, including effector-associated markers like *Klrg1* and *Cx3cr1*.

We next performed a comprehensive analysis of the heterogeneity in gene expression among P14 cells *within* each timepoint. To achieve this, we performed single cell RNA-seq on samples collected in an identical fashion to the bulk analysis. Hierarchical clustering analysis again identified two clusters of cells at each timepoint (except the naïve group) (**Fig. 5A**). These clusters are labeled as A and B for days 1 and 2, and MP and TE for day 8. At the center, there is an additional cluster which is comprised of proliferating cells from days 1, 2, and 3 post-infection. Pseudotime trajectory analysis via Monocle3 illustrated that naïve cells and cells with high levels of TCF-1 expression branched towards more terminally-differentiated subsets (**Fig. 5B**). Naïve-associated genes were immediately downregulated following infection, but they consistently remained higher in one subset of each subsequent timepoint, namely d1B and d2B (**Fig. 5C**). Chemokine and co-stimulatory signals were upregulated on day 1 post-infection, including *Il2, Cd200, Tnfrsf9, Tnfrsf4, Xcl1,* and *Cxcl10* (**Fig. 5D**). All except for *Cxcl10* were expressed more highly in subsets that lacked naïve-associated genes—d1A and d2A. Other genes were upregulated after day 1 and these included *Batf3* (exclusively expressed on day 2), as well as *Mki67, Il2ra, Pdcd1, Havcr2*, and *Ctla4* (**Fig. 5E**). Notably, *Mki67* was localized to the cluster of proliferating cells at the center of the UMAP. Finally, at day 8, MP and TE populations could be clearly distinguished—MPs expressed higher *Cxcr3* for example, while TEs expressed higher levels of *Tbx21, Klrg1, Il18rap, Cx3cr1,* and *Gzma* (**Fig. 5F**). These findings were validated by flow cytometry and by additional single cell RNA-seq that included simultaneous CITE-seq analysis of protein expression (**Fig. 6**). These transcriptomic analyses are summarized in **Figure 7**.

Given the surprising level of heterogeneity observed just 1 day after infection, we next wondered whether there was some degree of pre-existing heterogeneity among CD8 T cells from the P14 mice that might be confounding our results. We evaluated the phenotype of CD8 T cells from a naïve P14 mouse and found that they expressed higher levels of CD44, CXCR3, and Ly6C than WT B6 mice (**Fig. 8A**). Thus, we sorted CD44loCXCR3lo P14 CD8 T cells prior to transfer, and repeated our previous experiment with these "pure naïve" donor cells (**Fig. 8B**). Of course, we also transferred "dirty" unsorted P14 cells, as we had done before, for comparison. We found that, regardless of the donor population, P14 CD8 T cells could differentiate into equivalently heterogeneous populations (**Fig. 8C**). Clustering analysis demonstrated similar clustering and gene expression following a transfer of "dirty" versus "pure naïve" P14 cells (**Fig. 9A** and **B**).

IV. Discussion

Here, we uncover several early features of memory programming through in-depth analysis of flow cytometry and multiple RNA-seq approaches. Altogether, our results suggest that, following activation, antigen-specific CD8 T cells undergo rapid and complex re-programming. Activated CD8 T cells experience changes in gene expression occurring even before the first division, as well as following subsequent divisions.

We have identified several novel genes that may be associated with the early differentiation of memory precursors, given their co-expression with TCF-1. Thus, we propose a more detailed profile of the early pool of memory precursor "precursors." The earliest memory precursors may be marked by sustained expression of *Tcf7, Il7r, Sell, Cxcr3, Cxcl10,* and *Batf3*, as well as very transient expression of effector molecules such as *Gzmb*, *Pdcd1,* and *Il2ra*. The precise functional

role of each of these markers in determining survival and memory fate remains to be determined, however. This could be achieved through the transfer of targeted knock-out P14 cells.

Ultimately, our findings provide insight into some of the gene expression programs and fate decisions that may be required to generate functional memory cells. Uncovering these processes will enable us to quickly predict the long-term course of an immune response. We can use this information to determine vaccine efficacy and to develop novel vaccines with better memory responses.

V. Materials and Methods

Mice and viruses. All animal experiments were performed in accordance with Emory University Institutional Animal Care and Use Committee. C57BL/6J female mice were purchased from Jackson Laboratory and P14 CD45.1$^+$ female mice (on the C57BL/6J background) were bred in-house. For acute infections and analysis of early CD8 T cell responses, we performed a transfer of 1x10^6 CD45.1$^+$ P14 CD8 T cells into CD45.2$^+$ C57BL/6J mice 1 day prior to infection with 2x10^6 pfu i.v. of LCMV Armstrong. Mice were sacrificed on days 1, 2, and 3 post-infection, while some mice remained uninfected as naïve controls. For day 8 analyses, 4,000 P14 CD8 T cells were instead transferred 1 day prior to infection with 2x10^5 pfu i.p. of LCMV Armstrong. Timepoints were staggered such days 1, 2, 3, and 8 were harvested on 1 day. For some experiments, CD44loCXCR3lo CD8 T cells were sorted from the bulk naïve P14 population prior to the transfer.

Cell isolation. Spleens were isolated from mice and smashed through 70um nylon cell strainers to remove clumps. Cells were spun down and resuspended in 2 ml of Ack lysis buffer for 2 minutes in order to lyse the RBCs. After incubation, an additional 35 ml of RPMI + 5% FBS was added to

dilute the buffer, and the cells were spun down again. The resulting cell pellet was resuspended in PBS + 2% FBS + 0.5mM EDTA and cells were transferred to a 96-well round-bottom plate.

Flow cytometry. Surface staining was performed by incubating cells with fluorochrome-conjugated antibodies against CD8, CD4, CD19, PD-1, CD44, CD45.1, CD45.2, CD25, CD69, and CD62L (BD Bioscience, eBioscience, and Biolegend). Cells were incubated on ice for 30 minutes in PBS + 2% FBS + 0.5mM EDTA. Cell viability was determined with the Live/Dead fixable aqua or near IR dead cell stain kit (Invitrogen). Samples were acquired on a Symphony flow cytometer (BD Biosciences) and data were analyzed with FlowJo software (TreeStar).

Bulk RNA-seq and analysis. CD45.1$^+$ P14 CD8 T cells were isolated and FACS-sorted from uninfected mice or mice infected with LCMV Armstrong 1, 2, 3, or 8 days prior. Samples were sorted on a FACSAria II (BD Biosciences). After sorting, RNA was isolated from each sample using the All-Prep DNA/RNA Micro Kit (Qiagen) and then submitted to the Emory Yerkes Nonhuman Primate Genomics Core. Reads from RNA-sequencing were aligned to the mm10 genome [accessed through Ensembl (192)] with STAR version 2.7.

Single cell RNA-seq and analysis. Cells from all conditions (naïve and days 1, 2, 3, and 8 post-infection) were stained prior to the sort with CD4, CD19, CD8, CD45.1, PD-1, and Live/Dead. Additionally, each sample was also stained with 1 of 5 distinct hashtag labelling antibodies (TotalSeq-C0301 hashtag 1, TotalSeq-C0302 hashtag 2, TotalSeq-C0303 hashtag 3, TotalSeq-C0304 hashtag 4, TotalSeq-C0305 hashtag 5, all from Biolegend). This allowed us to combine the samples into a single capture post-sort. In some cases, the cells were also stained with CITE-

sequencing (CITE-seq) antibodies against PD-1, CD62L, CD127, CD69, CD25, CD8a, CD200, CD28, TCRb, and CD226 (Biolegend) prior to the sort. CD45.1^{+} P14 CD8 T cells were FACS-sorted from the stained samples on a FACSAria II (BD Biosciences). The capture was performed at the Emory Yerkes Nonhuman Primate Genomics Core. Gene expression and CITE-sequencing data were aligned and mapped with 10X Genomics' Cell Ranger (v6). Cells were excluded from further analysis if >4% of their reads mapped to mitochondrial genes, if they contained <1500 or >50000 UMIs, or had <800 detected genes. Cells were assigned to a sample group (naïve, day 1, etc.) if >85% of their barcoding antibody reads originated from a single hashtag antibody. Gene expression (RNA) counts were normalized in Seurat (v4) (194) using the SCTransform command. Counts were center log-ratio normalized and scaled with Seurat. Shared nearest neighbor clustering was performed in Seurat with 15 principal components, 100 neighbors, and a resolution of 0.47. UMAP dimensionality reduction was performed with identical parameters and a minimum distance of 0.5. A phylogenetic tree was also created with identical parameters, using Seurat's BuildClusterTree. For CITE-sequencing analysis, 16,452 cells passed the quality control criteria and were unambiguously assigned to a sample group; these cells were used for downstream analysis. UMAP was performed with gene expression data using 18 principal components, 200 neighbors, and a minimum distance of 0.1. Clusters were identified with Seurat's FindClusters command, using the igraph method and a resolution of 0.5. Additional plots were generated using ggplot2 or GraphPad Prism.

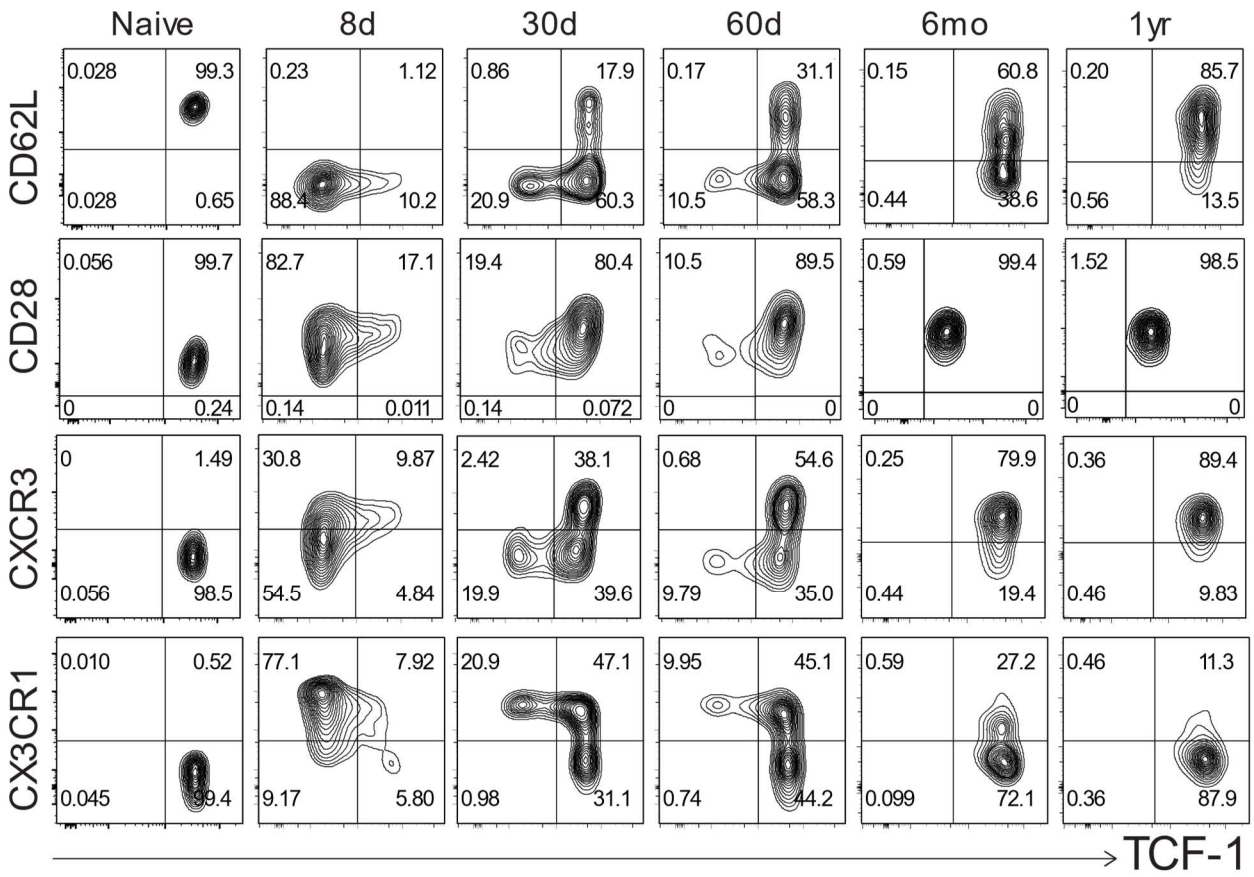

Figure 1. Long-lived GP33^{+} memory CD8 T cells express TCF-1, CD62L, CD28, & CXCR3. Representative flow plots showing the frequency of splenic GP33^{+} CD8 T cells that co-expressed TCF-1 along with the indicated markers. B6 mice were infected LCMV Armstrong (2×10^{5} pfu, i.p.) and responses are shown from 8 days to 1 year post-infection. A naïve, uninfected mouse is also shown for comparison.

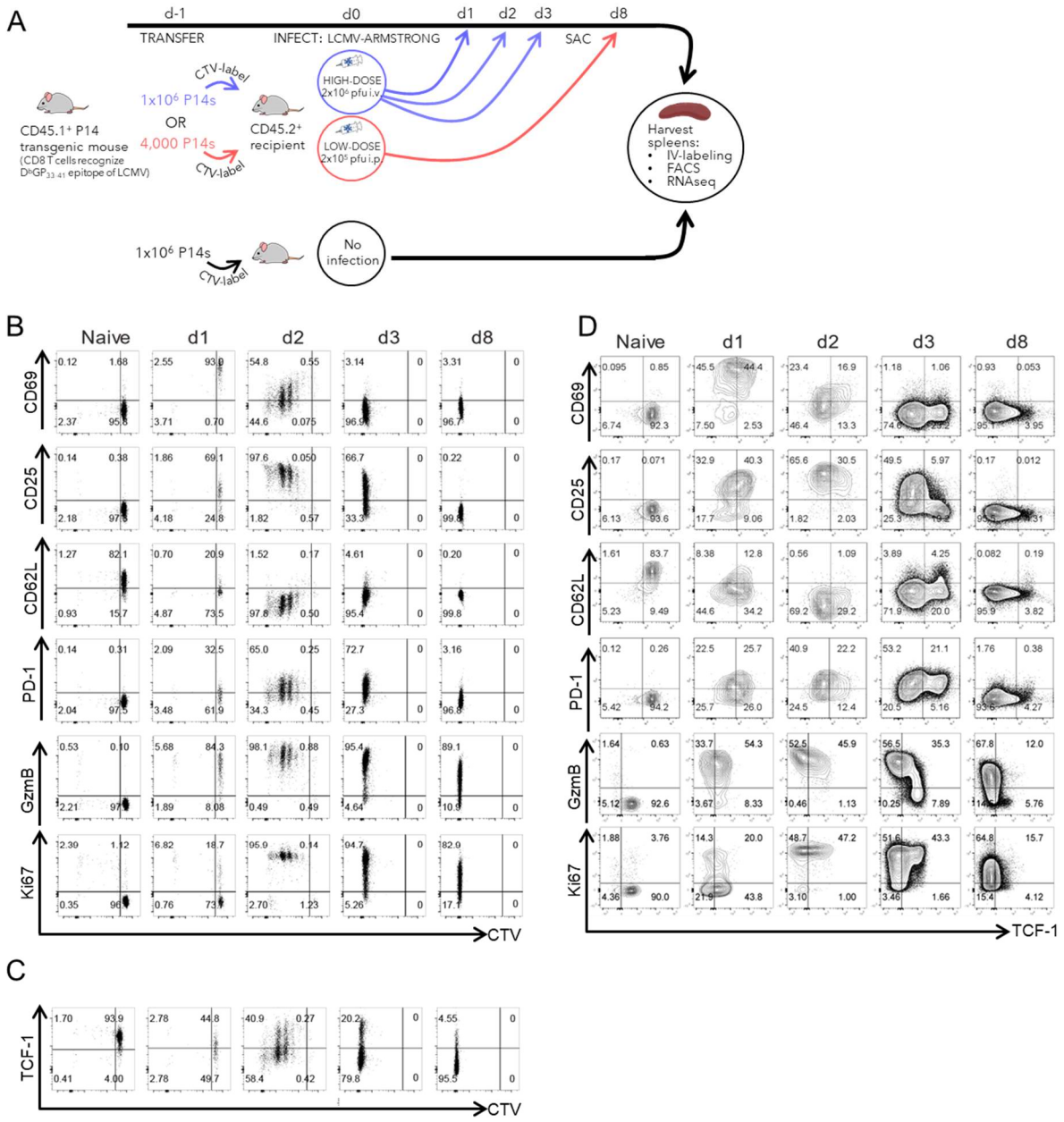

Figure 2. Surface phenotype of antigen-specific CD8 T cells early following infection. (A) Experimental scheme. CD8 T cells from CD45.1$^+$ P14 transgenic mice were labeled with cell-trace violet (CTV) tracking dye, then transferred into naïve CD45.2$^+$ B6 recipients. P14 mice have a clonal population of GP33-specific CD8 T cells. All recipients received 1x10^6 P14s, except for day 8 mice, which received only 4,000 P14s. Recipients were infected with 2x10^6 pfu LCMV Armstrong, i.v. in a staggered fashion, such that all mice were sacrificed on a single day. Splenocytes from mice were examined at 1, 2, 3, or 8 days post-infection. (B-C) Representative flow plots showing the kinetics of expression of the indicated markers by division, from 1 to 8 days post-infection. Samples are gated on donor P14 cells. The mean fluorescence of CTV is diluted with each division. (D) Representative flow plots showing the expression TCF-1 with the indicated markers.

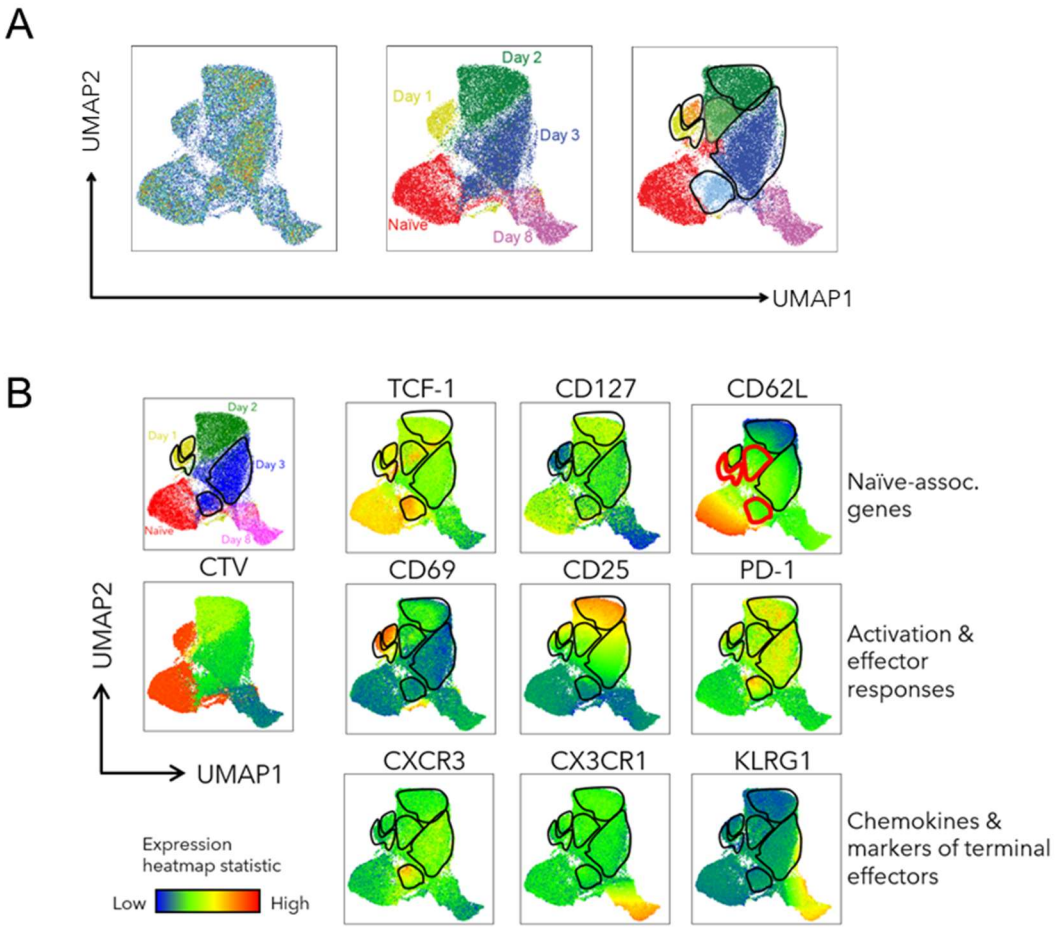

Figure 3. Early heterogeneity in surface marker expression among CD8 T cells. Flow cytometry data from samples collected on days 1, 2, 3, and 8, as well as from naïve mice, was re-analyzed using the FlowSOM algorithm to distinguish cell clusters. (A) Uniform Manifold Approximation and Projection (UMAP) of the pooled samples. Each timepoint can be visualized as a unique cluster. Two clusters were identified on days 1, 2, and 3. (B) Expression of markers among the clusters, which are circled with black lines. Red indicates high relative expression, while blue indicates low relative expression. Clusters outlined in red lines in the top right are putative memory precursor (MP) "precursor" clusters.

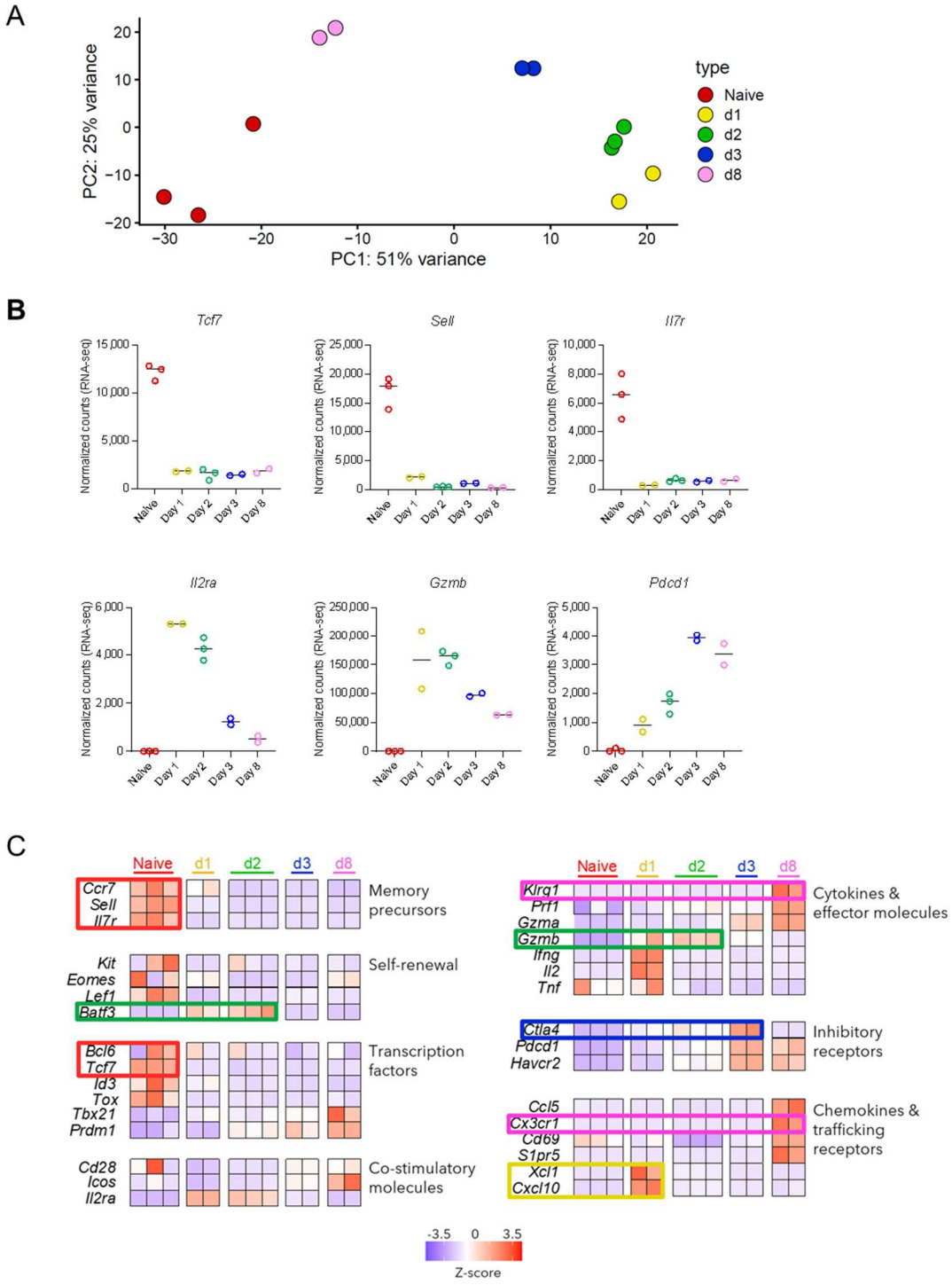

Figure 4. Transcriptional profiling reveals distinct gene expression programming on each day following infection. Bulk RNA-seq was performed on sorted CD45.1$^+$ P14 CD8 T cells from uninfected mice or mice infected with LCMV Armstrong 1, 2, 3, or 8 days prior. (A) Principal component analysis (PCA) identified two principal components that explained 76% of variance between the samples. Each sample is plotted on these two components. (B) Normalized counts of genes of interest across all timepoints. (C) Heatmap showing Z-scores of top DEGs and other genes of interest across all timepoints. Colored boxes highlight key genes upregulated at each timepoint.

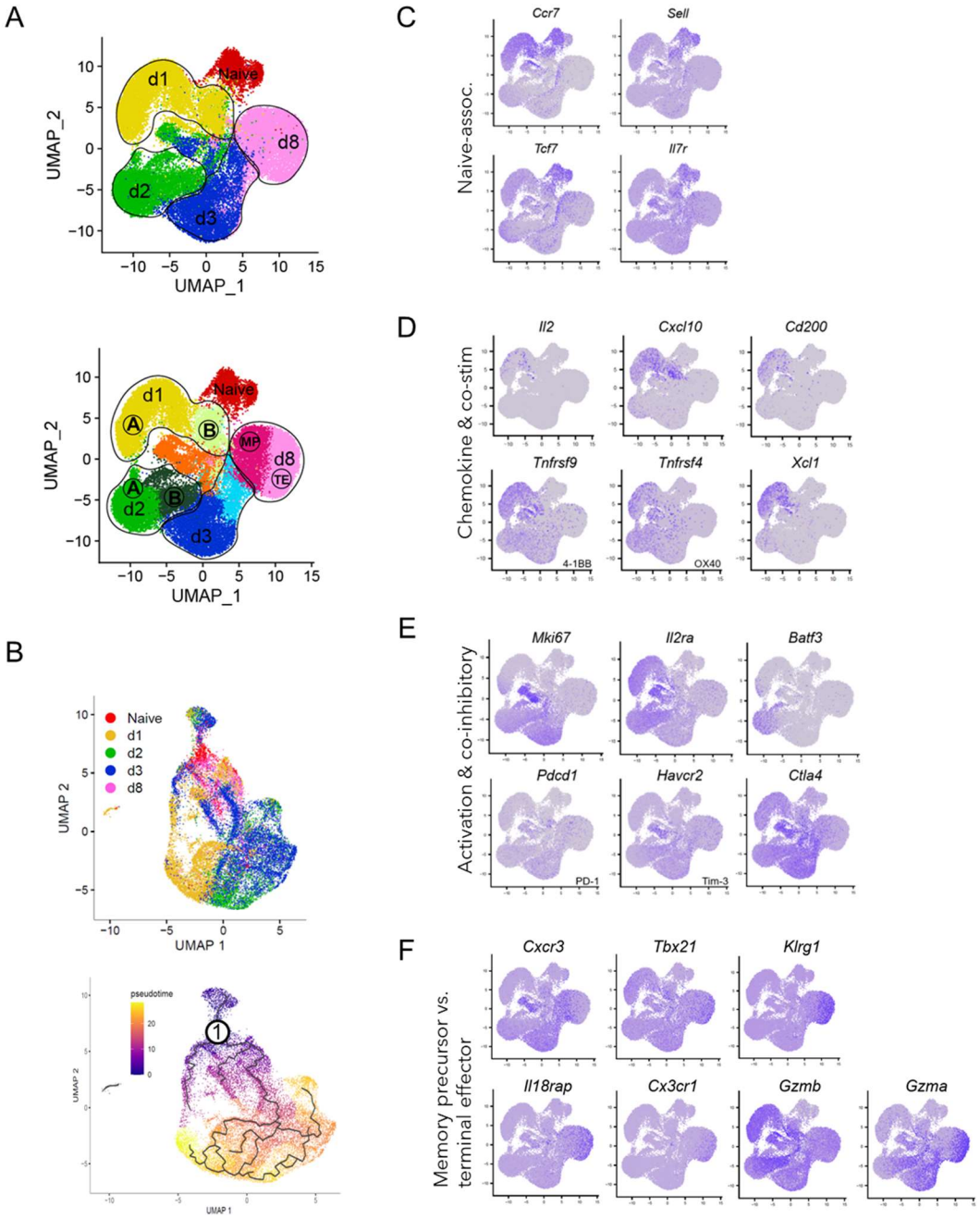

Figure 5. Single cell analysis reveals transcriptional heterogeneity at each timepoint. Single cell RNA-seq was performed on sorted CD45.1^{+} P14 CD8 T cells from uninfected mice or mice infected with LCMV Armstrong 1, 2, 3, or 8 days prior. Two individual experiments are pooled as one integrated dataset. (A) UMAP with unsupervised clustering analysis showing the transcriptional relationship between samples. Each sample is highlighted (top). Clustering analysis identified two major clusters on days 1, 2, 3, and 8, but only 1 for the naïve sample. In the center is an orange cluster of proliferating cells (bottom). (B) Pseudotime trajectory analysis performed by Monocle3 (195), rooted from the naïve group. Rooting from *Tcf7* expression results in a nearly identical trajectory analysis. (C-F) Expression of the indicated genes among the UMAP clusters.

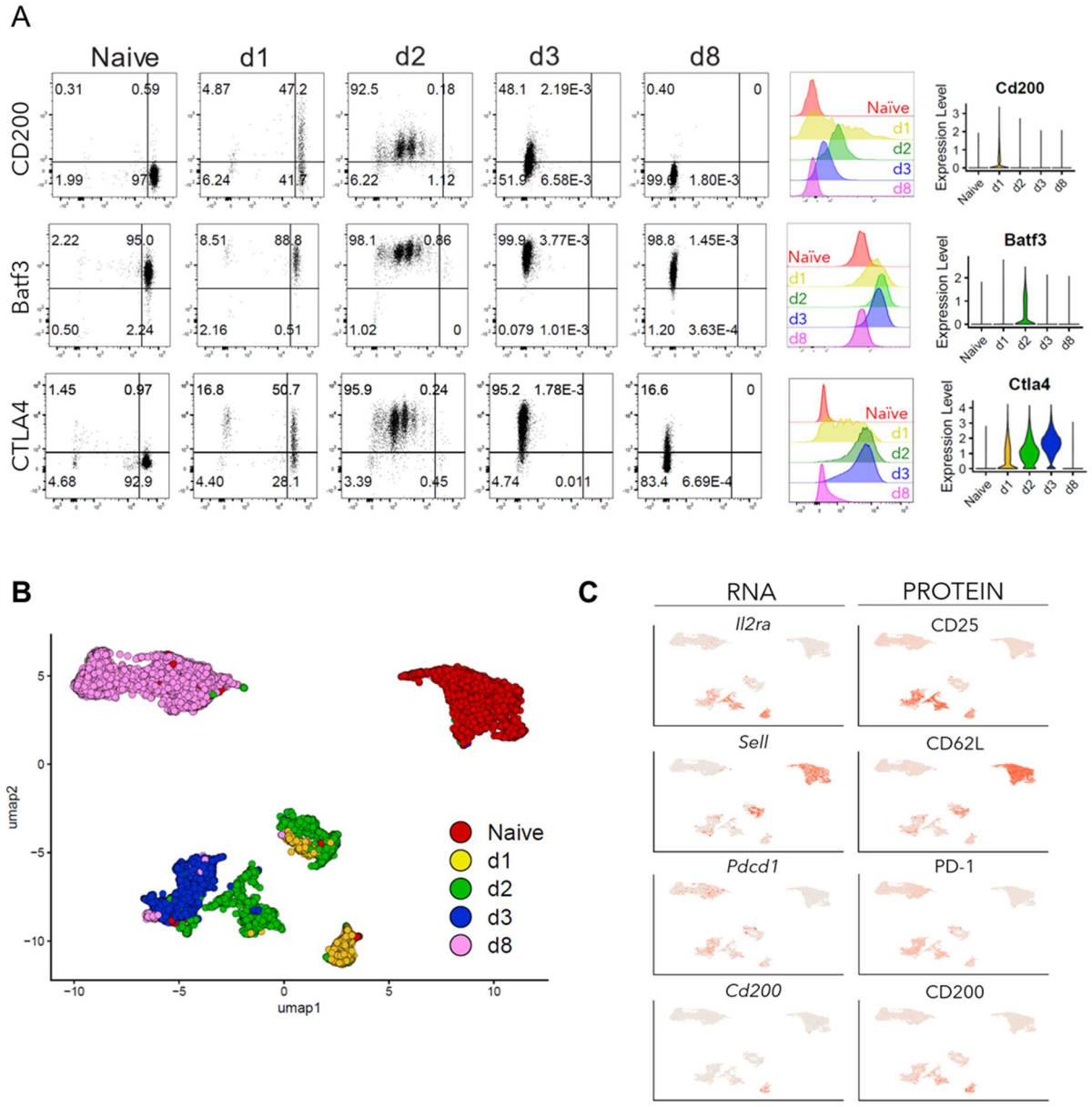

Figure 6. Transcriptional findings are consistent with surface expression profiles. (A) We performed flow cytometry analyses to validate transcriptional and protein expression. Representative flow plots and histograms are shown, as well as violin plots from the single cell RNA-seq. (B) We also performed CITE-seq analyses to simultaneously assess the protein and transcript levels. UMAP clustering of the samples is shown. (C) RNA and protein expression of the indicated markers among the UMAP clusters.

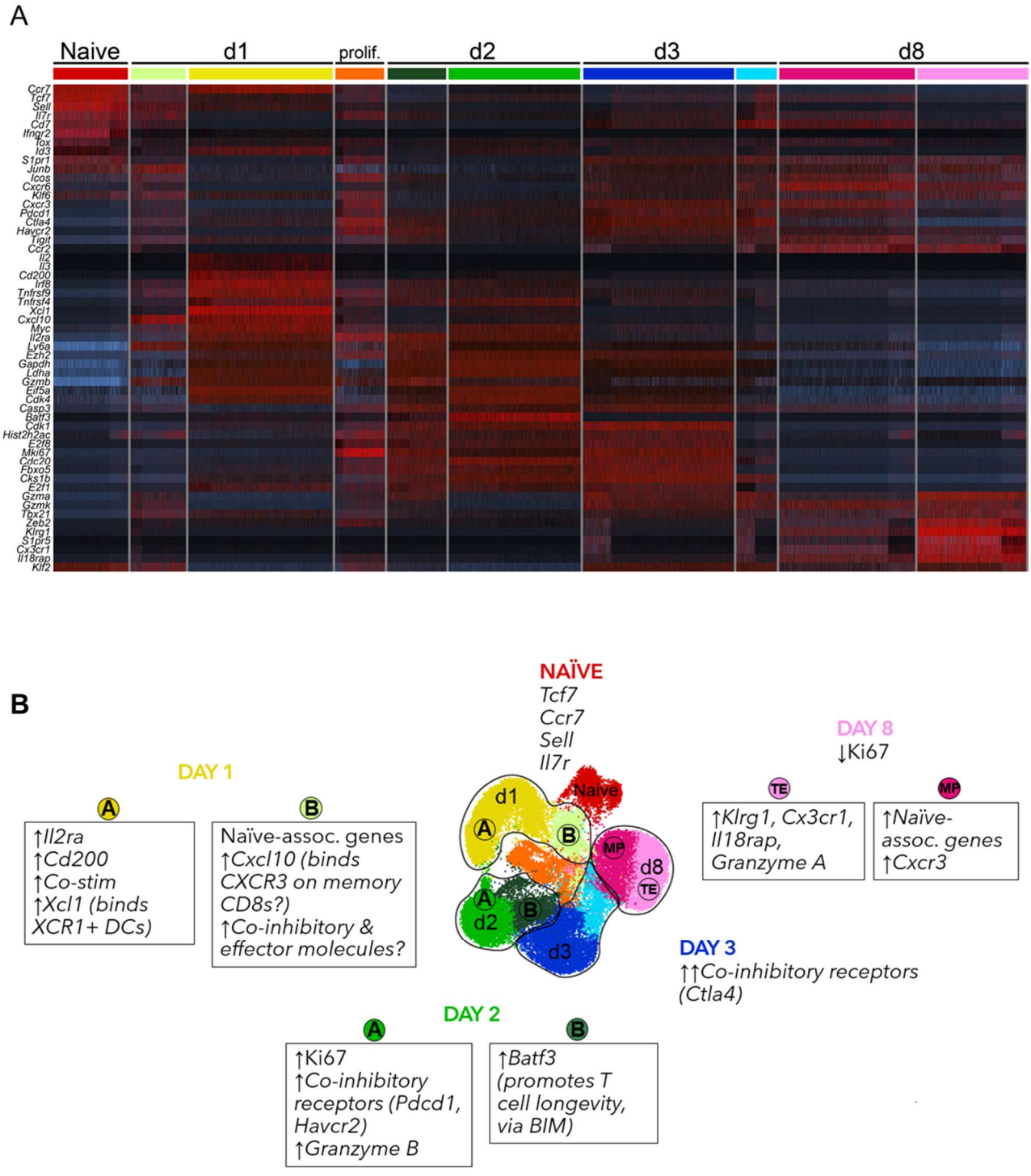

Figure 7. Summary of putative sub-populations at each timepoint based on transcriptional analyses. (A) Heatmap showing the expression of top DEGs as well as other genes of interest across all timepoints. (B) Summary of key genes involved in early CD8 T cell differentiation and their proposed roles in fate determination.

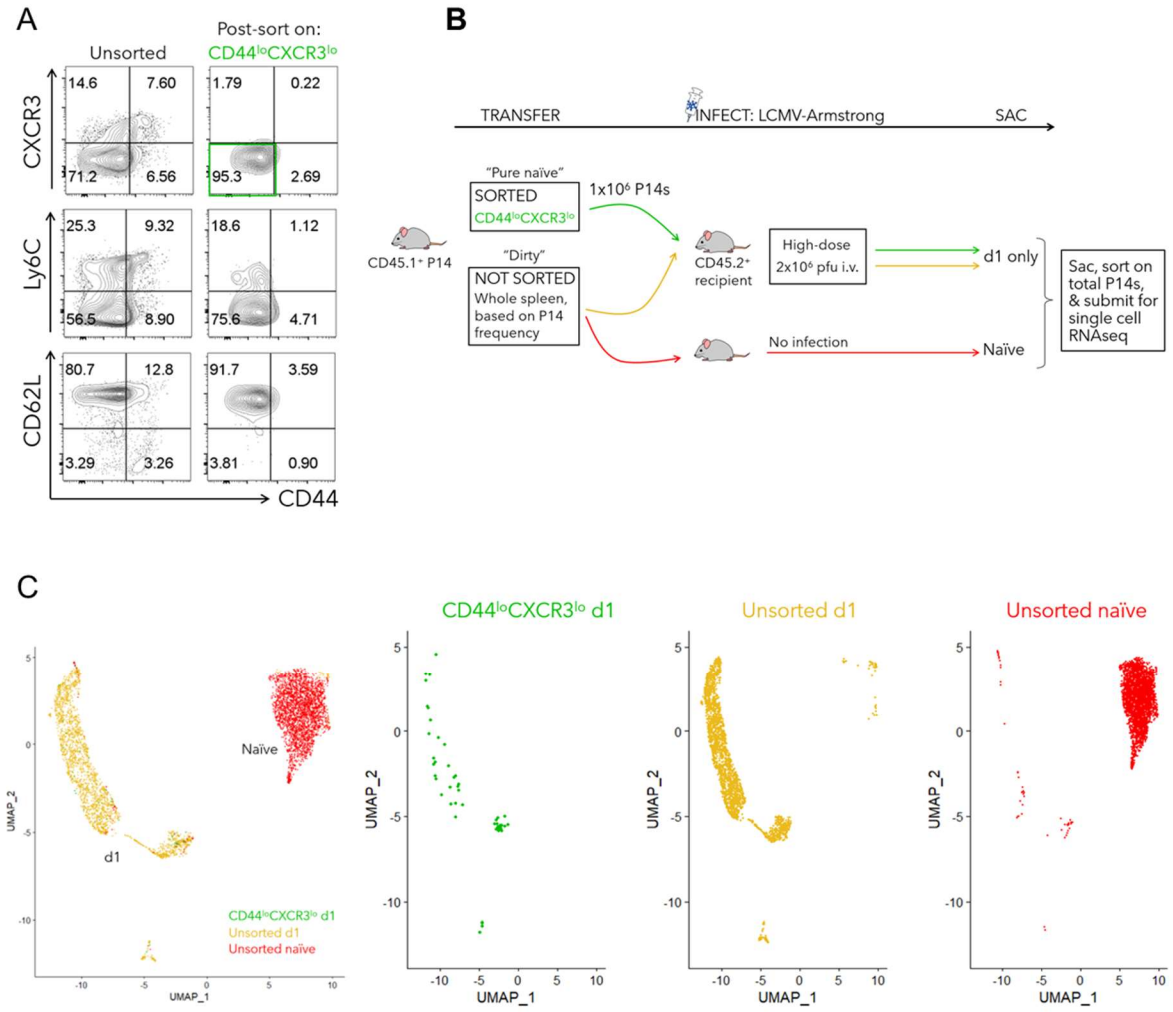

Figure 8. Heterogeneity in the naïve precursor population is not responsible for the heterogeneity observed post-infection. (A) P14 CD8 T cells express higher levels of CD44, Ly6C, and CXCR3 than their wild-type (WT) counterparts. So, we sorted CD44loCXCR3lo CD8 T cells from CD45.1$^+$ P14 mice prior to transfer to obtain a "pure naïve" donor population. (B) We also transferred non-sorted "dirty" P14 cells as a control. As before, P14 cells were transferred into CD45.2$^+$ B6 mice and these mice were infected with 2x10^6 pfu LCMV Armstrong, i.v. Non-sorted "dirty" mice were also transferred into recipients that remained uninfected. CD45.1$^+$ P14s were sorted 1 day post-infection and all samples were submitted for single cell RNA-seq. (C) UMAP clustering showing the sorted populations altogether (left) and individually (right).

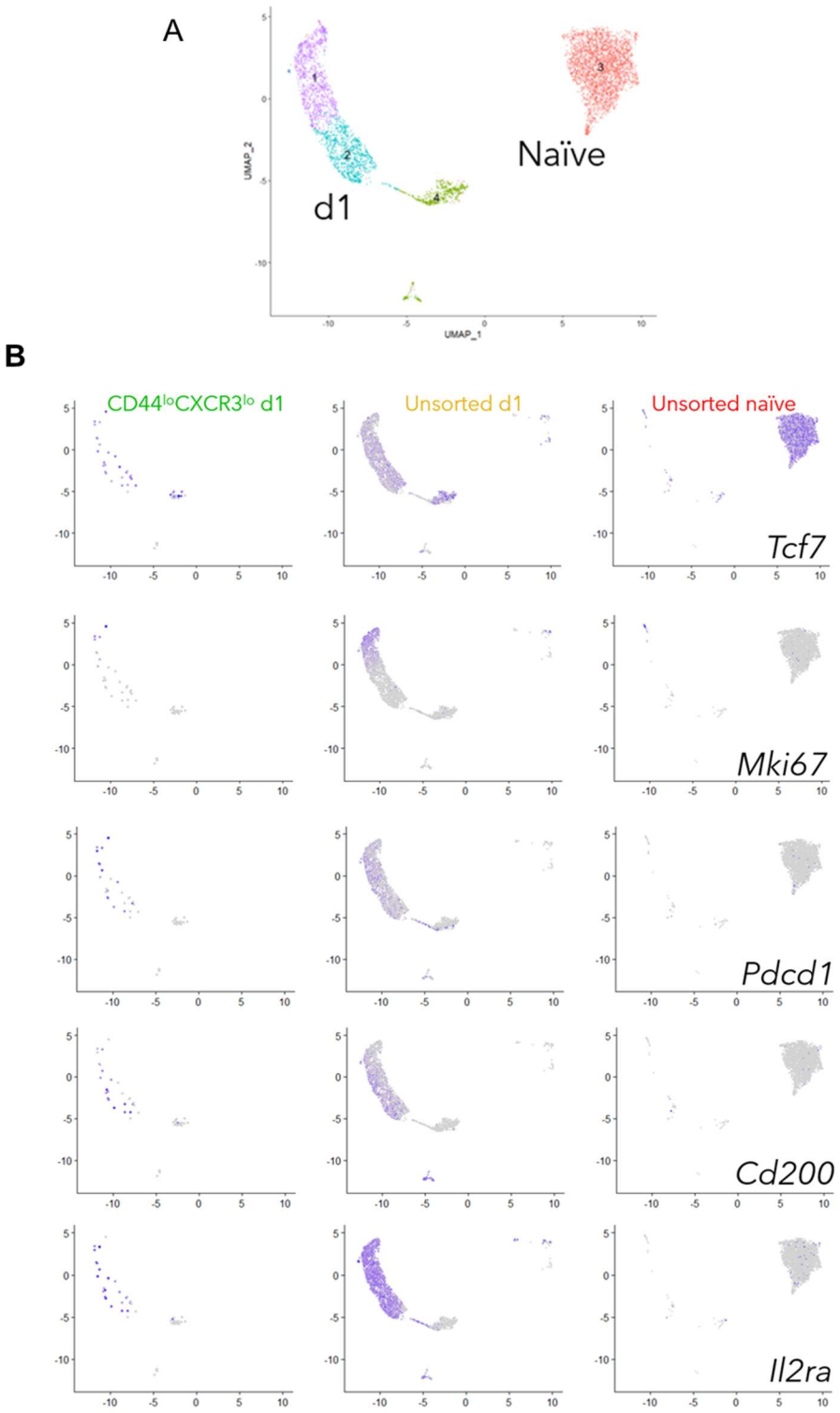

Figure 9. Expression of key markers is consistent between "dirty" and "pure naïve" precursor population. (A) UMAP clustering of the indicated samples. (B) Expression of key markers within each sample.

Chapter 4: Intracellular stores facilitate rapid expression of CD69 on antigen-specific and non-specific CD8 T cells following TCR or cytokine stimulation

Gill AL, Hudson WH, Xie X, Cuevas A, Ahn E, Araki K, Kaja MK, and Ahmed R. (2023). Intracellular CD69 stores facilitate rapid surface expression on CD8 T cells following either TCR or cytokine stimulation. *Nature Immunology*. (In preparation).

I. Summary

CD69 is a widely-used marker of cellular activation and tissue-residency. But its precise regulatory mechanisms remain poorly understood. We investigated which signals trigger surface expression, and we found that both TCR and non-TCR signaling could induce robust expression on naïve CD8 T cells within 24 hours. Interestingly, type I interferon signaling could induce CD69 surface expression on naïve, non-antigen specific CD8 T cells within this same timeframe. But we wondered how exactly naïve CD8 T cells could express CD69 so rapidly. We performed RNA-sequencing and, surprisingly, we found that naïve cells had high levels of *Cd69* mRNA. Polysome profiling on naïve CD8 T cells then demonstrated that this mRNA was being actively translated at steady state, and western blot analysis confirmed actual intracellular protein also present at steady state. These findings suggest that CD69 remains poised intracellularly in all naïve cells, waiting at the ready to localize to the cell surface and trigger activating signal transduction. Our studies can inform future use of CD69 as surface marker for cellular function, as the intracellular and extracellular profiles may not always align.

II. Introduction

Activation of CD8 T cells induces highly regulated changes in gene expression (16, 196–199). CD69 is classically viewed as the earliest marker of CD8 T cell activation, but the precise

mechanisms by which activating stimuli trigger surface expression—and trigger it so quickly—are incompletely understood.

Signaling from a wide variety of agents has been shown to induce CD69 expression on the cell surface, including anti-CD3/TCR, anti-CD2, interferon α/β, Poly (I:C), and PMA (200–204). At the transcriptional level, pro-inflammatory stimuli involving the NF-κB/Rel family of transcription factors (downstream of TNFa), as well as AP-1, specifically activate the CD69 gene promoter (205, 206). One study has even proposed that CD69 exists within the cytoplasm of non-activated T cells and that surface expression can occur independently of newly synthesized RNA or protein (207). This study examined changes in global RNA and protein synthesis following activation, however, and failed to examine the steady-state kinetics of *Cd69* transcription and translation alone.

Increasingly, CD69 has been implicated in a number of additional processes, including migration, lymphoid organ retention, and tissue residency. Following acute infection, CD69 is used as a marker of tissue-resident memory CD8 T cells (Trm) (55, 208). In chronic infection, CD69 has also been used to define a hierarchical pathway of differentiation and localization for exhausted CD8 T cells (136). These programs result from downstream CD69 signaling, upon binding its cognate ligands Galectin-1 or S100A8/S100A9(209–212). CD69 also establishes lateral interactions with the sphingosine 1-phosphate receptor (S1PR1) and the amino acid transporter complex LAT1-CD98—involved in T cell migration and cell metabolism, respectively (204, 213). The CD69-S1PR1 axis is well-studied and plays a major role in regulating the egress of CD8 T cells from lymphoid organs. Upon activation, CD8 T cells upregulate CD69, which promotes S1PR1 internalization and degradation, leading to transient lymph node retention; this has been proposed as a mechanism to ensure complete activation prior to egress (214, 215). More

broadly, CD69 signaling triggers an increase in intracellular calcium, resulting in the synthesis of several cytokines (IL-2, TNFa, and IFNg) and their receptors (IL-2Ra), enhancement of the expression of c-myc and c-fos protooncogenes, and cell proliferation (but not the induction of cytotoxicity programs) (200, 216–219).

Thus, CD69 plays diverse roles in CD8 T cell function, particularly in activation and migration. We sought to tease apart the precise mechanisms regulating CD69 induction. Although much is known about its activating signals, we wanted to clarify the contributions of both TCR and non-TCR stimuli. We also do not fully understand the transcriptional and translational kinetics of CD69 at steady-state in naïve CD8 T cells, nor how these kinetics change following TCR or non-TCR stimulation. If we are to use CD69 as a definitive marker of functional status and homing potential, it is crucial that we understand how its expression is regulated in all CD8 T cell states.

Here, we examine early CD69 expression in CD8 T cells in both *in vitro* and *in vivo* settings. We determined that acute infection resulted in upregulation of CD69 on both naïve, antigen-specific and non-specific CD8 T cells alike. Of course, TCR stimulation triggered upregulation of CD69 on antigen-specific CD8 T cells, but we found that type I interferon was required for expression in the non-specific CD8 T cell population. This upregulation occurred within 24 hours, at which time nearly ~100% of antigen-specific and ~70% of non-specific CD8 T cells were $CD69^{+}$. We sought to understand how such a rapid and robust phenotypical change might occur, and we found that a tightly regulated transcriptional network exists at steady-state. To our surprise, although naïve CD8 T cells lack surface CD69, they have high levels of *Cd69* mRNA by RNA-seq analysis. Furthermore, we found that, at baseline, they actively transcribe *Cd69* mRNA and translate CD69 protein. This pre-formed CD69 remains poised intracellularly, waiting for an activating stimulus. These results suggest that activation-induced surface-level

CD69 expression is therefore not driven by *de novo* translation, but rather due to translocation of pre-formed protein to the cell surface. These findings have broad implications for the routine use of CD69 as a marker of cellular activation and migration. Importantly, they explain why naïve CD8 T cells have such high levels of *Cd69* mRNA and how CD69 can be expressed so rapidly upon activation.

III. Results

In this study, we investigated the expression of CD69 on the surface of CD8 T cells following activation. We utilized the mouse model of lymphocytic choriomeningitis virus (LCMV) infection to evaluate CD69 expression on both antigen-specific and non-antigen specific CD8 T cells. By transferring CD45.1$^+$ LCMV GP33-specific CD8 T cells from P14 transgenic mice into recipient CD45.2$^+$ mice, we were able to analyze the GP33-specific donor CD8 T cells (P14 cells) as a distinct population from the CD45.2$^+$ endogenous compartment (**Fig. 1a**). Just 1 day after LCMV infection, CD69 was dramatically upregulated on the cell surface. Importantly, this upregulation occurred on both P14 and endogenous CD8 T cells, with ~100% of P14s and ~70% of endogenous CD8 T cells expressing CD69 at this timepoint (**Fig. 1b** and **c**). On the other hand, CD25 (IL-2Ra) and PD-1 were only expressed by the LCMV-specific P14 CD8 T cells, and not by the endogenous population. The upregulation of CD69 was seen on antigen-specific CD8 T cells even before their first division (**Fig. 2**). Cell-trace violet (CTV) staining of the P14 cells prior to transfer showed that the undivided CTVhi P14 cells were already almost uniformly CD69$^+$. We also found that CD69 was rapidly expressed on both CD44hi (activated) and CD44lo (naïve) CD8 T cells, regardless of whether they were antigen-specific or non-specific (**Fig. 3**).

We next wanted to determine the basis for such immediate and robust expression of CD69 on the cell surface. First, we sought to characterize which precise activating signals could stimulate CD69 upregulation, hypothesizing a role for both TCR and non-TCR signals based on numerous prior studies. We turned to an *in vitro* system, which would allow us to tease apart the individual contributions of cognate peptide versus cytokine stimulation. We isolated naïve P14 cells and cultured them for 6 or 24 hours with GP33 peptide or interferon-β, and then we analyzed their phenotypic profiles (**Fig. 4a**). CD69 was robustly upregulated following both GP33 and interferon stimulation (**Fig. 4b-c**). In contrast, CD25 and PD-1 were only upregulated following peptide stimulation.

To confirm the role of TCR signaling in CD69 upregulation, we utilized an LCMV mutant strain with a single-amino-acid substitution in the GP33 glycoprotein (**Fig. 5a**)(186). This mutation significantly decreases the efficiency of antigen presentation to CD8 T cells, as the mutant GP33 has significantly reduced binding affinity to MHC. To investigate the role of non-TCR signaling in CD69 surface expression, we performed an *in vivo* interferon blockade with an aIFNAR-1 blocking antibody. Following P14 transfer, we infected mice with either the WT or mutant LCMV strain, and some WT and mutant-infected mice received interferon blockade additionally (**Fig. 5b**). As with the *in vitro* studies, both TCR and interferon signaling could upregulate CD69 (**Fig. 5c** and **d**). Of course, infection with the WT virus resulted in surface expression of CD69 in nearly 100% of P14 cells. But infection with the mutant virus induced a similar response, suggesting that there may be some redundancy to the TCR signal. We hypothesized that type I interferon might provide this alternate signal. Interferon blockade delivered to mice infected with the WT virus did not reduce CD69 expression, presumably due to intact TCR signaling. But blockade in mutant virus-infected mice nearly eliminated CD69 expression. In contrast, upregulation of CD25 and

PD-1 was entirely TCR-dependent. Expression of these markers decreased only upon infection with the mutant form of the virus and not by interferon blockade.

We next sought to determine which signals were driving CD69 expression in non-antigen specific CD8 T cells. We performed another type I interferon blockade and this time analyzed the endogenous CD8 T cell population. As suspected, CD69 was upregulated on non-specific CD8 T cells following either WT or mutant LCMV infection, but aIFNAR-1 blockade abrogated this effect (**Fig. 6a** and **b**). Type I interferon was thus a key modulator of CD69 expression in non-antigen specific, as well as antigen-specific CD8 T cells . We next wanted to confirm our findings in a setting of complete genetic ablation of the type I IFN signaling cascade. We directly infected either WT or IFNAR-1 KO mice with WT LCMV and analyzed the total population of CD8 T cells 1 day after infection (**Fig. 7a**). We found that CD69 upregulation among total CD8 T cells was dramatically reduced in the KO mouse (**Fig. 7b**). Altogether, these studies demonstrated that interferon was a primary driver of CD69 surface expression on non-specific CD8 T cells following infection.

Importantly, rapid surface expression of CD69 on the total population of CD8 T cells is not unique to the LCMV system. In fact, this is also seen following many different kinds of systemic infections, including vesicular stomatitis virus (VSV), yellow fever virus (YFV), vaccinia virus, and *Listeria monocytogenes* (**Fig. 8**).

We next wondered, how do naïve CD8 T cells (antigen-specific and non-specific alike) express CD69 on the surface so quickly after an activating stimulus—and to such a robust extent? Nearly 100% are $CD69^{+}$ within just 1 day. This is a remarkably short period time in the context of gene induction. To understand the molecular mechanisms underlying this observation, we performed RNA-sequencing (RNA-seq) on P14 cells that were sorted from an uninfected and an

infected mouse (1 day post-infection). We sought to compare the protein and transcript levels of CD69. Surprisingly, in stark contrast to their lack of surface protein, naïve P14s had high levels of *Cd69* transcript (**Fig. 9a**). Transcript levels were roughly unchanged after 1 day of infection, while levels of surface CD69 sky-rocketed. Pearson's r correlation between normalized RNA counts and surface mean fluorescence intensity (MFI) reflected this discordance (r = 0.083) (**Fig. 9b** and **c**). This trend was not seen for *Il2ra* (encoding CD25), *Pdcd1* (encoding PD-1), or *Sell* (encoding CD62L). In this case, RNA and protein levels were much more closely correlated (Pearson's r = 0.41, 0.99, and 0.99, respectively). Naïve cells lacked *Il2ra* and *Pdcd1* transcripts and lacked protein as well. Naïve cells had high levels of *Sell* and CD62L, and these levels dropped upon infection.

These findings raised the question of whether CD69 protein expression in naïve CD8 T cells was translationally repressed, or whether CD69 protein was actually present but not delivered to the cell surface. To answer this, we performed polysome profiling of CD8 T cells from uninfected and day 1 LCMV-infected mice (**Fig. 10a**). The amount of RNA recovered from polysome fractions in P14 CD8 T cells on day 1 after infection was larger than that in naïve P14 CD8 T cells, indicating global translation activity is high in day 1 P14 CD8 T cells (**Fig. 10b**). Next, we examined translation of *Cd69* mRNA in comparison to that of *Cd8a* mRNA, which is actively translated regardless of T cell status, and Rps6 mRNA, translation of which is positively correlated with T cell activation. A large amount of C*d69* mRNA was detected in polysomes in both naïve and day 1 P14 CD8 T cells, similar to the pattern of *Cd8a* mRNA data (**Fig. 10c**). This indicated that *Cd69* was being actively translated in naïve cells.

Given that *Cd69* was being actively translated in naïve CD8 T cells, but was not detected on the cell surface, we next performed a western blot analysis to examine the result of this active

translation (**Fig. 10d**). CD69 protein was found intracellularly in both naïve and day 1 LCMV-infected CD8 T cells. The protein levels did not appear to differ between naïve and day 1, as the transcript data would suggest. These findings are summarized in **Figure 11**.

These data provide a deeper understanding of the regulation of CD69 expression. We have uncovered the mechanism by which naïve CD8 T cells can express CD69 so rapidly upon their surfaces following activation. CD69 is both transcribed and translated in naïve CD8 T cells, remaining intracellular until an activating stimulus. Both interferon and TCR signaling can trigger its movement to the cell surface. An understanding of these processes may be of use to those using CD69 as a marker in a wide variety of immunological contexts.

IV. Discussion

CD69 is generously used as a marker of CD8 T cell activation and tissue-residency. Though seemingly disparate, our studies suggest that CD69 physiologically links these two processes. CD69 is upregulated following activating stimuli—TCR-dependent and independent alike. CD69 has been shown to control lymphocyte egress from lymph nodes through association with the G-protein-coupled sphingosine-1-phosphate receptor-1 (S1PR1) (204, 214, 220). Complexes between these two proteins form on the plasma membrane, resulting in inhibition of lymphoid tissue egress. Upregulation of CD69 upon activation can thus result in retention of CD8 T cells within lymphoid tissues and may explain the transient lymphopenia observed during numerous acute febrile illnesses (221–223). Alterations in lymphoid architecture and cellularity during immune responses are well-documented (90). In this way, CD69 can mediate transduction of an activation signal into regulation of cellular trafficking.

Additionally, upregulation of CD69 on non-antigen specific CD8 T cells via interferon signaling highlights the importance of non-antigen specific CD8 T cells in the antiviral response. Non-antigen specific CD8 T cells may also provide crucial effector functions, including cytokine secretion and cytotoxicity(224).

Amazingly, naïve CD8 T cells have enormous intracellular stockpiles of both CD69 mRNA and protein. Intracellular protein had previously been reported by Risso et al., but we show that *Cd69* mRNA is also being actively translated at steady-state, demonstrating that this is a more dynamic process that previously understood. Ultimately, the CD69 protein remains poised at the ready inside the cell, waiting for cognate TCR or interferon stimulation to migrate to the cell surface. These intracellular reserves enable rapid surface expression of CD69, triggering rapid inhibition of lymphocyte egress, among other downstream consequences. In this very early phase of the immune response, the rapid timing of these processes is clearly crucial. What remains unknown, however, is how exactly the activating signal is transduced such that pre-formed CD69 protein physically makes its way to the cell surface.

Our findings suggest that we should exercise caution in using CD69 to assign functional and activation status. Both RNA and protein exist in naïve cells. Therefore, expression of CD69 on the surface may be the only reliable way predict signaling along the CD69 axis. This of course necessitates the use of flow cytometry to discern this.

Altogether, we have shown that CD69 expression is more complicated than previously appreciated. This complexity may have crucial implications for how we use it as a marker in immunology. Intracellular RNA and protein may confound our interpretations of truly "naïve" cells. But this feature is also what enables naïve cells to express CD69 so rapidly, and now mechanistically explains their capacity for rapid recruitment to a new immune insult. Our results

highlight the necessity of understanding the function and regulation of surface markers. We provide a new context for CD69 in immunology.

V. Materials and Methods

Mice and viruses. All animal experiments were performed in accordance with Emory University Institutional Animal Care and Use Committee. C57BL/6J female mice were purchased from Jackson Laboratory and P14 CD45.1$^+$ female mice (on the C57BL/6J background) were bred in-house. For acute infections and analysis of early CD8 T cell responses, we performed a transfer of 1x10^6 CD45.1$^+$ P14 CD8 T cells into CD45.2$^+$ C57BL/6J mice 1 day prior to infection with 2x10^6 pfu i.v. of LCMV Armstrong or LCMV Clone 13. Mice were sacrificed on day 1 post-infection, while some mice remained uninfected as naïve controls. For some experiments, CD45.1$^+$ P14 mice were directly infected with 2x10^6 pfu i.v. of LCMV Armstrong and sacrificed on day 1 post-infection. To investigate the role of cognate antigen in upregulating CD69, a GP33 mutant LCMV Clone 13 strain was used. This strain contains a single-amino-acid substitution (valine to alanine) at position 35 of the viral glycoprotein, so the GP33 specific P14 TCR is unable to bind(225). To investigate the role of IFNR1 signaling in upregulating CD69, we used IFNR1-deficient mice on a 129/SvEv background (226). Finally, we investigated CD69 upregulation in a number of other viral contexts. We infected mice with 2x10^6 pfu of VSV, YFV, vaccinia virus, or Listeria monocytogenes i.p. and measured surface CD69 expression at 44 hours post-infection.

Cell isolation. Spleens were isolated from mice and smashed through 70um nylon cell strainers to remove clumps. Cells were spun down and resuspended in 2 ml of Ack lysis buffer for 2 minutes in order to lyse the RBCs. After incubation, an additional 35 ml of RPMI + 5% FBS was added to

dilute the buffer, and the cells were spun down again. The resulting cell pellet was resuspended in PBS + 2% FBS + 0.5mM EDTA and cells were transferred to a 96-well round-bottom plate.

Flow cytometry. Surface staining was performed by incubating cells with fluorochrome-conjugated antibodies against CD8, CD4, CD19, PD-1, CD44, CD45.1, CD45.2, CD69, and CD25 (BD Bioscience, eBioscience, and Biolegend). Cells were incubated on ice for 30 minutes in PBS + 2% FBS + 0.5mM EDTA. Cell viability was determined with the Live/Dead fixable aqua or near IR dead cell stain kit (Invitrogen). Samples were acquired on a Symphony flow cytometer (BD Biosciences) and data were analyzed with FlowJo software (TreeStar).

Interferon blockade. Mice received 500ug of aIFNAR-1 (BioXCell) i.p. on the day prior to infection and the day of the infection. Mice were sacrificed on day 1 post-infection.

***In vitro* culture.** Splenocytes were harvested from P14 mice and plated at 1x10^6 cells per ml in a 12-well plate in RPMI + 10% FBS. Cells were cultured with mouse interferon-β at 500U/ml (PBL Assay Science), GP33 peptide (100ng/ml), or nothing. In all cases, cells were cultured for 6 or 24 hours, harvested, and stained for flow cytometry analysis.

Bulk RNA-sequencing and analysis. CD45.1$^+$ P14 CD8 T cells were isolated and FACS-sorted from uninfected mice or mice infected with high-dose LCMV Armstrong 1 day prior to the sort. Samples were sorted on a FACSAria II (BD Biosciences). After sorting, RNA was isolated from each sample using the All-Prep DNA/RNA Micro Kit (Qiagen) and then submitted to the Emory

Yerkes Nonhuman Primate Genomics Core. Reads from RNA-sequencing were aligned to the mm10 genome (accessed through Ensembl(192)) with STAR version 2.7.

Polysome profiles and qRT-PCR. Polysome profiles were analyzed as described previously(196). Briefly, for naive CD8 T cells, a single cell suspension of spleen from uninfected P14 transgenic mice was prepared. For activated antigen-specific CD8 T cells, P14 transgenic mice were intravenously infected with LCMV Armstrong (2 x 10^6 PFU) and spleens from the LCMV-infected P14 mice were isolated 24 hours after infection. To purify naïve and activated P14 CD8 T cells, single cell suspension of spleen was stained with APC-conjugated anti-CD8a antibody, and the CD8 T cells were isolated by $CD8a^+$ isolation kit (Miltenyi Biotech). These CD8 T cells were further purified by anti-APC MicroBeads (Miltenyi Biotech). After MicroBeads purification, dead cells were removed by percoll density centrifugation. Cycloheximide (100 μg/ml, Sigma) were added in all buffers used during this purification process. Purified P14 cells (>90-95% purity) were lysed, and cell lysates were loaded onto 10%-50% sucrose gradient, followed by ultracentrifugation as described previously(196, 227). After ultracentrifugation, sucrose gradient was fractionated from the top of the tube. RNA was isolated from individual fractions using Trizol reagent (ThermoFisher). For quantification of RNA, Ribogreen RNA assay kit (ThermoFisher) was used, and RNA concentration was determined by NanoDrop 3300 fluorospectrometer (ThermoFisher). The amount of RNA in each fraction was normalized by the amount in the monosome fraction, which was set as 100%. For qRT-PCR, 10 pg of luciferase mRNA (Promega) was added to individual fractions of polysome profiles for normalization as described previously(228), and then RNA was extracted by Trizol reagent. Primers used in this study for qRT-PCR were QuantiTect primers purchased from Qiagen except for luciferase primers. The

followings are sequences for luciferase primers: forward; 5'-GAGATACGCCCTGGTTCCTG-3', reverse; 5'-ATAAATAACGCGCCCAACAC-3'. qRT-PCR was carried out by QuantiFast SYBR Green RT-PCR Kit (Qiagen). Values of gene expression determined by qRT-PCR in individual fractions of sucrose gradient were normalized to luciferase quantity, and then distribution of the gene expression in the gradient was plotted.

Western blot analysis. P14 mice were sacrificed after no infection or one day after infection with high-dose LCMV Armstrong. Splenocytes were harvested from mice and CD8 T cells were purified using the EasySep Mouse $CD8^+$ T Cell Isolation Kit (Stem Cell Technologies). Purified CD8 T cell samples were resolved via SDS-PAGE at room temperature. Protein transfer was conducted on ice in Bio-rad Mini Trans-Blot® Cell onto MeOH soaked PVDF membrane. Blot was then blocked for 30 minutes in blocking buffer (5% bovine serum albumin in TBST (20 mM Tris, pH 7.5; 150 mM NaCl; 0.1% Tween 20)). Blot incubated overnight at 4 °C in α-CD69 (Abcam; Cat # ab202909) and α-GAPDH (Cell Signaling Technology®; Cat # 5174) antibodies that were diluted 1:2000 and 1:10,000 in blocking buffer, respectively. Blot then rinsed and incubated in HRP-conjugated goat α-Rb antibody (Cell Signaling Technology®; Cat # 7074S) diluted 1:2000 in blocking buffer for 1 hour at room temperature. Blot rinsed again before finally adding luminol/enhancer and peroxide solutions from Clarity™ Western ECL substrate kit (Bio-rad; Cat # 170-5060) that were pre-mixed 1:1. Chemiluminescence detected on Bio-rad Chemidoc MP imaging system.

Statistical analysis. All experiments were analyzed using Prism 9 (GraphPad Software). Statistical differences were assessed using unpaired two-tailed t tests or one-way ANOVA with

Tukey's test for multiple comparisons. Pearson's correlation between normalized RNA counts (from RNA-seq) and MFI (from flow cytometry) was also performed.

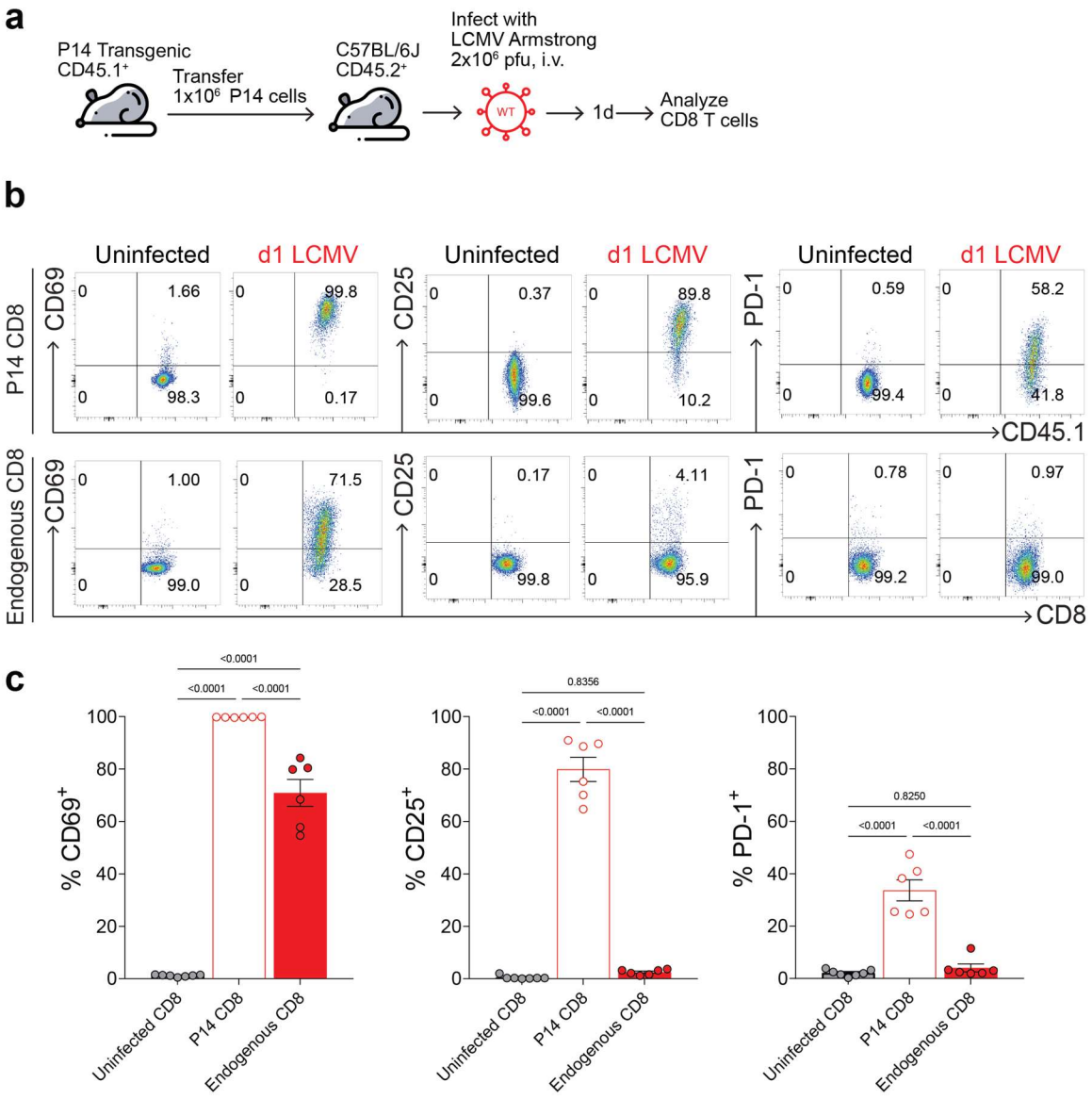

Figure 1. CD69 is upregulated on both antigen-specific and non-specific CD8 T cells early following cognate antigen stimulation. (**a**) Experimental scheme. 1x10^6 CD8 T cells from CD45.1$^+$ P14 transgenic mice were transferred into naïve CD45.2$^+$ C57BL/6J recipients. P14 mice have a clonal population of GP33-specific CD8 T cells. Recipients were infected with 2x10^6 pfu LCMV Armstrong, i.v. and sacrificed on day 1 post-infection. Some recipients remained uninfected to serve as naïve controls. (**b**) Representative flow plots showing CD69, CD25, and PD-1 expression on donor CD45.1$^+$ P14 CD8 T cells (top) or recipient endogenous CD8 T cells (bottom). (**c**) Quantification of the frequency of donor P14 cells or endogenous CD8 T cells expressing CD69, CD25, or PD-1. Mean ± SEM. One-way ANOVA with Tukey's test for multiple comparisons (c).

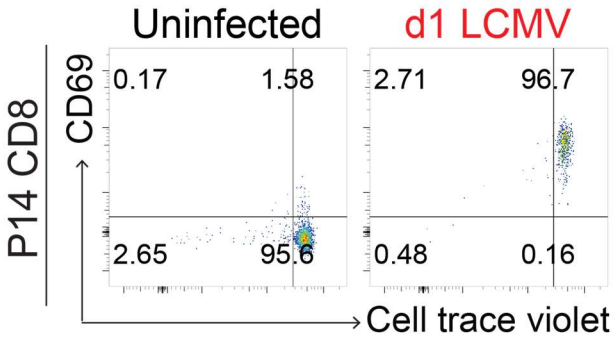

Figure 2. CD69 is upregulated on antigen-specific CD8 T cells prior to the first division. Representative flow plot showing the expression of CD69 on cell-trace violet (CTV)-labeled donor CD45.1^{+} P14 transgenic CD8 T cells (labeling was performed prior to the transfer).

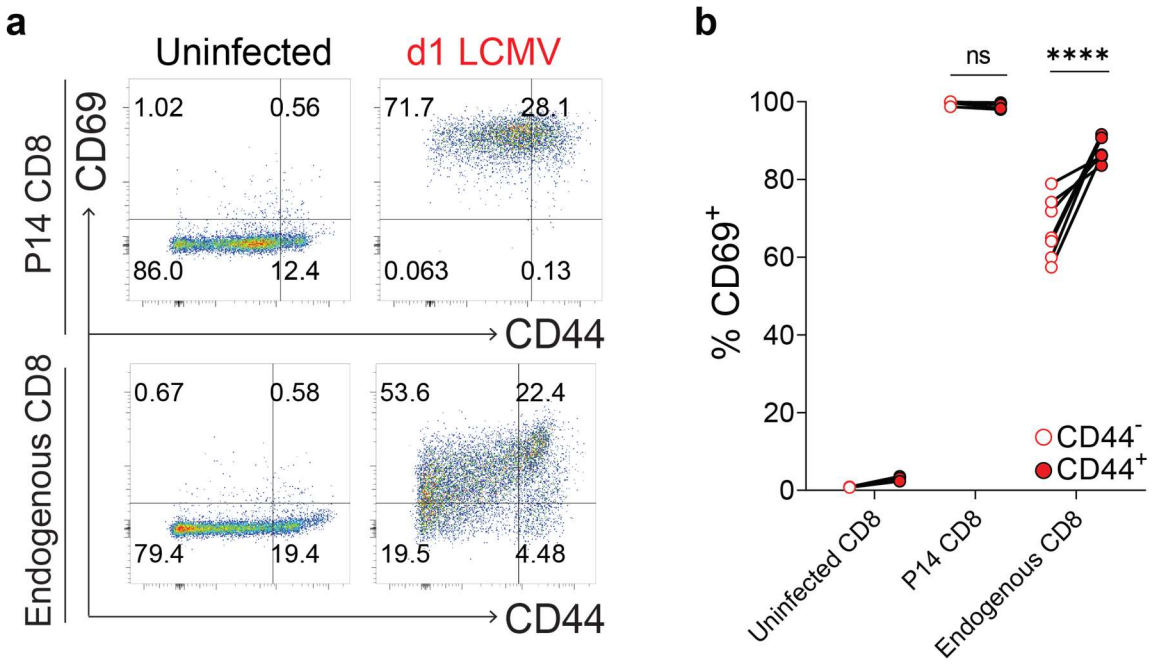

Figure 3. CD69 is upregulated on both CD44hi and CD44lo CD8 T cells. (a) Representative flow plots showing co-expression of CD69 with CD44 in naïve or infected mice among P14 cells or endogenous CD8 T cells. (b) Quantification of the frequency of $CD69^+$ CD8 T cells among uninfected, P14, and endogenous CD8 T cell populations, divided into CD44hi and CD44lo compartments. Unpaired, two-tailed t tests (b).

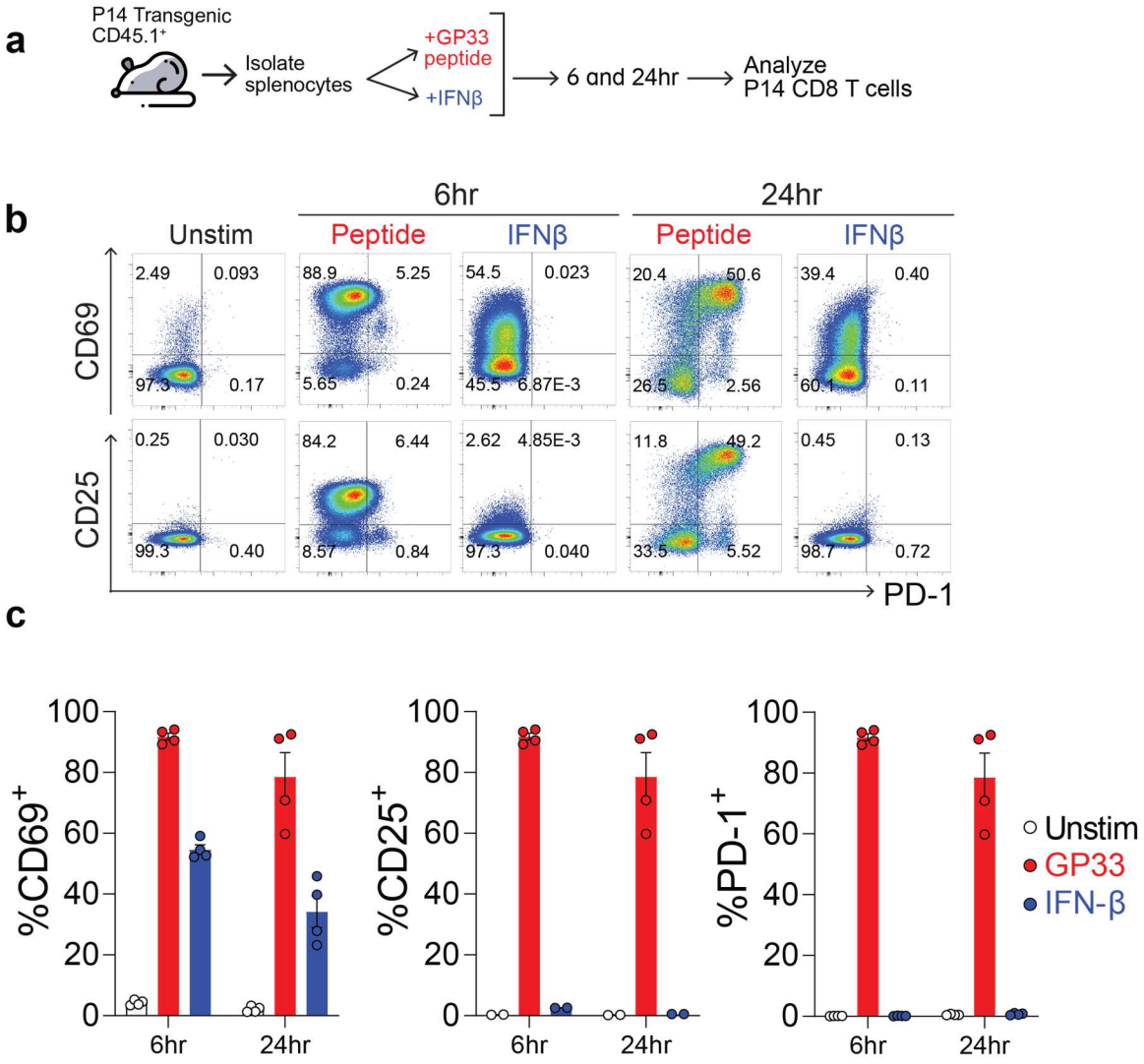

Figure 4. Both TCR and interferon can upregulate CD69 *in vitro*. (**a**) Splenocytes from P14 transgenic mice were harvested and plated for culture. GP33 cognate peptide or interferon-β were added to separate wells and cells were cultured for 6 or 24 hours, then analyzed by flow cytometry. (**b**) Representative flow plots showing the expression of CD69, CD25, and PD-1 on P14 CD8 T cells at 6 and 24 hours post-stimulation. (**c**) Quantification of the frequency of P14 CD8 T cells expressing the indicated markers.

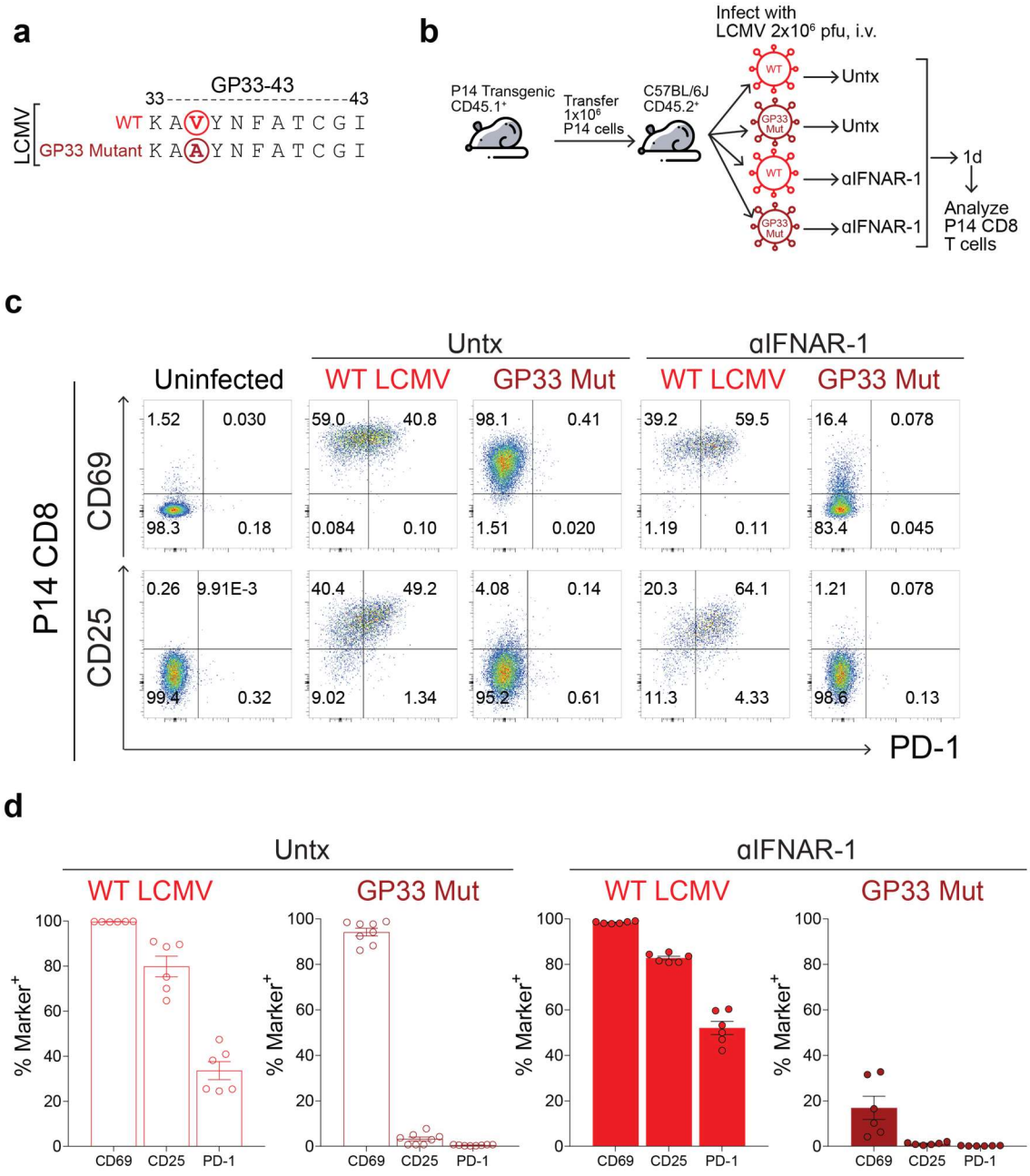

Figure 5. Both TCR and interferon can upregulate CD69 on antigen-specific CD8 T cells *in vivo*. (a) A mutant strain of LCMV has a single-amino-acid substitution (valine to alanine) at position 35 of the viral glycoprotein, reducing its affinity for MHC. (**b**) 1x10^6 CD8 T cells from CD45.1$^+$ P14 transgenic mice were transferred into naïve CD45.2$^+$ B6 recipients. Recipients were infected with 2x10^6 pfu, i.v. of mutant or WT LCMV, treated with either aIFNAR-1 or nothing, and then sacrificed on day 1 post-infection. Some recipients also remained uninfected. (**c**) Representative flow plots showing the expression of CD69, CD25, and PD-1 on donor P14 CD8

T cells, among the four treatment groups. (**d**) Quantification of the frequency of P14 CD8 T cells expressing CD69, CD25, or PD-1. Mean ± SEM.

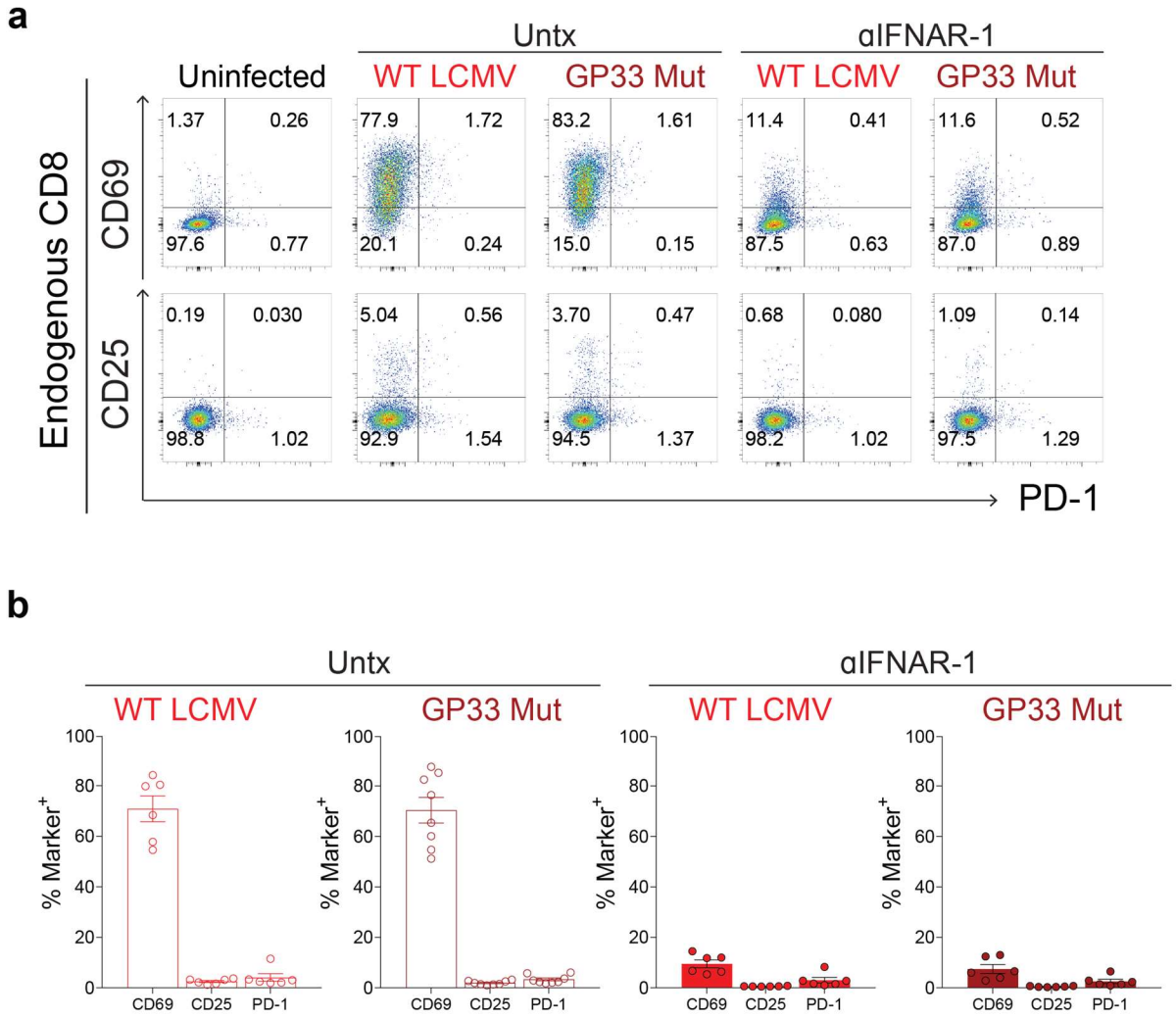

Figure 6. Interferon can upregulate CD69 on non-specific CD8 T cells *in vivo*. Experiment was performed as in Fig. 3. 1x10^6 CD8 T cells from CD45.1$^+$ P14 transgenic mice were transferred into naïve CD45.2$^+$ B6 recipients. Recipients were infected with 2x10^6 pfu, i.v. of mutant or WT LCMV, treated with either aIFNAR-1 or nothing, and then sacrificed on day 1 post-infection. (**a**) Representative flow plots showing the expression of CD69, CD25, and PD-1 on endogenous, non-P14 CD8 T cells, among the four treatment groups. (**b**) Quantification of the frequency of endogenous, non-P14 CD8 T cells expressing CD69, CD25, or PD-1. Mean ± SEM.

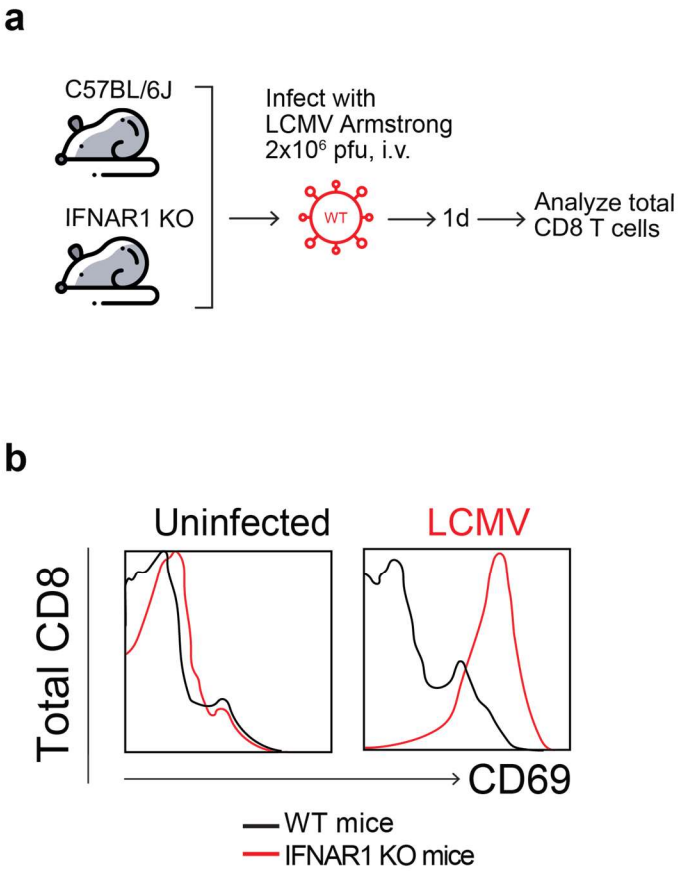

Figure 7. CD69 expression on non-specific CD8 T cells is interferon-dependent. (a) WT and IFNAR1 KO mice were directly infected with 2x10^6 pfu, i.v. of WT LCMV and levels of CD69 were measured at 1 day post-infection. (**b**) Representative histograms showing the mean fluorescence intensity (MFI) of CD69 on the surface of total CD8 T cells (*n*=1-5 mice per experiment; 5 experiments were performed).

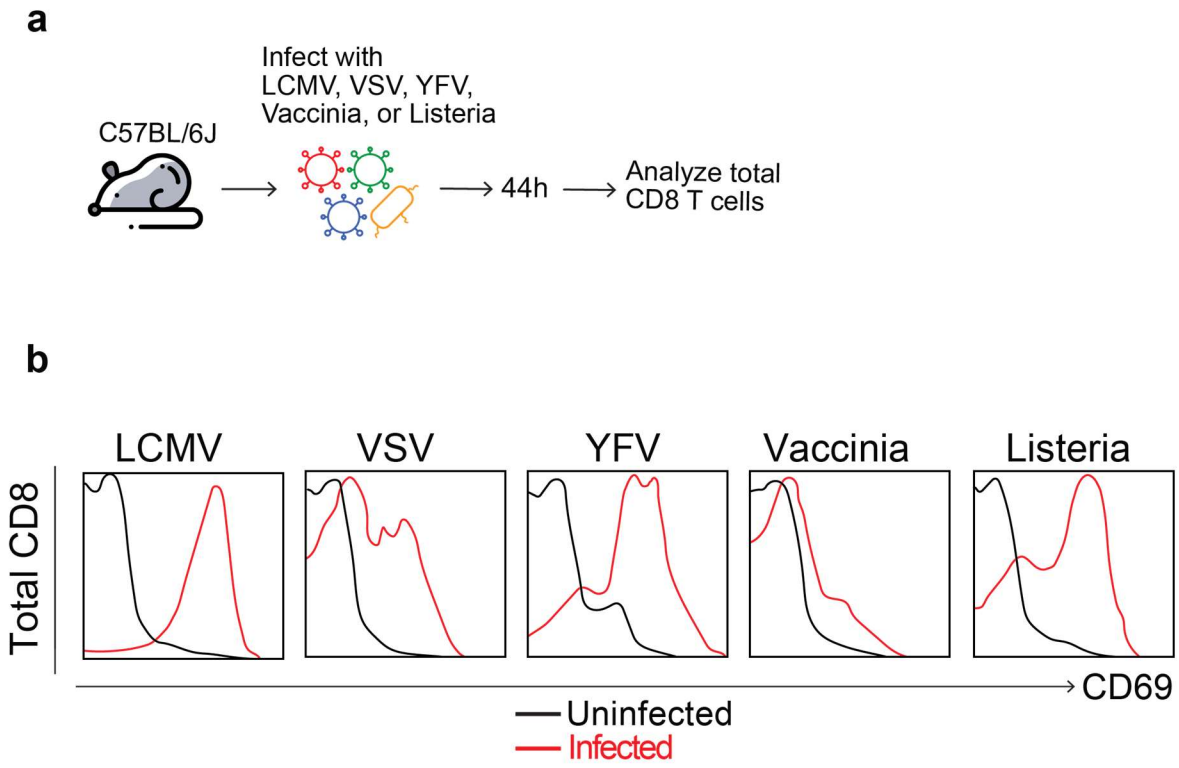

Figure 8. CD69 is upregulated in many **other** systemic **viral infections. (a)** B6 mice were infected with VSV, YFV, Vaccinia virus, or Listeria monocytogenes (2x10^6 pfu, i.p.) and surface levels of CD69 expression were examined at 44 hours post-infection. (**b**) Representative histograms showing the MFI of CD69 are shown, gated on total CD8 T cells (*n*=5 mice per virus).

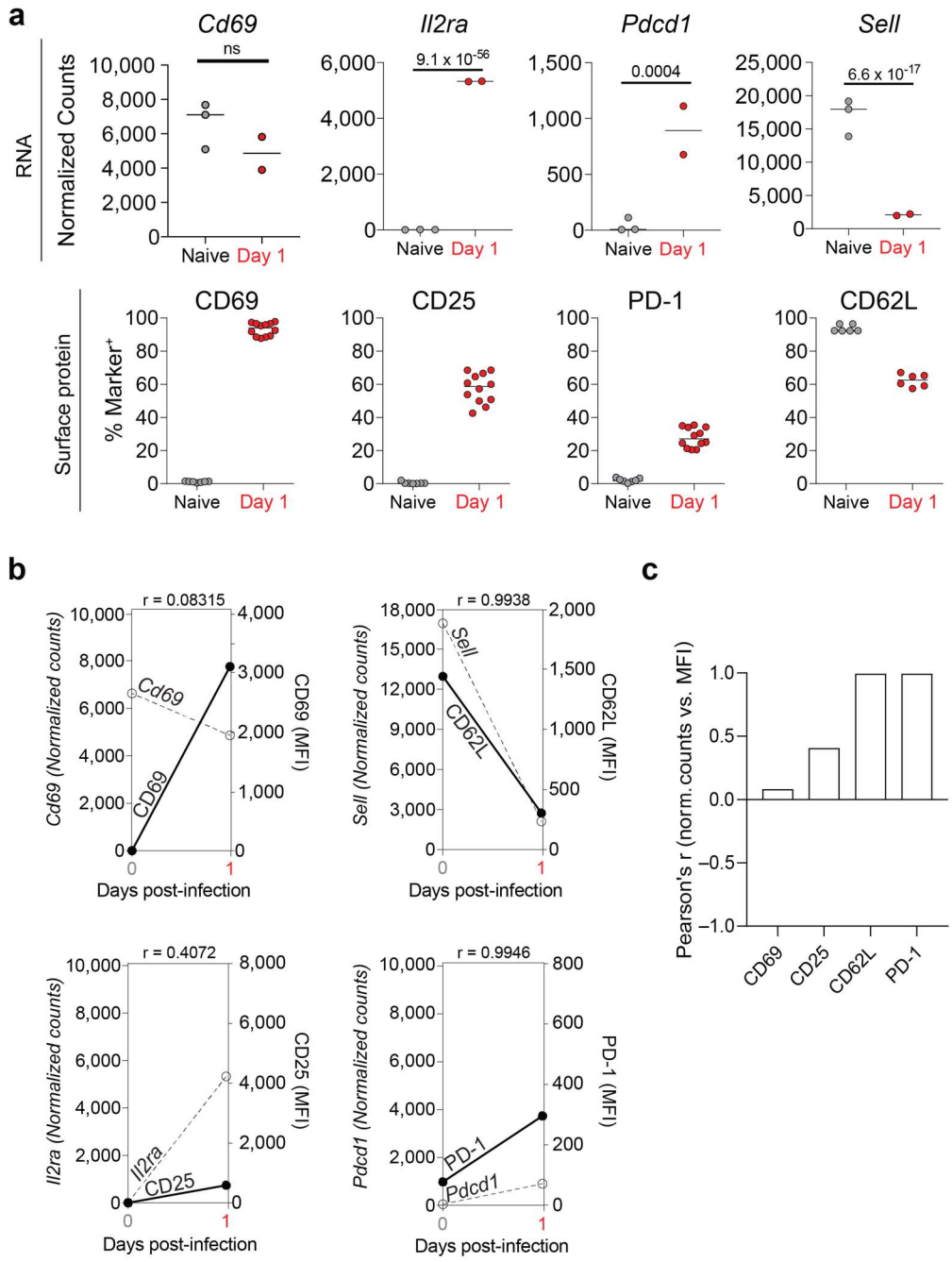

Figure 9. Naïve CD8 T cells express high levels of *Cd69* mRNA. (**a**) Expression of CD69, CD25, PD-1, and CD62L at the RNA level (top) and at the protein level (bottom). RNA levels are shown as normalized counts from RNA-seq analysis (*p* values are from Wald's test, performed by "DESeq2" in R). (**b**) Plots showing correlation of normalized RNA counts (solid line, left axis) with mean fluorescence intensity (MFI) from flow cytometry (dotted line, right axis). Pearson correlation coefficients were calculated for each pair and are shown above each plot. (**c**) Summary of Pearson's r values from (b).

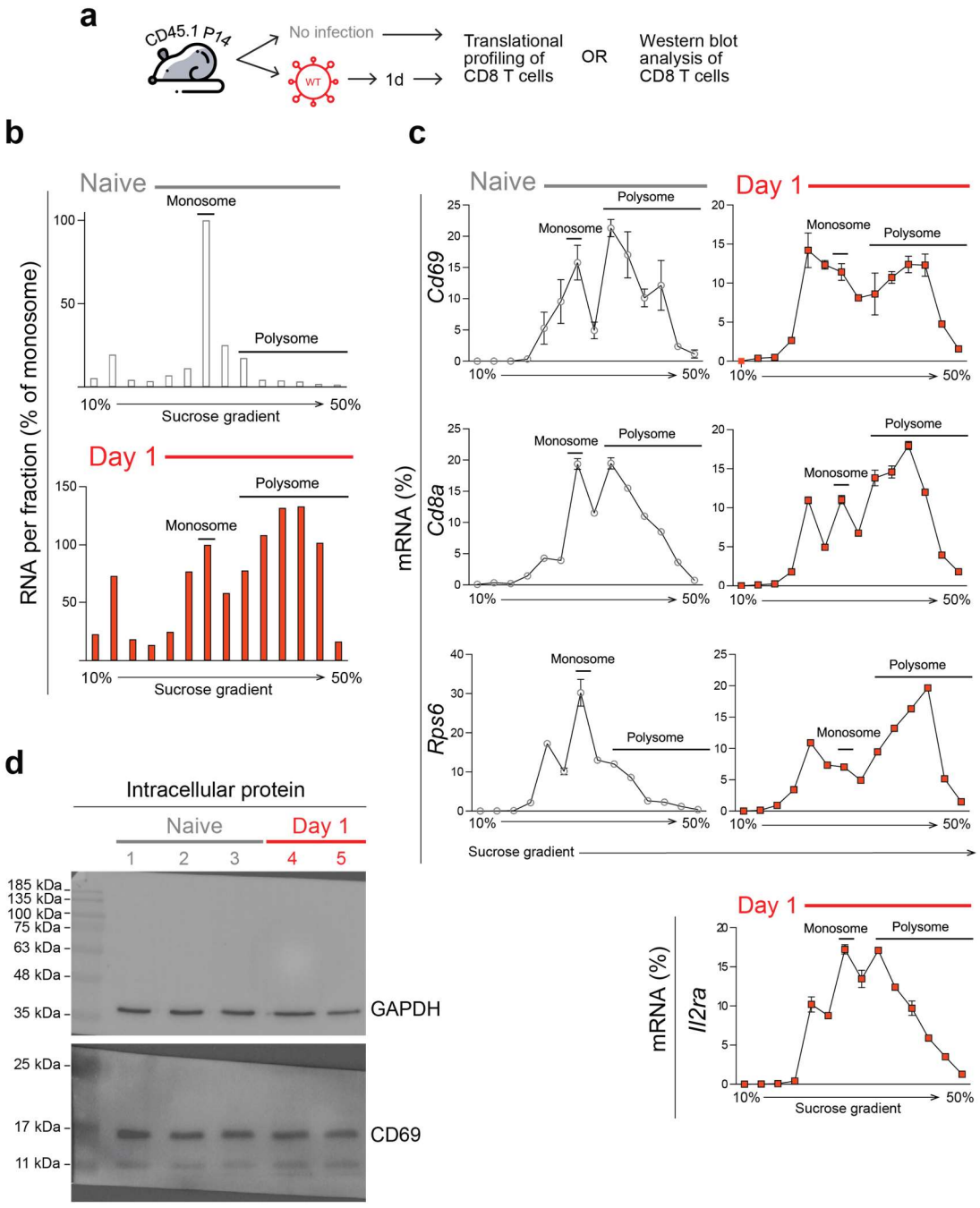

Figure 10. Naïve CD8 T cells actively translate *Cd69* mRNA and consequently have large intracellular stores of CD69 protein. (**a**) P14 transgenic mice were directly infected with WT LCMV ($2x10^6$ pfu, i.v.) and compared to uninfected controls. Translational profiling by sucrose gradient and western blot analysis were performed on purified total CD8 T cells at day 1 post-infection. (**b**) Total RNA in monosomes versus polysomes of CD8 T cells after 1 day of infection. (**c**) Percent of the indicated mRNA in monosomes versus polysomes. (**d**) Western blot analysis from CD8 T cell lysates. Membranes were probed for CD69 and GAPDH.

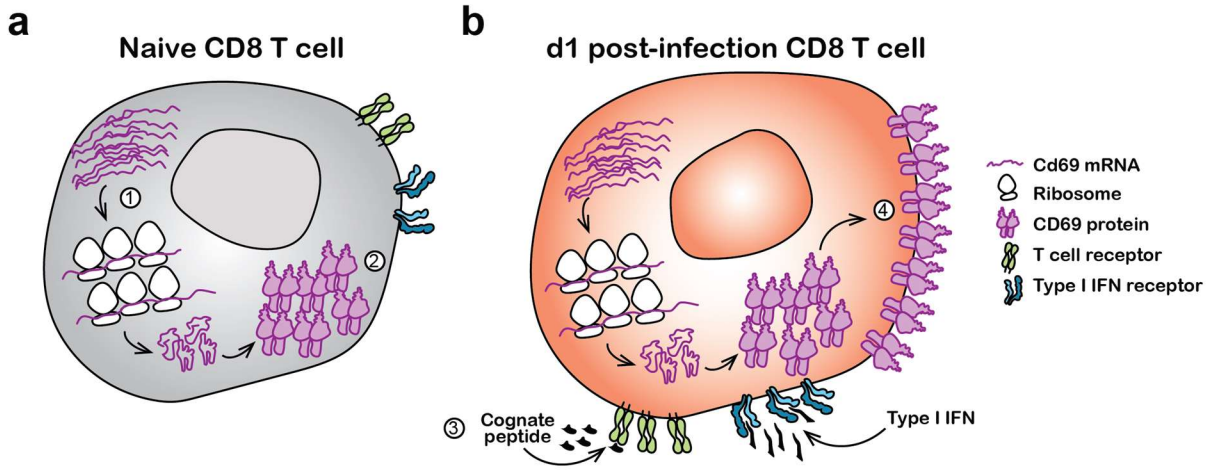

Figure 11. Summary of CD69 transcription and translation within naïve and activated CD8 T cells. (**a**) In naïve CD8 T cells, *Cd69* mRNA is actively translated (1), forming a pool of intracellular CD69 protein (2), which remains poised at the ready for cellular activation. (**b**) Upon TCR (cognate peptide) or cytokine (type I interferon) stimulation (3), CD69 is rapidly expressed on the cell surface (4).

Chapter 5: PD-1 blockade not only promotes effector cell differentiation, but also increases the self-renewal of stem-like CD8 T cells to maintain the number of progenitor cells

Gill AL, Wang PH, Lee J, Hudson WH, Ando S, Araki K, Hu Y, Wieland A, Im SJ, Gavora A, Freeman GJ, Hashimoto M, Reiner SJ, and Ahmed R. (2023). PD-1 blockade not only promotes effector cell differentiation, but also increases the self-renewal of stem-like CD8 T cells to maintain their numbers. *Science Immunology.* (Under revision).

I. Summary

PD-1^{+}TCF-1^{+} stem-like CD8 T cells act as critical resource cells for maintaining T cell immunity in chronic viral infections and cancer. Importantly, these are the cells that provide the proliferative burst of effector CD8 T cells after PD-1 therapy. An important question is what happens to the numbers of these stem-like CD8 T cells after PD-1 blockade. Is there a loss of these progenitor CD8 T cells? Also, what happens to the gene expression program and functionality of these cells following PD-1 therapy? We have addressed these key questions using the mouse model of chronic LCMV infection. We found that PD-1 blockade not only increases effector differentiation from the stem-like cells but also increases the self-renewal of these PD-1^{+}TCF-1^{+} CD8 T cells to maintain their numbers. This self-renewal was mTOR-dependent. Phenotypically, the stem-cell like transcriptional signature and *in vivo* functional properties of these progenitor CD8 T cells remained intact following PD-1 blockade. These findings have implications for PD-1 directed immunotherapy in humans.

II. Introduction

PD-1^{+}TCF-1^{+} stem-like CD8 T cells are crucial resource cells that sustain ongoing T cell responses during chronic viral infection and cancer (128, 130, 229–232). These quiescent stem-like CD8 T cells, also referred to as precursors of exhausted CD8 T cells, do not express effector

molecules and reside in lymphoid tissues where they undergo a slow self-renewal and can also proliferate and differentiate into effector CD8 T cells that eventually get exhausted (104, 107, 129, 134, 135, 137, 233, 234). Most importantly, PD-1 directed immunotherapy acts specifically on this subset of cells—inducing a proliferative burst that accelerates their differentiation into effectors (129, 137, 234). This substantial increase in the numbers of effector CD8 T cells emerging from the stem-like cells after removing the PD-1 brake, combined with PD-1 blockade at the target site results in efficient killing of virally-infected or tumor cells (137, 139, 235–237). PD-1 is now the leading immune check point inhibitor and PD-1 directed immunotherapy is approved for the treatment of several different cancers (238–243).

An important unanswered question is what happens to the numbers of PD-1^{+}TCF-1^{+} stem-like CD8 T cells after PD-1 therapy? Is there a loss of these progenitor CD8 T cells because many more of these cells are differentiating into effector cells? It is also not known what happens to the gene expression program and functionality of the stem-like CD8 T cells after PD-1 therapy. Do these cells still retain their ability to respond to PD-1 blockade? We have addressed these key questions in this study using the mouse model of chronic LCMV infection (113, 114, 244).

III. Results

Stem-like CD8 T cell numbers are maintained following PD-1 blockade

Mice chronically infected with LCMV (>day 45) were treated with αPD-1 or αPD-L1 antibody for two weeks and then examined for CD8 T cell responses in the spleen (Fig. 1A). As in earlier studies, PD-1 blockade resulted in an increase in the percentage and numbers of PD-1^{+} and LCMV-specific CD8 T cells, based on staining with H-2D^{b}GP33 and H-2D^{b}GP276 tetramers (Fig. 1B, C, and D) (151). Also consistent with previous studies, the largest increase both in terms of the

percentage and total numbers was seen in the PD-1^{+}Tim-3^{+}CX3CR1^{+} transitory effector CD8 T cells that are derived from the stem-like CD8 T cells (Fig. 1E, F, and G) (137, 139). Consequently, there was a significant decrease in the percentage of the PD-1^{+}TCF-1^{+} stem-like CD8 T cells (Fig. 2B-G). However, there was no decrease in the total numbers of these progenitor cells (Fig. 2H, I, and J). In fact, there was a significant increase in the numbers of the TCF-1^{+} stem-like cells after PD-1 blockade; this was seen for total PD-1^{+} progenitor cells and for LCMV-specific GP33^{+} and GP276^{+} progenitor CD8 T cells (Fig. 2H, I, and J). This is a surprising and potentially important finding that had been overlooked in earlier studies because the quantitation of the stem-like CD8 T cell subset after PD-1 blockade had not been extensively done. The data shown in Figure 1 are based on a large number of mice (n=54 to 75), thus providing good statistical significance. We also show the data from 12 different experiments (Fig. 3, experiments #1-12). It is worth noting that most of these individual experiments show the same pattern. However, in a few experiments the increase in the number of progenitor CD8 T cells is not statistically significant but it is still very clear that there is no decrease in their numbers. We also examined the stem-like CD8 T cell response after PD-1 blockade in the LCMV Clone 13 chronic infection model without transient CD4 T cell depletion and saw the same results; stem-like cells increased (or were at least maintained) following PD-1 blockade in both GP276^{+} and GP33^{+} populations (Fig. 4). Ultimately, we found that stem-like CD8 T cells were not only maintained at day 14 following PD-1 blockade, but their population also remained stable for another 8 weeks in the absence of further treatment (Fig. 5).

Stem-like CD8 T cells increase their self-renewal following PD-1 blockade

Why were stem-like CD8 T cells not depleted while PD-1 blockade was actively recruiting them to differentiate? We hypothesized that PD-1 blockade may contribute to their maintenance by increasing their proliferation. To address this we examined proliferation of stem-like CD8 T cells at days 8 and 14 after PD-1 blockade. We found that there was a significant increase in the percentage and numbers of $Ki67^{+}PD\text{-}1^{+}TCF\text{-}1^{+}$ CD8 T cells at day 8 after PD-1 blockade (Fig. 6A, D, and G). The same pattern was seen with LCMV-specific $PD\text{-}1^{+}TCF\text{-}1^{+}$ stem-like CD8 T cells (Fig. 6B-C, E-F, and H-I). At day 14 after PD-1 blockade the percentage of $Ki67^{+}$ stem-like CD8 T cells had returned to baseline levels but the total numbers of proliferating cells were still higher (Fig. 6G-I). These results show that PD-1 blockade not only promotes the differentiation of stem-like CD8 T cells into effector cells but it also increases the proliferation and self-renewal of the stem-like CD8 T cells. This ensures that the numbers of these critical resource CD8 T cells are maintained following PD-1 blockade. Upon further investigation, we also determined that PD-1 sustains CD8 T cells in an mTOR-dependent manner. We administered rapamycin to mice daily for a period of two weeks, in combination with αPD-L1 (Fig. 7A). Control mice received sham treatment during the same time period. Following αPD-L1 treatment, stem-like CD8 T cells significantly increased by absolute number on day 14, as previously shown, but the addition of rapamycin abrogated this effect, keeping their numbers at pre-treatment levels (Fig. 7B). On day 8 post-treatment, the absolute number of proliferating $Ki67^{+}TCF\text{-}1^{+}$ stem-like CD8 T cells was also reduced following the addition of rapamycin (Fig. 8A-C). Thus, mTOR signaling was needed for stem-like cells' increased self-renewal and the PD-1 inhibitory pathway also regulates this process.

Stem-like CD8 T cells' transcriptional program is conserved following PD-1 blockade

We next asked whether this proliferative response following PD-1 therapy changes the transcriptional program of the stem-like CD8 T cells. Of course, prior studies have demonstrated transcriptional and epigenetic stability of exhausted CD8 T cells following immunotherapy (121, 245), but we sought to study the effect of PD-1 blockade on the stem-like progenitor population exclusively. To do this, we sorted stem-like CD8 T cells and the more differentiated Tim-3$^+$ CD8 T cells from LCMV chronically infected mice that had been treated with αPD-1 antibody for 14 days or from chronically infected mice that had received no treatment (Fig. 9A). RNA-seq analysis was done on these sorted CD8 T cell subsets from the two groups of mice. We found that the treated stem-like CD8 T cells were transcriptionally almost identical to untreated stem-like cells. Using principal component analysis (PCA), we compared the subsets and treatment groups: sorted stem-like cells clustered together tightly along both PC1 and PC2—regardless of prior treatment (Fig. 9B). A heatmap of selected genes also showed minimal to no changes in the stem-like CD8 T cells after PD-1 blockade (Fig. 9C). We further confirmed these findings by doing single cell RNA-seq (scRNA-seq) on LCMV GP33 tetramer sorted CD8 T cells from untreated or PD-1 treated chronically infected mice (Fig. 9D, E, and F)**.** Taken together, these results show that the canonical gene expression program of LCMV-specific PD-1$^+$TCF-1$^+$ stem-like CD8 T cells is not changed by PD-1 therapy.

Stem-like CD8 T cells' functional program is conserved following PD-1 blockade

The most critical question was whether the functionality of the stem-like CD8 T cells was intact after the first cycle of PD-1 treatment. Do these CD8 T cells retain the ability to proliferate

and differentiate following a viral challenge? And, most importantly, can these PD-1 treated stem-like CD8 T cells respond efficiently to a second round of PD-1 blockade?

To address the first question, we transferred stem-like cells from untreated or cycle 1 αPD-1-treated chronically infected mice into naïve recipients and challenged these mice with LCMV Clone 13 (Fig. 10A). Robust proliferation of donor stem-like CD8 T cells was observed in the blood between days 0 and 14 post-infection with equivalent expansion of untreated stem-like cells and PD-1 treated stem-like cells (Fig. 10B, right). As expected, there was minimal expansion of the more differentiated Tim-3^{+}PD-1^{+} CD8 T cells (Fig. 10B, left). A similar pattern was seen in the spleen, liver, and lung at day 14 after infection with stem-like CD8 T cells from both groups of mice expanding equally well (Fig. 10C-I). Phenotypically, donor stem-like cells underwent the classical differentiation to become Tim-3^{+}TCF-1^{-}, while a small proportion remained Tim-3-TCF-1^{+} (Fig. 10J). Thus, no defect was observed in the proliferative capacity of cycle 1-treated versus untreated stem-like cells in any tissue examined.

Anti-PD-1 treatment did not dampen the magnitude of proliferation or the differentiation of stem-like CD8 T cells in response to Clone 13 challenge. But we next wondered: can αPD-1-treated stem-like cells respond to secondary PD-1 blockade? Do stem-like cells retain their proliferative capacity following treatment in the setting of chronic infection? We isolated cycle 1 αPD-1-treated stem-like cells, transferred them into infection-matched, untreated recipients, and treated them with a second round of αPD-1 (or isotype) (Fig. 11A). We found that cycle 1-treated stem-like cells were able to mount a robust proliferative response following an additional cycle of PD-1 blockade, as compared the cycle 1-treated stem-like cells that did not receive a second round of therapy—by both frequency and total number of cells in the PBMC, spleen, liver, and lung (Fig. 11B-G). Responses were equivalent to those from cycle 1 blockade alone (Fig. 12). Also, cycle 1

treatment did not alter the characteristic differentiation of Tim-3^{+}TCF-1^{-} effector cells from the treated stem-like population (Fig. 11H and I).

IV. Discussion

These studies using the mouse model of chronic LCMV infection have addressed a critical and unanswered question about what happens to the numbers and function of PD-1^{+}TCF-1^{+} stem-like CD8 T cells after PD-1 therapy. Previously, we found that PD-1 blockade increases the proliferation and differentiation of stem-like CD8 T cells into highly functional effectors, but we now show that PD-1 blockade also increases the self-renewal of these cells (Fig. 13). Increased self-renewal prevents depletion of this crucial resource population. This finding suggests that PD-1 signaling regulates stem-like CD8 T cells' self-renewal and highlights an important feature of chronic infection: homeostatic maintenance of the stem-like population.

We speculate that there are key mechanisms which regulate stem-like CD8 T cells' survival and proliferation at steady-state, and that PD-1 signaling may regulate these processes. Stem-like CD8 T cells express higher transcript levels of cytokines (*Tnf* and *Il2*), co-stimulatory molecules (*Icos* and *Cd28*), and survival molecules (*Tcf7, Lef1, Il7r,* and *Id3*) as compared to their more-differentiated counterparts. PD-1 signaling may directly modulate cytokine and/or co-stimulatory signals to sustain a slow turnover at steady state, explaining why blockade of these signals results in massive proliferation.

We also propose several mechanisms by which stem-like cells self-renew to maintain their numbers. We found that mTOR signaling is required for early proliferation of the stem-like population following PD-1 blockade. This pathway can be manipulated in humans and thus modulation of stem-like cell numbers may also be possible in the clinic.

Finally, we show that stem-like CD8 T cells remain transcriptionally and functionally intact following PD-1 blockade. This was surprising to us but may be of tremendous relevance to clinical checkpoint therapy. We can now predict that PD-1 blockade is unlikely to deplete or functionally diminish stem-like CD8 T cells in clinical settings. It will be especially interesting to see if this holds when PD-1 therapy is continued for extended periods of time. Above all, our results suggest that poor clinical responses to PD-1 therapy may not originate from defects within the stem-like compartment; it may be of use to find other targets of therapeutic intervention.

V. Materials and Methods

Mice and viruses. LCMV infections were performed as previously described (129). All animal experiments were performed in accordance with Emory University Institutional Animal Care and Use Committee. C57BL/6J and CD45.1 congenic female mice were purchased from Jackson Laboratory. For chronic infections, 6-8 week old mice were injected intraperitoneally (i.p.) with 300 μg of the $CD4^+$ T cell-depleting antibody GK1.5 (Bio X Cell) one day before and one day after intravenous (i.v.) injection with 2×10^6 pfu LCMV Clone 13. Some experiments were also performed without this transient CD4 depletion.

PD-1 blockade. LCMV chronically infected mice (>45 days post-infection) received either PD-1 blockade or no treatment. Mice that received PD-1 blockade were injected i.p. with either 200ug of mouse anti-mouse αPD-1 (clone 2203, D265A mutation in the Fc portion) or 200ug of rat anti-mouse αPD-L1 (clone 10F.9G2). Control mice received 200ug of isotype control in PBS or nothing. Mice were injected every three days and sacrificed 14 days after the first dose.

Administration of rapamycin. Rapamycin (Wyeth) was administered to mice i.p. daily for 8 days or 2 weeks. The daily dose of rapamycin was 600 μg kg^{-1} (blood levels; 40–100 ng ml^{-1}). Control mice received daily sham treatment (injection of the buffer without rapamycin).

Cell isolation. Spleens were isolated from mice and smashed through 70um nylon cell strainers to remove clumps. Cells were spun down at 2,000 RPM for 10 minutes, and the supernatant was removed. After resuspending the pellet, cells were incubated at room temperature with 1 ml of Ack lysis buffer for 2 minutes in order to lyse the RBCs. After incubation, an additional 35 ml of RPMI + 5% FBS was added to dilute the Ack lysis buffer, and the cells were spun down at 2,000 RPM for 10 minutes. The resulting cell pellet was resuspended in PBS + 2% FBS + 0.5mM EDTA and cells were transferred to a 96-well round-bottom plate for staining. For lungs, tissue was incubated at 37°C with Collagenase-I prior to straining. For both the liver and lungs, lymphocytes were isolated via Percoll gradient.

Flow cytometry. Surface staining was performed by incubating cells with fluorochrome-conjugated antibodies against CD8, CD4, CD19, PD-1, CD44, Tim-3, CD101, CX3CR1, CD45.1, and CD45.2 (BD Bioscience, eBioscience, and Biolegend). Cells were incubated on ice for 30 minutes in PBS + 2% FBS + 0.5mM EDTA. Ki67, Granzyme B, and TCF-1 (BD Bioscience, eBioscience, and Cell Signaling Technology) were stained intracellularly with the eBioscience Foxp3/Transcription Factor Fixation/Permeabilization Kit (Thermofisher). For detecting LCMV-specific CD8 T cell responses, peptides bound to major histocompatibility complex (pMHC) tetramers were prepared against LCMV GP33 and LCMV GP276 proteins, as described previously (12, 191). Cell viability was determined with the Live/Dead fixable aqua or near IR dead cell stain

kit (Invitrogen). Samples were acquired on an LSR II or Symphony flow cytometer (BD Biosciences) and data were analyzed with FlowJo software (TreeStar).

Bulk RNA-sequencing and analysis. PD-1^{+}Tim-$3^{+}$$CD73^{-}$ (terminally-differentiated) and PD-1^{+}Tim-$3^{-}$$CD73^{+}$ (stem-like) $CD8^{+}$ T cells were isolated from mice infected with LCMV Clone 13 >45 days prior to the sort. Using FACS, the two populations were sorted on day 14 following αPD-1 blockade or isotype treatment. Naive $CD44^{lo}CD62L^{hi}$ CD8 T cells from uninfected mice were also isolated by FACS. Samples were sorted on a FACSAria II (BD Biosciences). After sorting, RNA was isolated from each sample using the All-Prep DNA/RNA Micro Kit (Qiagen) and then submitted to the Emory Yerkes Nonhuman Primate Genomics Core. Reads from RNA-seq were aligned to the mm10 genome [accessed through Ensembl (192)] with STAR version 2.7.

Single cell RNA-sequencing and analysis. scRNAseq data was obtained from Hashimoto et al. (236). In their processing, mice infected with LCMV Clone 13 for >45 days were treated with αPD-L1 or left untreated. On day 14 post-treatment, mice were sacrificed and $GP33^{+}$ $CD8^{+}$ T cells were magnetically enriched and then sorted on a FACS Aria II (BD Biosciences). The initial study included additional treatment groups, but in our study only the naïve, untreated, and αPD-L1 sequencing results were re-analyzed. The Yerkes Nonhuman Primate Genomics Core generated a single cell gene expression library, and this data was aligned using CellRanger version 4 (10X Genomics). Outlier cells with high numbers of reads originating from mitochondrial genes and presumed doublets were excluded from the dataset. Genes encoded on mitochondrial chromosomes were also excluded from analysis. Data was normalized and scaled using the Seurat package [v4.0.4 (246–249)] and plots were made with ggplot2 or GraphPad Prism. Shared nearest

neighbor clustering was performed in Seurat with 200 neighbors, 6 principal components (1-7, excluding principal component 4, which was primarily based on ribosomal genes), and a resolution of 0.8. UMAP dimensionality reduction was performed with identical parameters and a minimum distance of 2. A phylogenetic tree was also created with identical parameters, using Seurat's BuildClusterTree. For analysis of the stem-like cluster individually, prior clustering was used to generate a new data object, on which additional UMAP dimensionality reduction was performed (with 500 neighbors, principal components 1-7 [excluding 4], a resolution of 0.9, and a minimum distance of 1).

Adoptive transfer experiments. For the transfer followed by LCMV challenge: Mice infected with LCMV Clone 13 (as above) for >45 days were injected αPD-1 or IgG1 isotype control in PBS. Injections were given every three days and mice were sacrificed on day 14 and pooled into αPD-1-treated or isotype-treated groups. $CD8^+$ T cells in the samples were purified with the EasySep Mouse $CD8^+$ T Cell Isolation Kit (StemCell Technologies), then two CD8 T cell subsets were sorted from each treatment group using FACS: PD-1^+Tim-$3^+$$CD73^-$ (terminally-differentiated) and PD-1^+Tim-$3^-$$CD73^+$ (stem-like). Cells were reconstituted in RPMI and 2-2.5 $\times 10^4$ sorted cells from each group were transferred i.v. into uninfected, age-matched CD45.1^+ recipients. On the next day, the recipients were challenged with 2×10^6 pfu LCMV Clone 13, i.v. Recipients were bled one week post-transfer, and then sacrificed two weeks post-transfer, at which time cells were isolated from the spleen, liver, lung, and PBMC, and stained as above.

For the transfer followed by secondary PD-1 blockade: Mice infected with LCMV Clone 13 (as above) for >45 days were injected with αPD-1 every three days. On day 14, mice were sacrificed and isolated splenocytes were pooled, purified with the EasySep Mouse $CD8^+$ T Cell

Isolation Kit (StemCell Technologies), and sorted using FACS into a pure population of PD-1^{+}Tim-$3^{-}$$CD73^{+}$ stem-like CD8 T cells. Sorted cells were reconstituted in RPMI and 1×10^{5} cells were transferred i.v. into infection-matched $CD45.1^{+}$ recipients. Recipients were then treated with a second cycle of PD-1 blockade and sacrificed two weeks later. At this time, cells were isolated from the spleen, liver, lung, and PBMC, and stained as above. In some experiments, isotype-treated donor stem-like CD8 T cells were also isolated, sorted, and transferred, followed by secondary blockade.

Statistical analysis. All experiments were analyzed using Prism 9 (GraphPad Software). Statistical differences were assessed using unpaired two-tailed t tests, one-way ANOVA with Tukey's test for multiple comparisons, or two-way ANOVA with Sidak's or Dunnett's tests for multiple comparisons.

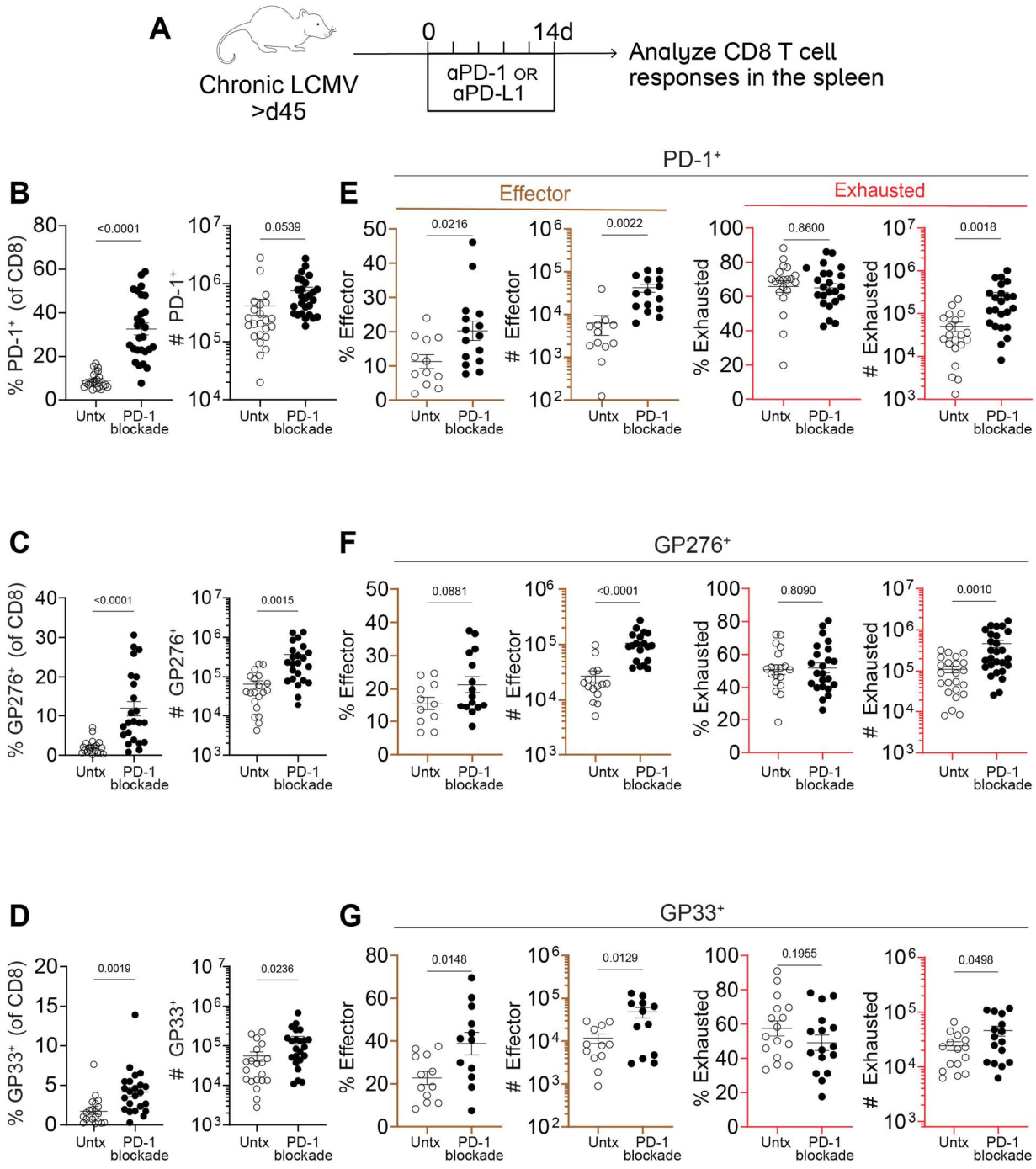

Figure 1. PD-1 blockade promotes effector cell differentiation. (A) LCMV chronically infected mice were treated with αPD-1 or αPD-L1 every three days for two weeks. CD8 T cell responses were analyzed on day 14. (B-D) Frequency and absolute number of indicated LCMV-specific CD8 T cells within the spleen. (E-G) Frequency and absolute number of indicated LCMV-specific CD8 T cells that have a transitory effector (Tim-3$^+$CX3CR1$^+$) or terminally-differentiated (Tim-3$^+$CD101$^+$) phenotype. Mean ± SEM. Unpaired two-tailed t tests (B-G).

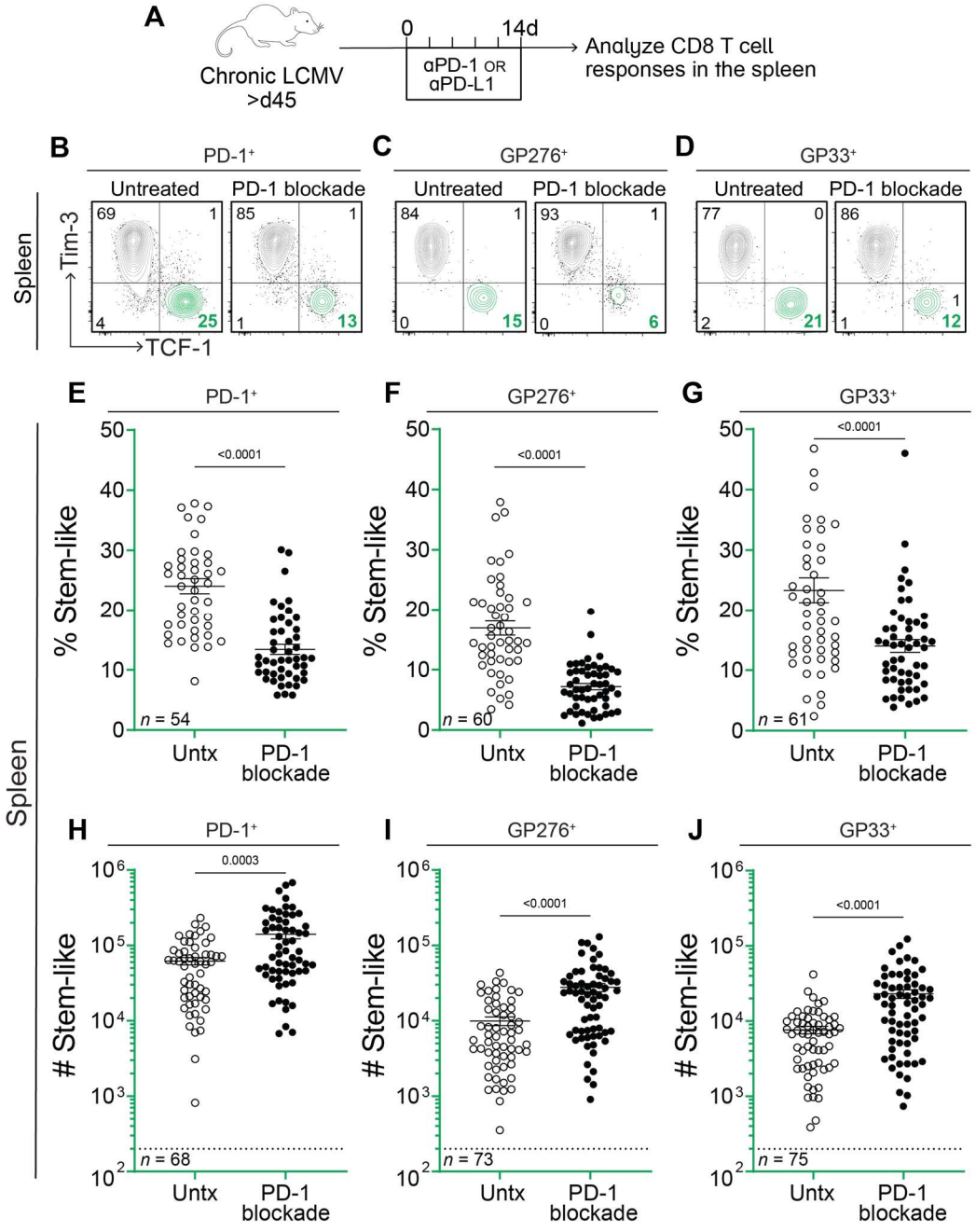

Figure 2. PD-1 blockade decreases the frequency of stem-like CD8 T cells but their numbers increase. (A) LCMV chronically infected mice were treated with αPD-1 or αPD-L1 every three days for two weeks. CD8 T cell responses were analyzed on day 14. (B-D) Representative flow plots showing expression of TCF-1 and Tim-3 on total PD-1$^+$, GP276$^+$, and GP33$^+$ CD8 T cells with and without αPD-1/L1 treatment. (E-G) Frequency of TCF-1$^+$Tim-3$^-$ stem-like cells among the LCMV-specific CD8 T cell populations indicated above each plot. (H-J) Absolute number of stem-like cells among the LCMV-specific populations indicated above each plot. Dotted lines indicate the limit of detection. The number of mice in each plot is shown in the bottom left corner. Mean ± SEM. Unpaired two-tailed t tests (E-J).

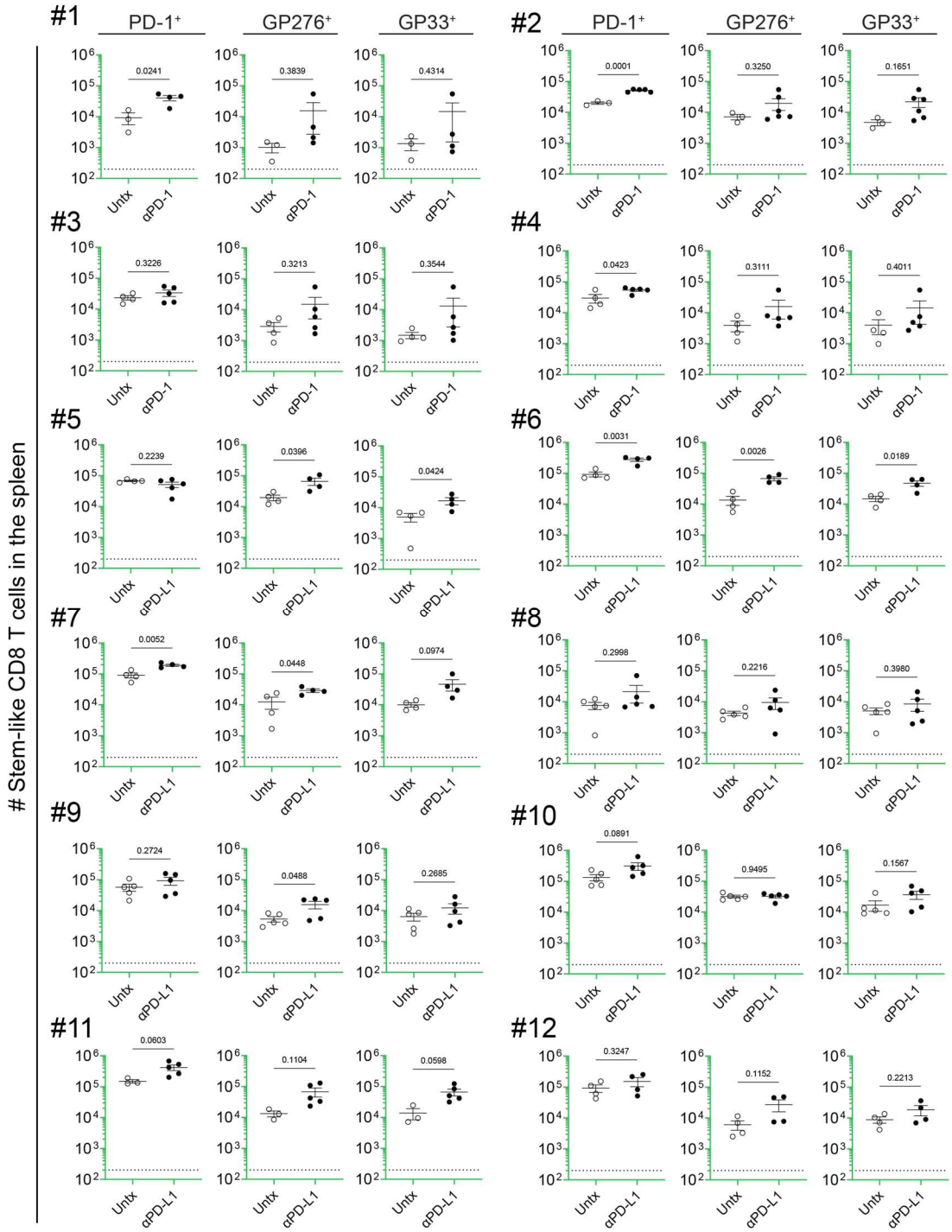

Figure 3. Quantitation of stem-like CD8 T cells after PD-1 blockade. Stem-like CD8 T cell numbers following PD-1 blockade in 12 separate experiments. (#1-12) Absolute number of stem-like cells among PD-1$^+$, GP276$^+$, and GP33$^+$ CD8 T cells within the spleen. Each panel represents one single experiment. Plots in Fig. 1 were generated from pooling this data. Mice were treated with αPD-1 for experiments #1-4 or αPD-L1 for experiments #5-12. Mean ± SEM. Unpaired two-tailed t tests (#1-12).

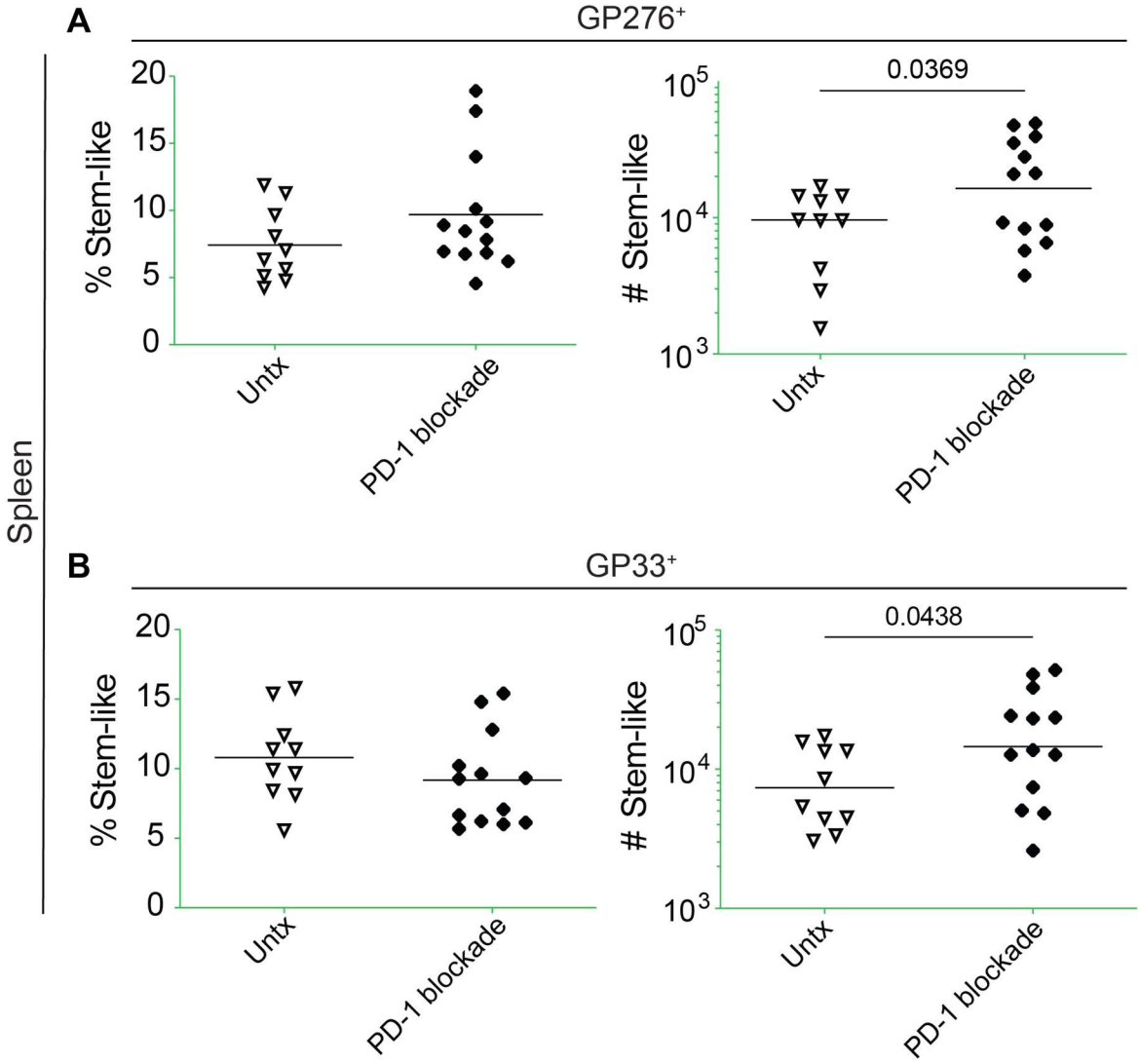

Figure 4. Quantitation of stem-like CD8 T cells after PD-1 blockade in chronic LCMV infection without transient CD4 depletion. Chronically LCMV-infected mice (infected without CD4 depletion) were treated with αPD-L1 for two weeks, starting on day 20 post-infection. (A-B) Frequency and absolute number of PD-1^{+}TCF-1^{+} cells among GP276^{+} and GP33^{+} CD8 T cells. Mean ± SEM. Unpaired two-tailed t tests (A and B).

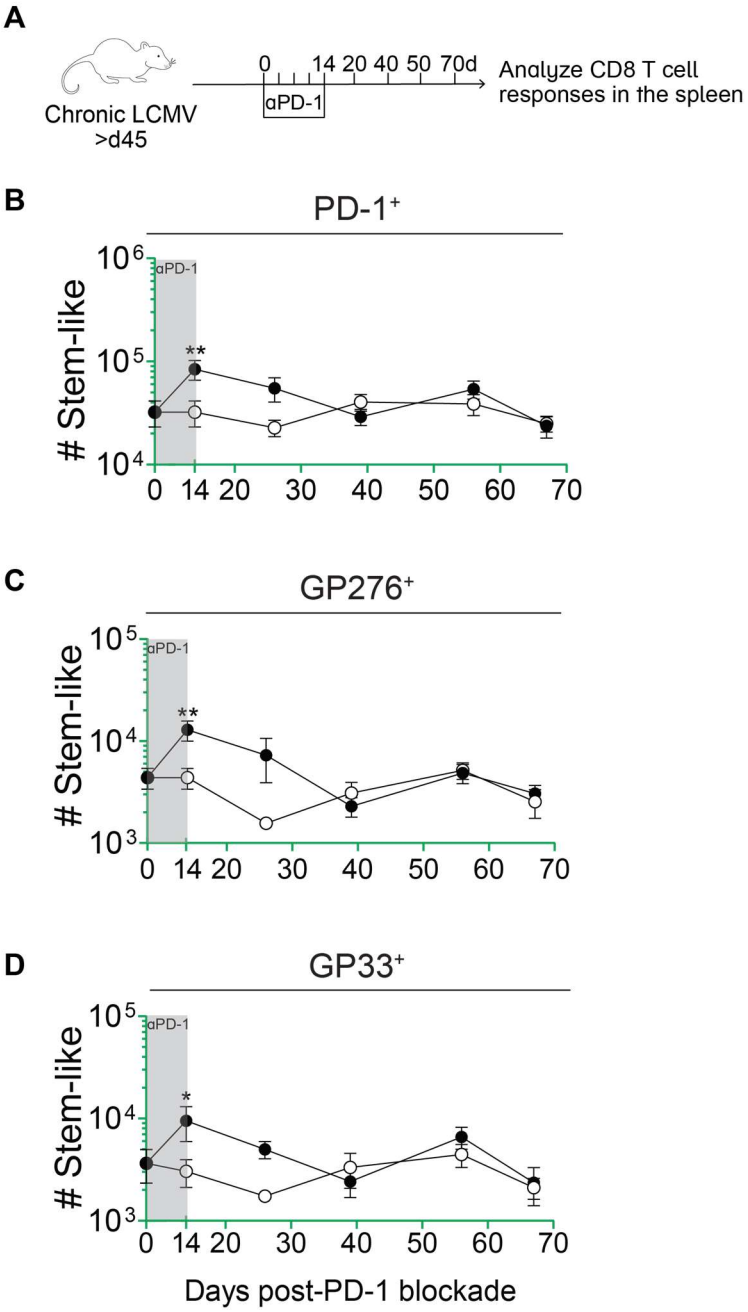

Figure 5. Stem-like CD8 T cells are maintained up to 8 weeks following initial PD-1 blockade. (A) LCMV chronically infected mice were treated with αPD-1 every three days for two weeks. Following treatment cessation, CD8 T cell responses were analyzed at weeks 2, 4, 6, 8, and 10. (B-D) Absolute number of stem-like cells among the LCMV-specific populations indicated above each plot. Mean ± SEM. Two-way ANOVA with Dunnett's test for multiple comparisons (B-D).

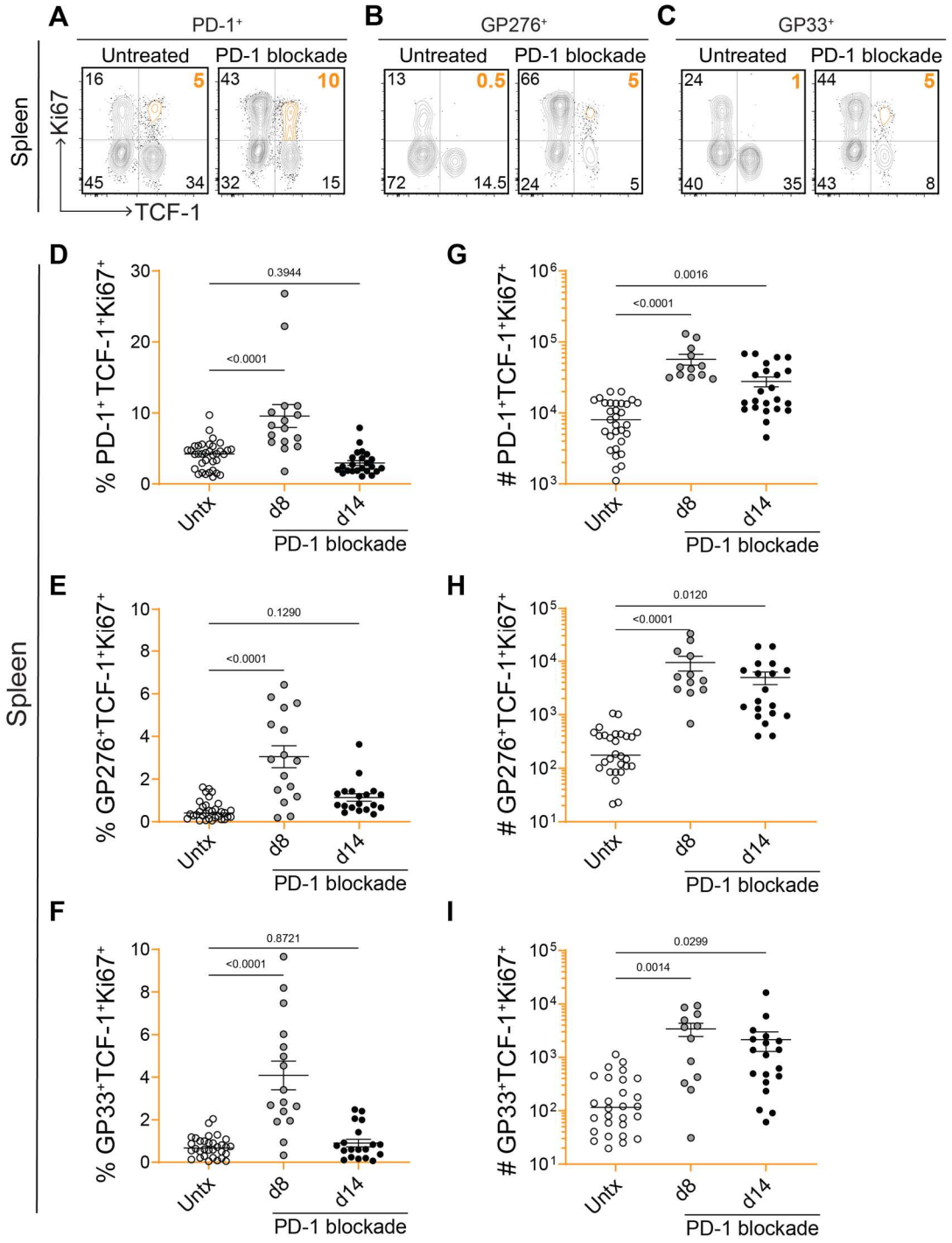

Figure 6. Increased proliferation and self-renewal of stem-like CD8 T cells after PD-1 blockade. (A-C) Representative flow plots showing expression of TCF-1 and Ki67 on total PD-1$^+$, GP276$^+$, and GP33$^+$ CD8 T cells on day 8 post-PD-1 blockade. (D-I) Frequency and absolute number of PD-1$^+$, GP276$^+$, or GP33$^+$ CD8 T cells that were TCF-1$^+$Ki67$^+$ on days 8 and 14 post-blockade. Mean ± SEM. One-way ANOVA with Tukey's test for multiple comparisons (D-I).

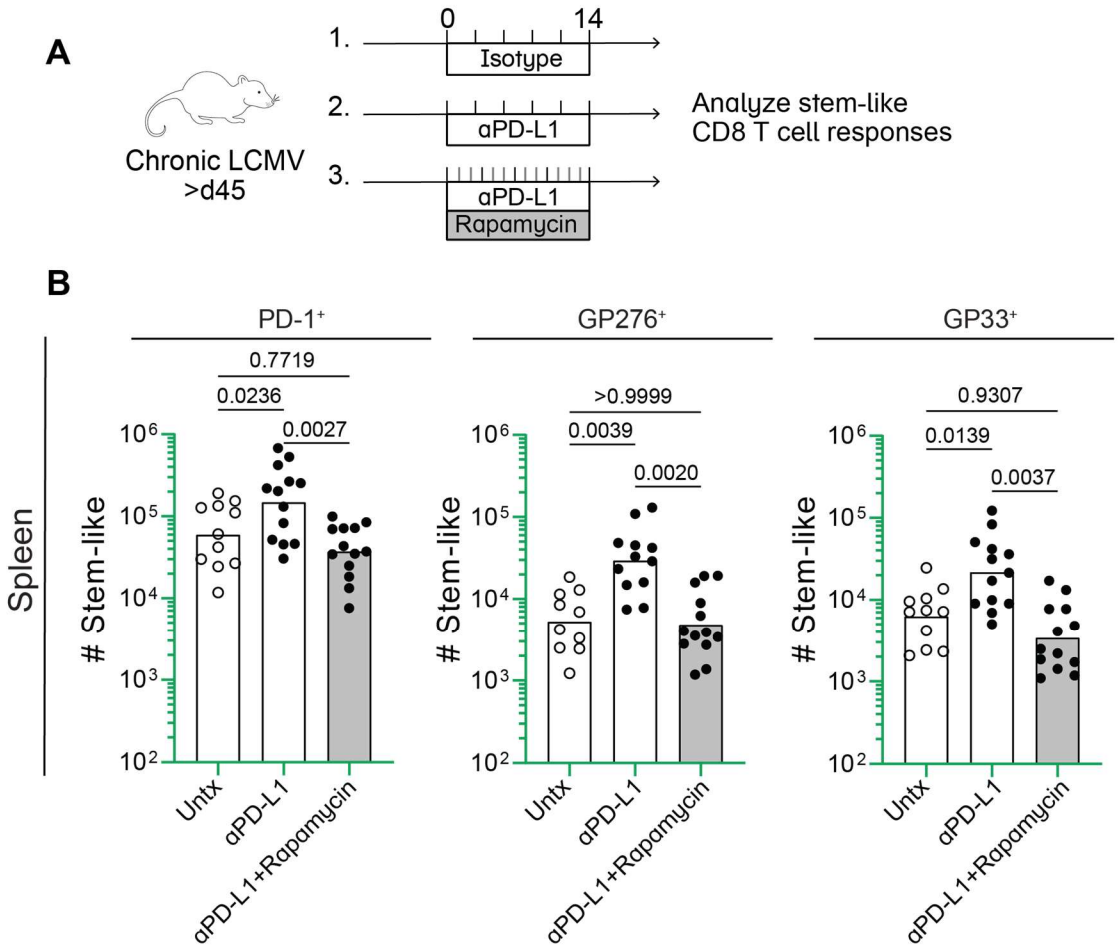

Figure 7. mTOR mediates expansion of stem-like CD8 T cells following PD-1 blockade. (A) Rapamycin was administered to mice daily for a period of two weeks, in combination with αPD-L1. Control mice received sham treatment during the same time period. (B) Absolute number of stem-like CD8 T cells in the spleen among total PD-1^{+}, GP276^{+}, and GP33^{+} CD8 T cells following treatment with isotype, αPD-L1, or αPD-L1 in combination with rapamycin. Mean ± SEM. One-way ANOVA with Tukey's test for multiple comparisons.

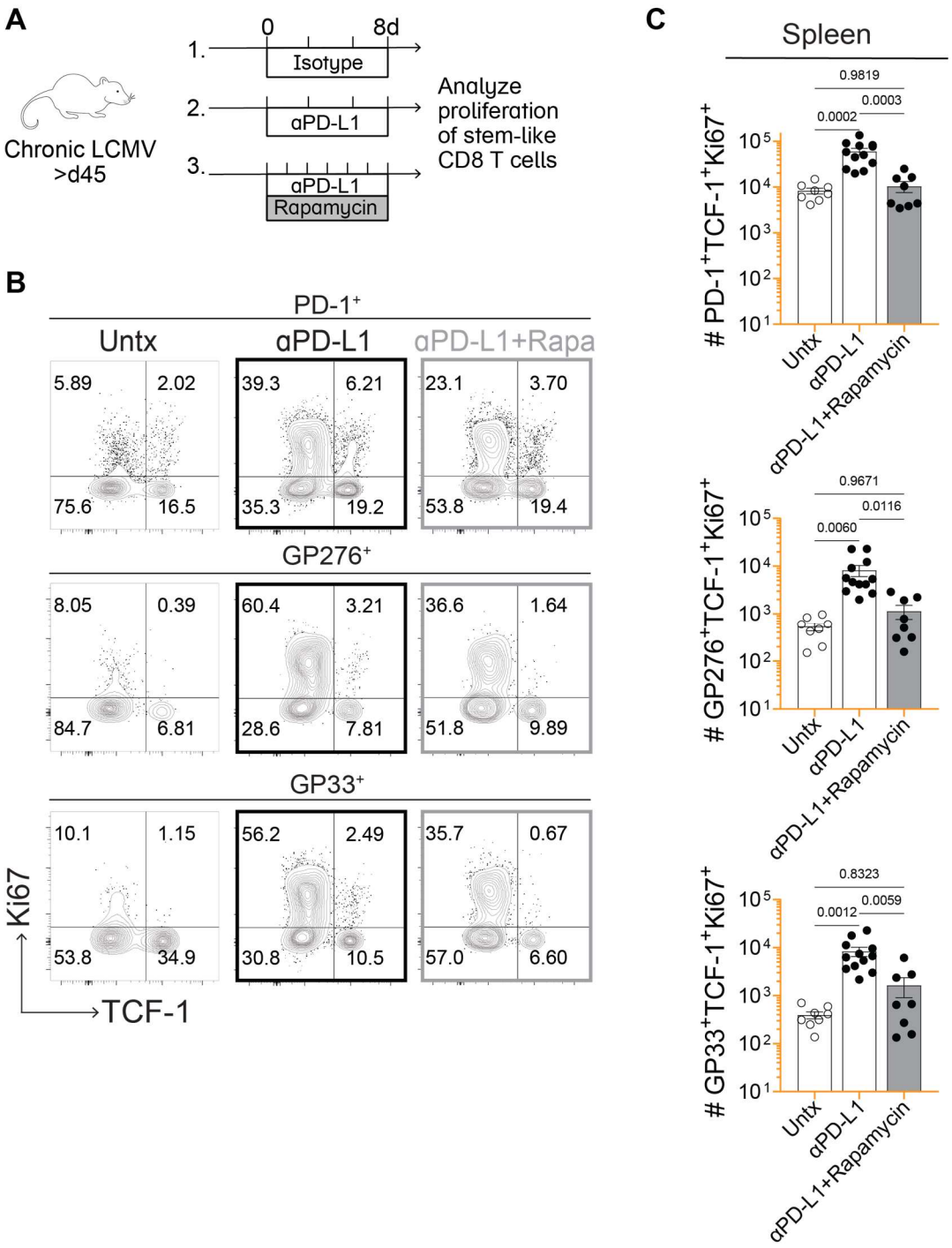

Figure 8. mTOR mediates proliferation of stem-like CD8 T cells following PD-1 blockade. (A) Rapamycin was administered to mice daily for a period of 8 days, in combination with αPD-L1. Control mice received sham treatment during the same time period. (B) Representative flow plots showing expression of TCF-1 and Ki67 on total PD-1$^+$, GP276$^+$, and GP33$^+$ CD8 T cells on day 8 following PD-1 blockade or combination therapy. (C) Absolute number of TCF-1$^+$Ki67$^+$ stem-like CD8 T cells among the LCMV-specific populations indicated above each plot on day 8 post-treatment. Mean ± SEM. One-way ANOVA with Tukey's test for multiple comparisons.

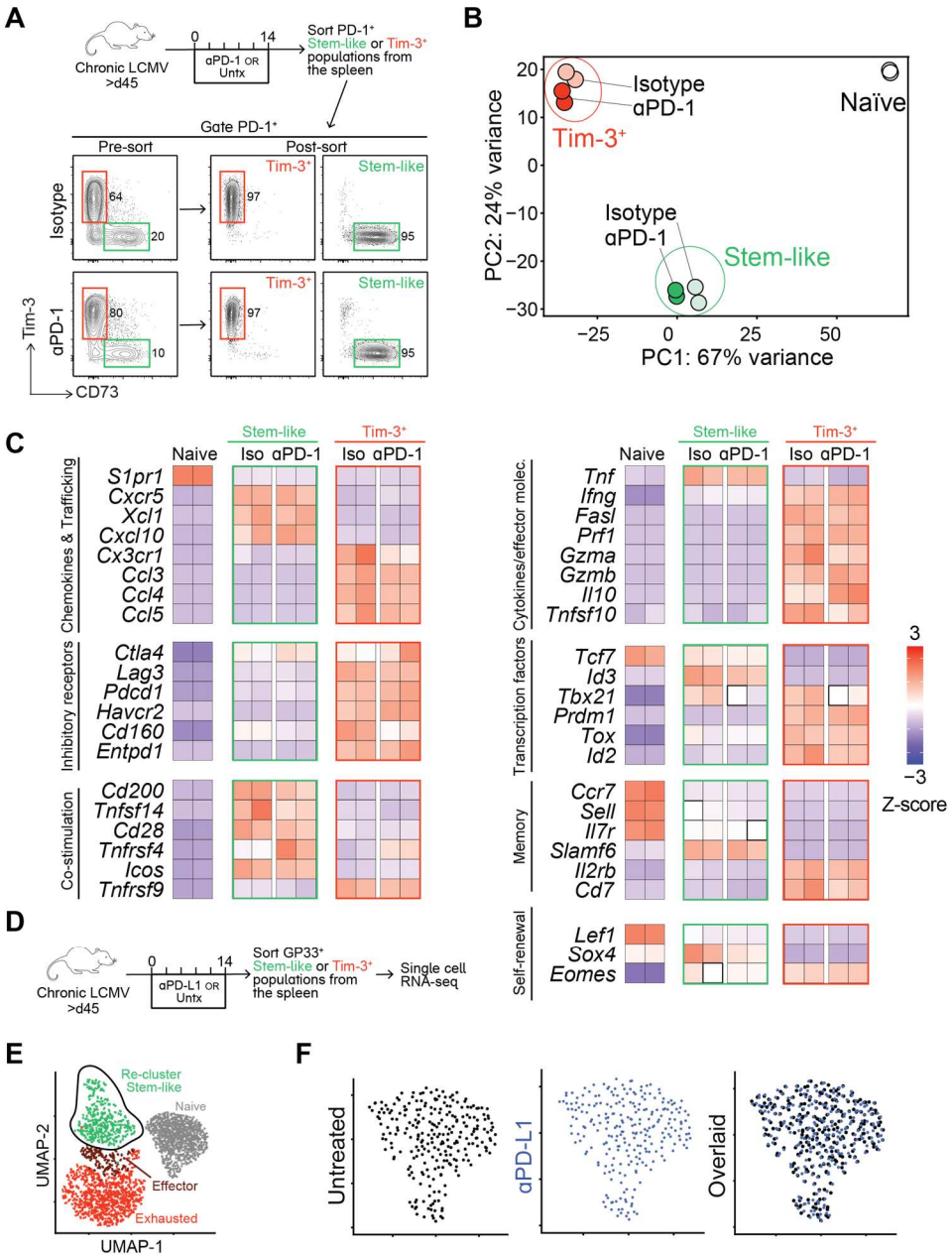

Figure 9. The transcriptional program of stem-like CD8 T cells is conserved after PD-1 blockade. **(A)** Stem-like (PD-1^{+}Tim-3^{-}CD73^{+}) and Tim-3^{+} (PD-1^{+}Tim-3^{+}CD73^{-}) CD8 T cells were sorted from isotype and αPD-1-treated mice at day 14 post-treatment. Representative flow plots showing the pre- and post-sort populations. Naïve CD44^{lo}CD62L^{hi} CD8 T cells were also sorted separately and analyzed as a control. **B**) Principal component analysis (PCA). Each sample is plotted on the top two components (PC1 and PC2). (**C**) Heatmap showing Z-scores of top differentially-expressed genes (DEGs) and genes of interest across the samples. (**D**) scRNA-seq analysis of GP33^{+} CD8 T cells sorted from naïve, untreated, and αPD-L1-treated mice at day 14 post-treatment. (**E**) UMAP with unsupervised clustering analysis showing the transcriptional relationship between samples. (**F**) Re-clustering analysis of the stem-like cell cluster from (E) and comparison of treated and untreated samples by UMAP.

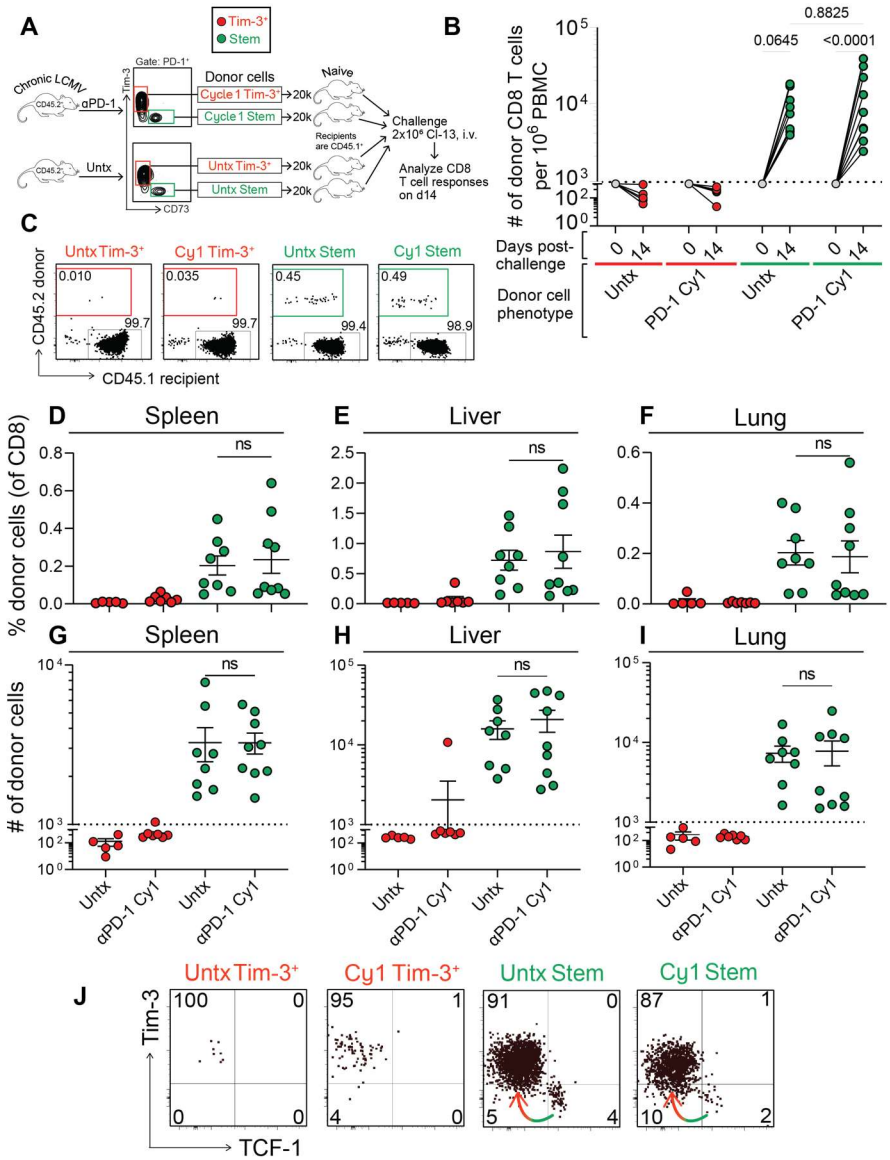

Figure 10. Stem-like CD8 T cells that have received cycle 1 PD-1 therapy can robustly proliferate in response to viral challenge. (A) Stem-like (PD-1$^+$Tim-3$^-$CD73$^+$) and Tim-3+ (PD-1$^+$Tim-3$^+$CD73$^-$) CD8 T cells were each sorted from isotype or cycle 1 αPD-1-treated CD45.2$^+$ donor mice. These subsets were transferred into naïve CD45.1$^+$ recipients that were challenged with LCMV Clone 13 (2×10^6 pfu, i.v.) the next day. Donor CD8 T cell responses were analyzed on day 14 post-challenge. (B) Expansion of donor cells among PBMC by day 14 post-challenge. Dotted line indicates the limit of detection based on 5% estimated take of donor cells within the recipient. (C) Frequency of donor (CD45.2$^+$) and recipient (CD45.1$^+$) CD8 T cells in the spleen. Treatment of the donor cells prior to transfer is shown above each plot. (D-F) Summary of the frequency of donor CD8 T cells within the spleen, liver, or lung. (G-I) Summary of the absolute number of donor CD8 T cells within the spleen, liver, or lung. (J) Phenotype of donor CD8 T cells based on Tim-3 and TCF-1 expression. Colored arrows indicate the direction of differentiation. Mean ± SEM. Two-way ANOVA with Sidak's test for multiple comparisons (B) and one-way ANOVA with Tukey's test for multiple comparisons (D-I).

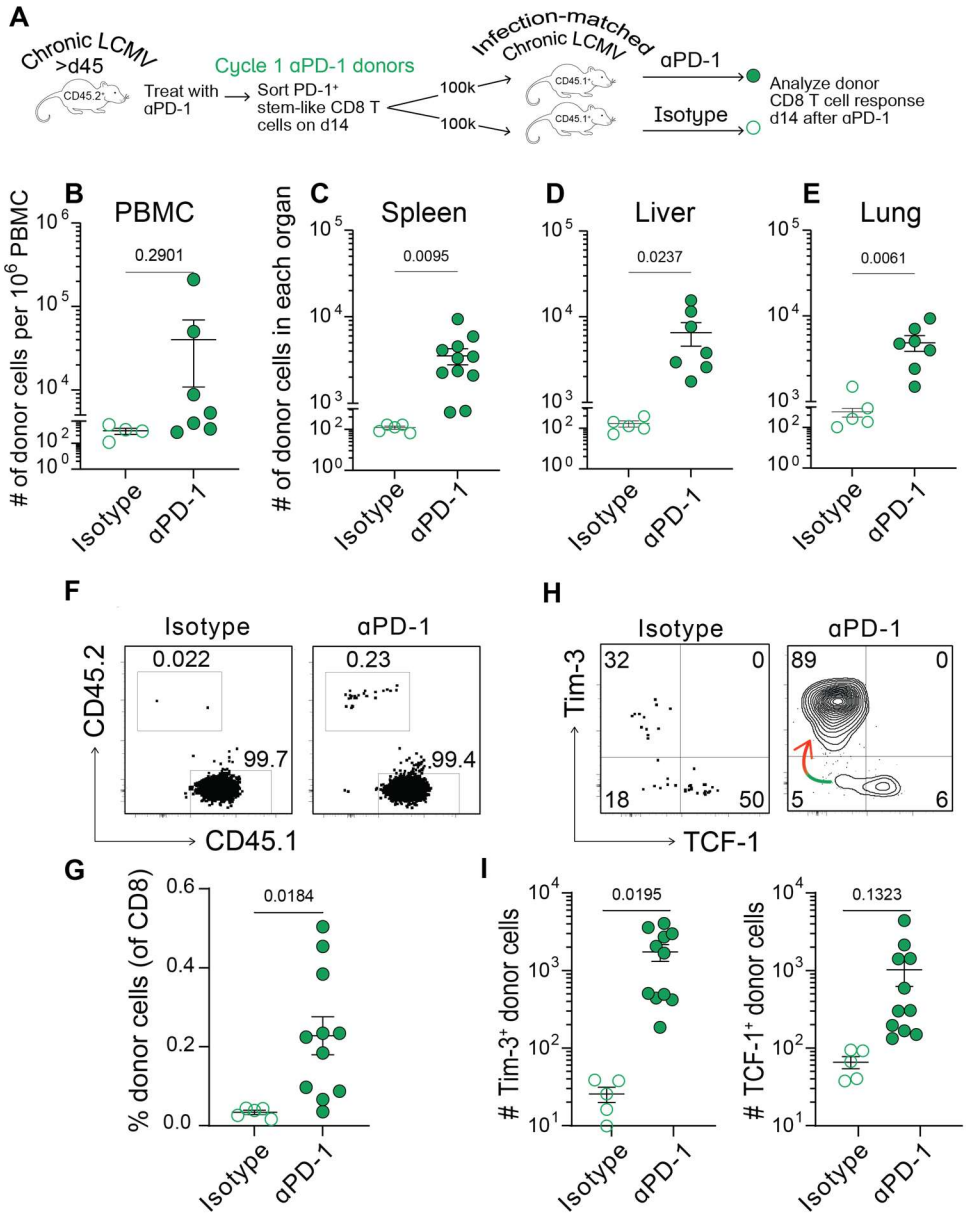

Figure 11. Stem-like CD8 T cells that have received cycle 1 PD-1 therapy can respond to an additional cycle. (A) Stem-like CD8 T cells were sorted from cycle 1 αPD-1-treated CD45.2$^+$ donor mice. These cells were transferred into infection-matched CD45.1$^+$ recipients that were then treated with an additional round of αPD-1. Donor CD8 T cell responses were analyzed on day 14. (B-E) Absolute number of donor CD8 T cells within the PBMC, spleen, liver, or lung at day 14 post-blockade. (F) Frequency of donor (CD45.2$^+$) and recipient (CD45.1$^+$) CD8 T cells following the recipient's treatment (αPD-1 or isotype). (G) Summary of the frequency of donor CD8 T cells following the recipient's treatment. (H) Phenotype of the donor CD8 T cell population after treatment, based on Tim-3 and TCF-1 expression. Colored arrow indicates the direction of differentiation. (**I**) Absolute number of Tim-3$^+$TCF-1$^-$ and Tim-3$^-$TCF-1$^+$ donor CD8 T cells after treatment. Mean ± SEM. Unpaired two-tailed t tests (B-E, G, and I).

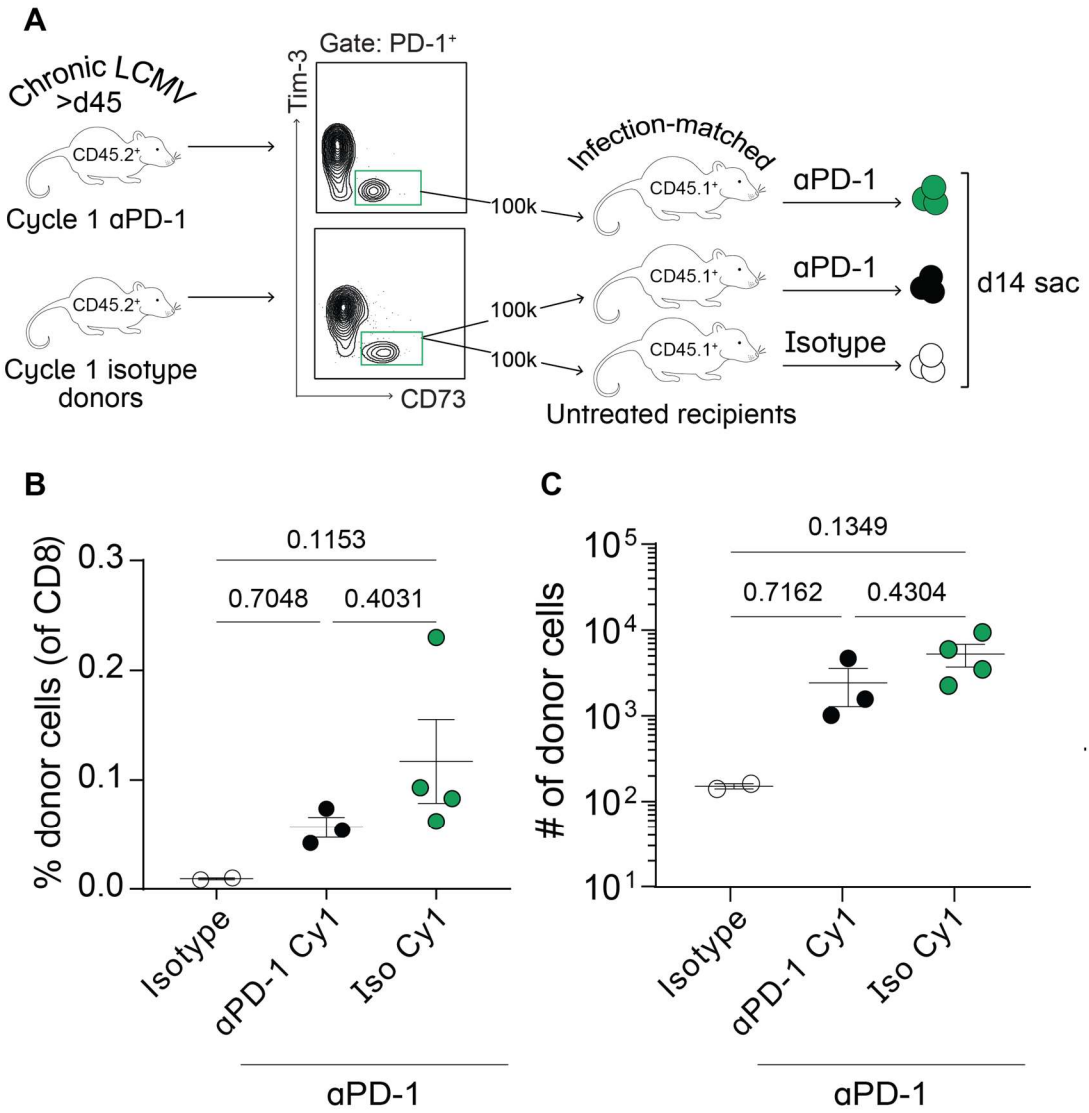

Figure 12. **Cycle 1-treated and untreated mice respond equally well to two week PD-1 therapy**. (**A**) Stem-like CD8 T cells were sorted from Cycle 1 αPD-1-treated or isotype-treated CD45.2$^+$ donor mice and transferred into infection-matched CD45.1$^+$ recipients. These recipients were then treated with an additional round of αPD-1 or isotype for two weeks. Donor CD8 T cell responses were analyzed on day 14. (**B**) Frequency and absolute number (**C**) of donor CD8 T cells within the spleen post-secondary isotype treatment or αPD-1 blockade. Mean ± SEM. One-way ANOVA with Tukey's test for multiple comparisons (B and C).

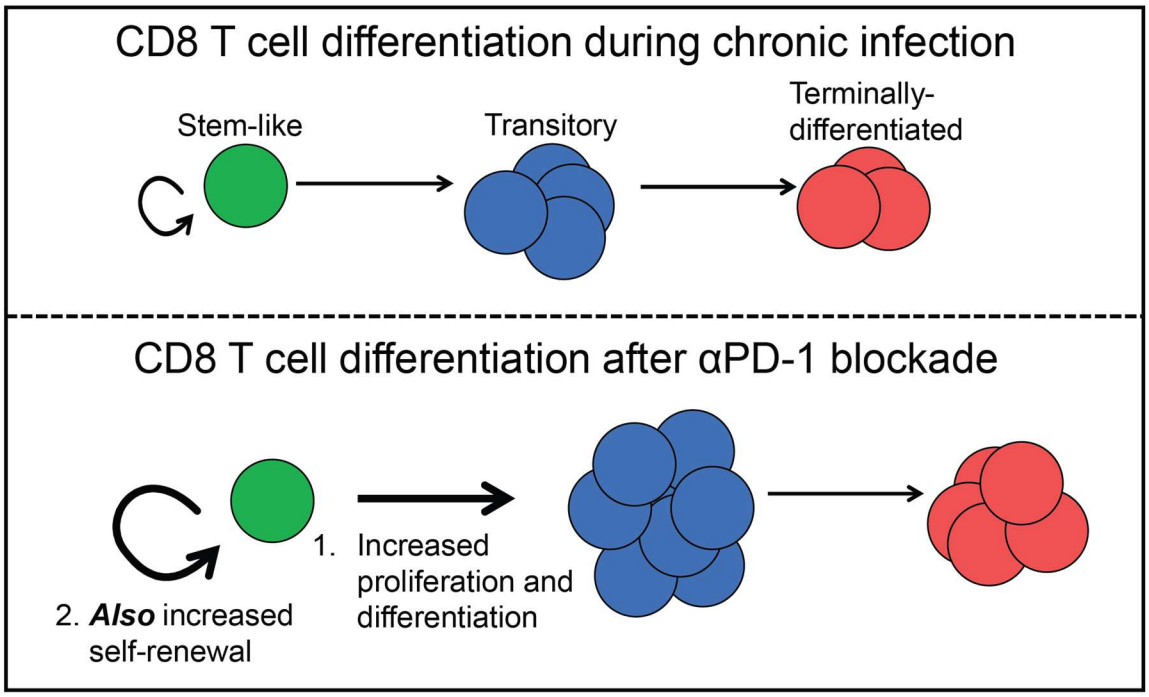

Figure 13. CD8 T cell differentiation during chronic infection and after PD-1 blockade. At steady state during chronic infection, stem-like CD8 T cells undergo slow self-renewal and steadily turn over into transitory effector CD8 T cells. These cells sustain the antiviral response, but gradually become exhausted. Following PD-1 blockade, these processes are accelerated: stem-like cells undergo a proliferative burst to increase the pool of effector cells, while also increasing their self-renewal, so their population is not depleted.

Chapter 6: Discussion

I. Evidence of early memory precursor "precursors"

Understanding the origin of memory CD8 T cells is of immense importance, as this will enable us to develop vaccines and therapeutic interventions that optimize memory CD8 T cell responses. The goal is to design vaccines the induce better memory responses, and T cell therapies that provide more functional and longer-lived responses.

Chapter 2 provided a deeper investigation of the longitudinal phenotype and localization of memory CD8 T cells. These analyses demonstrated that memory CD8 T cells express TCF-1, IL-7Ra, CD62L, CXCR3, and CD28. These cells also localize to the white pulp of the spleen as early as 1 to 2 weeks post-infection. These characteristics define a highly functional, long-lived memory phenotype, which we can use as metric to predict memory responses at earlier points in the infection. Chapter 3 investigated these early responses. We found that, as suspected, the same markers (and many others) could be used to distinguish CD8 T cells that were destined to survive and seed the memory pool versus die. In fact, early heterogeneity in the CD8 T cell response suggested that memory precursors emerge very early following infection—as early as 1 day later. In this case, we suggest their characterization as memory precursor "precursors."

We primarily distinguished the memory precursor precursors though transcriptomic analyses. Using unsupervised clustering, we were able to identify at least two distinct populations of activated, antigen-specific CD8 T cells on days 1, 2, and 3 following infection (as well as day 8, of course, when MPs and TEs were readily detected). The early memory precursor population expressed higher levels of key genes as compared to a more activated population. Genes upregulated in the early memory precursors in this interval included *Tcf7, Il7r, Ccr7, Sell*, *Cxcl10,* and *Cxcr3*, while genes upregulated in the second, activated population included *Il2ra, Cd200,*

Tnfrsf9, Tnfrsf4, Xcl1, Tbx21, Klrg1, Il18rap, Cx3cr1, and *Gzma*. Of note, *Cxcr3* is expressed as early as day 2 and expression is maintained on long-lived memory cells for at least 1 year post-infection. *Cxcl10* is also expressed as early as day 1 post-infection, and this chemokine binds CXCR3. This could indicate that early antigen-specific activation prompts scanning of the memory pool for cognate memory cells, and their effector functions can be immediately elaborated.

Interestingly, it seemed that during this early period of time, a number of co-inhibitory receptors and effector-associated proteins were transiently expressed on the memory precursor precursors—this included CD69, CD25, PD-1, and Granzyme B. Long-lived memory CD8 T cells clearly undergo a complex, highly regulated process of differentiation. We propose that, immediately following activation, naïve antigen-specific CD8 T cells proliferate, some seeing more antigen than others. It is possible that those cells seeing more antigen upregulate co-inhibitory receptors more quickly, which dampens their response and pre-disposes them towards survival and a memory fate. This effector history is a hallmark of memory CD8 T cells, as they gradually de-differentiate following clearance of a viral infection, but retain a demethylated imprint at key effector genes.

II. Functional role of CD69 in orchestrating the early immune response

CD69 is widely used as a marker of early CD8 T cell activation and tissue-residency. Chapter 4 established that discrete signals can trigger CD69 upregulation. Importantly, we showed that naïve CD8 T cells are actually pre-loaded with *Cd69* mRNA and protein, which enables rapid surface expression. Association of CD69 with S1PR1 downstream inhibits lymphocyte egress from lymph nodes (through inhibition of S1PR1/S1P interactions) (204, 214, 220). In this way, CD69 orchestrates the architecture and cellularity of lymphoid organs following an infection—

mediating a transient pause of lymphocytes within the lymphoid parenchyma. This pause may ensure that naive and memory CD8 T cells receive appropriate activating and co-stimulatory signals before entering the periphery. This finding would also partly explain the transient lymphopenia observed following many acute febrile illnesses (221–223). Previous studies have additionally demonstrated an interferon-γ-mediated transient drop in CCL21 and CXCL13 within lymphoid tissues following viral infection (~days 3-8 post-infection). This results in reduced local accumulation of T cells and APCs and may help to curtail the immune response, as well promote the generation of memory. Localized control of lymphocyte retention versus egress from lymphoid organs is therefore of critical importance in determining the outcome of an infection and the quality of memory cells that it elicits.

We also determined that rapid surface expression of CD69 occurs not only in antigen-specific, but also in non-antigen specific CD8 T cells. This finding suggests a further layer of immunological control throughout the entire organism—CD69 is expressed on most hematopoietic cells, including NK cells, monocytes, and gamma delta (γδ) T cells. Type I interferon, as well as IL-15 and IL-18, can trigger CD69 upregulation in non-specific CD8 T cells (224). These "bystander" CD8 T cells can participate in protective immunity by secreting cytokines, such as interferon-γ, and by exerting cytotoxicity through granzyme B and NK cell-activating receptors, such as NKG2D. Thus, CD69 is able to exert precise, early control of an infection throughout an entire immunological system; this likely determines its long-term outcome.

III. PD-1 regulates stem-like CD8 T cells' self-renewal

Chapter 5 demonstrated that stem-like CD8 T cells actually increase in number following PD-1 blockade. Moreover, stem-like cells also begin to express Ki67 as early as day 8 post-

treatment and continue to express it through day 14. These findings suggest that PD-1 signaling regulates the homeostatic turnover of stem-like cells. We hypothesize that PD-1 may act to maintain quiescence within the stem-like niche, part of a program which sequesters and protects stem-like cells from overstimulation, allowing them to retain their hallmark pluripotency. Our findings align with previous studies, which have demonstrated that stem-like cells acquire a lymphoid tissue-resident program, and do not circulate once the chronic phase of an infection is established (16, 33). We hypothesize that PD-1 blockade eases their quiescence and unleashes their proliferative potential specifically, and perhaps primarily, through modulation of PD-1 signal transduction. We propose that PD-1 is a master regulator of stem-like CD8 T cell turnover—restraining their differentiation in the setting of chronic infection in order to prevent depletion of an essential reservoir. PD-1 blockade unlocks stem-like cells' proliferative potential, while they remain functionally and transcriptionally unchanged.

A number of studies have suggested that maintenance of the stem-like population may require a protective niche—for example, within the splenic WP. It has been proposed that this niche may also be required for successful response to PD-1-directed immunotherapy (135, 250–253). In recent studies from Dahling et al., cDC1s were specifically shown to provide a specialized niche for sequestering the stem-like CD8 T cells (135).

Work by Dammeijer et al. has revealed another key role for DCs in this system. In this case, aPD-L1 antibodies were shown to specifically target PD-L1$^+$ cDC2s in tumor-draining lymph nodes, thereby suggesting the necessity of cDC2s for therapeutic response (250). In our own preliminary studies, we have shown that TLR7 agonism can improve effector CD8 T cell expansion, especially in combination with aPD-1 blockade. Together, these findings demonstrate

the emerging notion that effective antigen presentation is required for the generation of robust CD8 T cell responses following PD-1 blockade.

IV. PD-1 blockade does not functionally or transcriptionally alter stem-like CD8 T cells

We have also shown that the functional and transcriptional programming of stem-like CD8 T cells is unchanged by PD-1 blockade. These findings suggest that heterogeneity within human responses to PD-1-directed immunotherapy may not be due to defects within the stem-like compartment. From our continuous blockade studies, we show that, as in humans, the first cycle of PD-1 blockade induces the best proliferative response. But taken together with our adoptive transfer experiments, which demonstrate intact proliferative capacity on the part of the stem-like cells, we believe that PD-1 blockade may induce certain environmental changes that limit further therapeutic benefit. Additional preliminary observations from our lab show that even 6 weeks of "recovery" time following one round of therapy is not sufficient to induce a second, equally robust proliferative burst. Numerous other groups have also reported that aPD-1-induced environmental changes can limit the efficacy of PD-1 blockade—most examine how PD-1 blockade can re-shape the tumor microenvironment (254, 255), but some also examine responses in an antiviral context (156, 256). Taken together, these findings lead us to believe that the magnitude of response to PD-1 blockade may be determined by more than stem-like cells' proliferative potential. Instead, the magnitude likely depends on the quality and number of other immune cells surrounding the stem-like cells within their niche. These findings have vast implications for immune checkpoint targeting therapies, suggesting that stem cell-extrinsic, rather than intrinsic, factors play a more pivotal role in their success.

References

1. Blattman JN, Antia R, Sourdive DJD, Wang X, Kaech SM, Murali-Krishna K, Altman JD, Ahmed R. 2002. Estimating the Precursor Frequency of Naive Antigen-specific CD8 T Cells. J Exp Med 195:657–664.

2. Lewis SM, Williams A, Eisenbarth SC. 2019. Structure and function of the immune system in the spleen. Science Immunology 4:eaau6085.

3. Masopust D, Ahmed R. 2004. Reflections on CD8 T-cell activation and memory. Immunol Res 29:151–160.

4. Lanier LL, O'Fallon S, Somoza C, Phillips JH, Linsley PS, Okumura K, Ito D, Azuma M. 1995. CD80 (B7) and CD86 (B70) provide similar costimulatory signals for T cell proliferation, cytokine production, and generation of CTL. J Immunol 154:97–105.

5. Azuma M, Cayabyab M, Buck D, Phillips JH, Lanier LL. 1992. CD28 interaction with B7 costimulates primary allogeneic proliferative responses and cytotoxicity mediated by small, resting T lymphocytes. J Exp Med 175:353–360.

6. Elgueta R, Benson MJ, de Vries VC, Wasiuk A, Guo Y, Noelle RJ. 2009. Molecular mechanism and function of CD40/CD40L engagement in the immune system. Immunol Rev 229:10.1111/j.1600-065X.2009.00782.x.

7. Croft M, So T, Duan W, Soroosh P. 2009. The Significance of OX40 and OX40L to T cell Biology and Immune Disease. Immunol Rev 229:173–191.

8. Chen L, Flies DB. 2013. Molecular mechanisms of T cell co-stimulation and co-inhibition. 4. Nat Rev Immunol 13:227–242.

9. Curtsinger JM, Lins DC, Mescher MF. 2003. Signal 3 Determines Tolerance versus Full Activation of Naive CD8 T Cells. J Exp Med 197:1141–1151.

10. Butz EA, Bevan MJ. 1998. Massive Expansion of Antigen-Specific CD8+ T Cells during an Acute Virus Infection. Immunity 8:167–175.

11. Doherty PC. 1998. The Numbers Game for Virus-Specific CD8+ T Cells. Science 280:227–227.

12. Murali-Krishna K, Altman JD, Suresh M, Sourdive DJD, Zajac AJ, Miller JD, Slansky J, Ahmed R. 1998. Counting Antigen-Specific CD8 T Cells: A Reevaluation of Bystander Activation during Viral Infection. Immunity 8:177–187.

13. Lau LisaL, Jamieson BD, Somasundaram T, Ahmed R. 1994. Cytotoxic T-cell memory without antigen. Nature 369:648–652.

14. Grayson JM, Murali-Krishna K, Altman JD, Ahmed R. 2001. Gene expression in antigen-specific CD8+ T cells during viral infection. J Immunol 166:795–799.

15. Teague TK, Hildeman D, Kedl RM, Mitchell T, Rees W, Schaefer BC, Bender J, Kappler J, Marrack P. 1999. Activation changes the spectrum but not the diversity of genes expressed by T cells. Proceedings of the National Academy of Sciences 96:12691–12696.

16. Kaech SM, Hemby S, Kersh E, Ahmed R. 2002. Molecular and Functional Profiling of Memory CD8 T Cell Differentiation. Cell 111:837–851.

17. Bachmann MF, Barner M, Viola A, Kopf M. 1999. Distinct kinetics of cytokine production and cytolysis in effector and memory T cells after viral infection. European Journal of Immunology 29:291–299.

18. Oehen S, Brduscha-Riem K. 1998. Differentiation of Naive CTL to Effector and Memory CTL: Correlation of Effector Function with Phenotype and Cell Division. The Journal of Immunology 161:5338–5346.

19. Wherry EJ, Ahmed R. 2004. Memory CD8 T-Cell Differentiation during Viral Infection. Journal of Virology 78:5535–5545.

20. Cerwenka A, Morgan TM, Dutton RW. 1999. Naive, Effector, and Memory CD8 T Cells in Protection Against Pulmonary Influenza Virus Infection: Homing Properties Rather Than Initial Frequencies Are Crucial. The Journal of Immunology 163:5535–5543.

21. Hamann A, Klugewitz K, Austrup F, Jablonski-Westrich D. 2000. Activation induces rapid and profound alterations in the trafficking of T cells. European Journal of Immunology 30:3207–3218.

22. Walsh CM, Matloubian M, Liu CC, Ueda R, Kurahara CG, Christensen JL, Huang MT, Young JD, Ahmed R, Clark WR. 1994. Immune function in mice lacking the perforin gene. Proceedings of the National Academy of Sciences 91:10854–10858.

23. Heusel JW, Wesselschmidt RL, Shresta S, Russell JH, Ley TJ. 1994. Cytotoxic lymphocytes require granzyme B for the rapid induction of DNA fragmentation and apoptosis in allogeneic target cells. Cell 76:977–987.

24. Froelich CJ, Orth K, Turbov J, Seth P, Gottlieb R, Babior B, Shah GM, Bleackley RC, Dixit VM, Hanna W. 1996. New Paradigm for Lymphocyte Granule-mediated Cytotoxicity: TARGET CELLS BIND AND INTERNALIZE GRANZYME B, BUT AN ENDOSOMOLYTIC AGENT IS NECESSARY FOR CYTOSOLIC DELIVERY AND SUBSEQUENT APOPTOSIS *. Journal of Biological Chemistry 271:29073–29079.

25. Zhan Y, Carrington EM, Zhang Y, Heinzel S, Lew AM. 2017. Life and Death of Activated T Cells: How Are They Different from Naïve T Cells? Frontiers in Immunology 8.

26. Badovinac VP, Porter BB, Harty JT. 2002. Programmed contraction of CD8 + T cells after infection. Nat Immunol 3:619–626.

27. Kaech SM, Wherry EJ. 2007. Heterogeneity and Cell-Fate Decisions in Effector and Memory CD8+ T Cell Differentiation during Viral Infection. Immunity 27:393–405.

28. Wherry EJ, Ahmed R. 2004. Memory CD8 T-Cell Differentiation during Viral Infection. Journal of Virology 78:5535–5545.

29. Wherry EJ, Teichgräber V, Becker TC, Masopust D, Kaech SM, Antia R, von Andrian UH, Ahmed R. 2003. Lineage relationship and protective immunity of memory CD8 T cell subsets. Nature Immunology 4:225–234.

30. Kaech SM, Tan JT, Wherry EJ, Konieczny BT, Surh CD, Ahmed R. 2003. Selective expression of the interleukin 7 receptor identifies effector CD8 T cells that give rise to long-lived memory cells. Nature Immunology 4:1191–1198.

31. Huster KM, Busch V, Schiemann M, Linkemann K, Kerksiek KM, Wagner H, Busch DH. 2004. Selective expression of IL-7 receptor on memory T cells identifies early CD40L-dependent generation of distinct CD8+ memory T cell subsets. PNAS 101:5610–5615.

32. Sarkar S, Kalia V, Haining WN, Konieczny BT, Subramaniam S, Ahmed R. 2008. Functional and genomic profiling of effector CD8 T cell subsets with distinct memory fates. The Journal of Experimental Medicine 205:625–640.

33. Kalia V, Sarkar S, Subramaniam S, Haining WN, Smith KA, Ahmed R. 2010. Prolonged Interleukin-2Rα Expression on Virus-Specific CD8+ T Cells Favors Terminal-Effector Differentiation In Vivo. Immunity 32:91–103.

34. Kalia V, Sarkar S. 2018. Regulation of Effector and Memory CD8 T Cell Differentiation by IL-2—A Balancing Act. Front Immunol 9.

35. Williams MA, Bevan MJ. 2007. Effector and Memory CTL Differentiation. Annual Review of Immunology 25:171–192.

36. Surh CD, Sprent J. 2008. Homeostasis of Naive and Memory T Cells. Immunity 29:848–862.

37. Akondy RS, Fitch M, Edupuganti S, Yang S, Kissick HT, Li KW, Youngblood BA, Abdelsamed HA, McGuire DJ, Cohen KW, Alexe G, Nagar S, McCausland MM, Gupta S, Tata P, Haining WN, McElrath MJ, Zhang D, Hu B, Greenleaf WJ, Goronzy JJ, Mulligan MJ, Hellerstein M, Ahmed R. 2017. Origin and differentiation of human memory CD8 T cells after vaccination. Nature 552:362–367.

38. Kalia V, Sarkar S, Ahmed R. 2010. CD8 T-Cell Memory Differentiation during Acute and Chronic Viral Infections, p. 79–95. *In* Zanetti, M, Schoenberger, SP (eds.), Memory T Cells. Springer New York, New York, NY.

39. Youngblood B, Hale JS, Kissick HT, Ahn E, Xu X, Wieland A, Araki K, West EE, Ghoneim HE, Fan Y, Dogra P, Davis CW, Konieczny BT, Antia R, Cheng X, Ahmed R. 2017. Effector CD8 T cells dedifferentiate into long-lived memory cells. Nature 552:404–409.

40. Henning AN, Roychoudhuri R, Restifo NP. 2018. Epigenetic control of CD8 + T cell differentiation. Nat Rev Immunol 18:340–356.

41. Minervina AA, Pogorelyy MV, Komech EA, Karnaukhov VK, Bacher P, Rosati E, Franke A, Chudakov DM, Mamedov IZ, Lebedev YB, Mora T, Walczak AM. 2019. Comprehensive analysis of antiviral adaptive immunity formation and reactivation down to single-cell level. bioRxiv 820134.

42. Woodland DL, Kohlmeier JE. 2009. Migration, maintenance and recall of memory T cells in peripheral tissues. Nature Reviews Immunology 9:153–161.

43. DiSpirito JR, Shen H. 2010. Quick to remember, slow to forget: rapid recall responses of memory CD8 + T cells. Cell Res 20:13–23.

44. Akondy RS, Monson ND, Miller JD, Edupuganti S, Teuwen D, Wu H, Quyyumi F, Garg S, Altman JD, Del Rio C, Keyserling HL, Ploss A, Rice CM, Orenstein WA, Mulligan MJ, Ahmed R. 2009. The Yellow Fever Virus Vaccine Induces a Broad and Polyfunctional Human Memory CD8+ T Cell Response. The Journal of Immunology 183:7919–7930.

45. Demkowicz WE, Ennis FA. 1993. Vaccinia Virus-Specific CD8+ Cytotoxic T Lymphocytes in Humans. J Virol 67:7.

46. Nanan R, Rauch A, Kämpgen E, Niewiesk S, Kreth HW. 2000. A novel sensitive approach for frequency analysis of measles virus-specific memory T-lymphocytes in healthy adults with a childhood history of natural measles. Journal of General Virology 81:1313–1319.

47. Campbell JJ, Murphy KE, Kunkel EJ, Brightling CE, Soler D, Shen Z, Boisvert J, Greenberg HB, Vierra MA, Goodman SB, Genovese MC, Wardlaw AJ, Butcher EC, Wu L. 2001. CCR7 Expression and Memory T Cell Diversity in Humans. The Journal of Immunology 166:877–884.

48. Sallusto F, Lenig D, Förster R, Lipp M, Lanzavecchia A. 1999. Two subsets of memory T lymphocytes with distinct homing potentials and effector functions. Nature 401:708–712.

49. Lefrançois L, Masopust D. 2002. T cell immunity in lymphoid and non-lymphoid tissues. Current Opinion in Immunology 14:503–508.

50. Masopust D, Vezys V, Marzo AL, Lefrançois L. 2001. Preferential Localization of Effector Memory Cells in Nonlymphoid Tissue. Science 291:2413–2417.

51. Sallusto F, Geginat J, Lanzavecchia A. 2004. Central Memory and Effector Memory T Cell Subsets: Function, Generation, and Maintenance. Annual Review of Immunology 22:745–763.

52. Tripp RA, Hou S, Doherty PC. 1995. Temporal loss of the activated L-selectin-low phenotype for virus-specific CD8+ memory T cells. The Journal of Immunology 154:5870–5875.

53. Bromley SK, Thomas SY, Luster AD. 2005. Chemokine receptor CCR7 guides T cell exit from peripheral tissues and entry into afferent lymphatics. Nature Immunology 6:895–901.

54. Schenkel JM, Masopust D. 2014. Tissue-Resident Memory T Cells. Immunity 41:886–897.

55. Gebhardt T, Wakim LM, Eidsmo L, Reading PC, Heath WR, Carbone FR. 2009. Memory T cells in nonlymphoid tissue that provide enhanced local immunity during infection with herpes simplex virus. Nature Immunology 10:524–530.

56. Jiang X, Clark RA, Liu L, Wagers AJ, Fuhlbrigge RC, Kupper TS. 2012. Skin infection generates non-migratory memory CD8+ TRM cells providing global skin immunity. Nature 483:227–231.

57. Masopust D, Choo D, Vezys V, Wherry EJ, Duraiswamy J, Akondy R, Wang J, Casey KA, Barber DL, Kawamura KS, Fraser KA, Webby RJ, Brinkmann V, Butcher EC, Newell KA, Ahmed R. 2010. Dynamic T cell migration program provides resident memory within intestinal epithelium. J Exp Med 207:553–564.

58. Anderson KG, Sung H, Skon CN, Lefrancois L, Deisinger A, Vezys V, Masopust D. 2012. Cutting Edge: Intravascular Staining Redefines Lung CD8 T Cell Responses. The Journal of Immunology 189:2702–2706.

59. Anderson KG, Mayer-Barber K, Sung H, Beura L, James BR, Taylor JJ, Qunaj L, Griffith TS, Vezys V, Barber DL, Masopust D. 2014. Intravascular staining for discrimination of vascular and tissue leukocytes. Nature Protocols 9:209–222.

60. Rosato PC, Beura LK, Masopust D. 2017. Tissue resident memory T cells and viral immunity. Current Opinion in Virology 22:44–50.

61. Hofmann M, Pircher H. 2011. E-cadherin promotes accumulation of a unique memory CD8 T-cell population in murine salivary glands. PNAS 108:16741–16746.

62. Lefrançois L. 2006. Development, trafficking, and function of memory T-cell subsets. Immunological Reviews 211:93–103.

63. Mueller SN, Mackay LK. 2016. Tissue-resident memory T cells: local specialists in immune defence. Nature Reviews Immunology 16:79–89.

64. Skon CN, Lee J-Y, Anderson KG, Masopust D, Hogquist KA, Jameson SC. 2013. Transcriptional downregulation of S1pr1 is required for establishment of resident memory CD8+ T cells. Nat Immunol 14:1285–1293.

65. Liu L, Fuhlbrigge RC, Karibian K, Tian T, Kupper TS. 2006. Dynamic Programing of CD8+ T Cell Trafficking after Live Viral Immunization. Immunity 25:511–520.

66. Masopust D, Vezys V, Wherry EJ, Barber DL, Ahmed R. 2006. Cutting Edge: Gut Microenvironment Promotes Differentiation of a Unique Memory CD8 T Cell Population. The Journal of Immunology 176:2079–2083.

67. Casey KA, Fraser KA, Schenkel JM, Moran A, Abt MC, Beura LK, Lucas PJ, Artis D, Wherry EJ, Hogquist K, Vezys V, Masopust D. 2012. Antigen-Independent Differentiation

and Maintenance of Effector-like Resident Memory T Cells in Tissues. The Journal of Immunology 188:4866–4875.

68. Cepek KL, Shaw SK, Parker CM, Russell GJ, Morrow JS, Rimm DL, Brenner MB. 1994. Adhesion between epithelial cells and T lymphocytes mediated by E-cadherin and the α E β 7 integrin. Nature 372:190–193.

69. Mackay LK, Rahimpour A, Ma JZ, Collins N, Stock AT, Hafon M-L, Vega-Ramos J, Lauzurica P, Mueller SN, Stefanovic T, Tscharke DC, Heath WR, Inouye M, Carbone FR, Gebhardt T. 2013. The developmental pathway for CD103+CD8+ tissue-resident memory T cells of skin. Nature Immunology 14:1294–1301.

70. Schön MP, Arya A, Murphy EA, Adams CM, Strauch UG, Agace WW, Marsal J, Donohue JP, Her H, Beier DR, Olson S, Lefrancois L, Brenner MB, Grusby MJ, Parker CM. 1999. Mucosal T Lymphocyte Numbers Are Selectively Reduced in Integrin αE (CD103)-Deficient Mice. The Journal of Immunology 162:6641–6649.

71. Wakim LM, Woodward-Davis A, Liu R, Hu Y, Villadangos J, Smyth G, Bevan MJ. 2012. The Molecular Signature of Tissue Resident Memory CD8 T Cells Isolated from the Brain. The Journal of Immunology 189:3462–3471.

72. Lee Y-T, Suarez-Ramirez JE, Wu T, Redman JM, Bouchard K, Hadley GA, Cauley LS. 2011. Environmental and Antigen Receptor-Derived Signals Support Sustained Surveillance of the Lungs by Pathogen-Specific Cytotoxic T Lymphocytes. Journal of Virology 85:4085–4094.

73. Schenkel JM, Fraser KA, Masopust D. 2014. Cutting Edge: Resident Memory CD8 T Cells Occupy Frontline Niches in Secondary Lymphoid Organs. The Journal of Immunology 192:2961–2964.

74. Overstreet MG, Gaylo A, Angermann BR, Hughson A, Hyun Y-M, Lambert K, Acharya M, Billroth-MacLurg AC, Rosenberg AF, Topham DJ, Yagita H, Kim M, Lacy-Hulbert A, Meier-Schellersheim M, Fowell DJ. 2013. Inflammation-induced interstitial migration of effector CD4+ T cells is dependent on integrin αV. Nature Immunology 14:949–958.

75. Harris TH, Banigan EJ, Christian DA, Konradt C, Tait Wojno ED, Norose K, Wilson EH, John B, Weninger W, Luster AD, Liu AJ, Hunter CA. 2012. Generalized Lévy walks and the role of chemokines in migration of effector CD8+ T cells. Nature 486:545–548.

76. Andrian UH von, Mempel TR. 2003. Homing and cellular traffic in lymph nodes. Nat Rev Immunol 3:867–878.

77. Masopust D, Schenkel JM. 2013. The integration of T cell migration, differentiation and function. Nature Reviews Immunology 13:309.

78. Brinkman CC, Peske JD, Engelhard VH. 2013. Peripheral Tissue Homing Receptor Control of Naïve, Effector, and Memory CD8 T Cell Localization in Lymphoid and Non-Lymphoid Tissues. Front Immunol 4.

79. Farnsworth RH, Karnezis T, Maciburko SJ, Mueller SN, Stacker SA. 2019. The Interplay Between Lymphatic Vessels and Chemokines. Front Immunol 10.

80. Fletcher AL, Acton SE, Knoblich K. 2015. Lymph node fibroblastic reticular cells in health and disease. Nat Rev Immunol 15:350–361.

81. Kaiser A, Donnadieu E, Abastado J-P, Trautmann A, Nardin A. 2005. CC Chemokine Ligand 19 Secreted by Mature Dendritic Cells Increases Naive T Cell Scanning Behavior and Their Response to Rare Cognate Antigen. The Journal of Immunology 175:2349–2356.

82. Rosen SD. 2004. Ligands for L-Selectin: Homing, Inflammation, and Beyond. Annual Review of Immunology 22:129–156.

83. Arnon TI, Xu Y, Lo C, Pham T, An J, Coughlin S, Dorn GW, Cyster JG. 2011. GRK2-Dependent S1PR1 Desensitization Is Required for Lymphocytes to Overcome Their Attraction to Blood. Science 333:1898–1903.

84. Cyster JG, Schwab SR. 2012. Sphingosine-1-Phosphate and Lymphocyte Egress from Lymphoid Organs. Annual Review of Immunology 30:69–94.

85. Lo CG, Xu Y, Proia RL, Cyster JG. 2005. Cyclical modulation of sphingosine-1-phosphate receptor 1 surface expression during lymphocyte recirculation and relationship to lymphoid organ transit. J Exp Med 201:291–301.

86. Gregory JL, Walter A, Alexandre YO, Hor JL, Liu R, Ma JZ, Devi S, Tokuda N, Owada Y, Mackay LK, Smyth GK, Heath WR, Mueller SN. 2017. Infection Programs Sustained Lymphoid Stromal Cell Responses and Shapes Lymph Node Remodeling upon Secondary Challenge. Cell Reports 18:406–418.

87. Janatpour MJ, Hudak S, Sathe M, Sedgwick JD, McEvoy LM. 2001. Tumor Necrosis Factor–dependent Segmental Control of MIG Expression by High Endothelial Venules in Inflamed Lymph Nodes Regulates Monocyte Recruitment. J Exp Med 194:1375–1384.

88. Malhotra D, Fletcher AL, Astarita J, Lukacs-Kornek V, Tayalia P, Gonzalez SF, Elpek KG, Chang SK, Knoblich K, Hemler ME, Brenner MB, Carroll MC, Mooney DJ, Turley SJ. 2012. Transcriptional profiling of stroma from inflamed and resting lymph nodes defines immunological hallmarks. Nat Immunol 13:499–510.

89. McLachlan JB, Hart JP, Pizzo SV, Shelburne CP, Staats HF, Gunn MD, Abraham SN. 2003. Mast cell–derived tumor necrosis factor induces hypertrophy of draining lymph nodes during infection. Nat Immunol 4:1199–1205.

90. Mueller SN, Hosiawa-Meagher KA, Konieczny BT, Sullivan BM, Bachmann MF, Locksley RM, Ahmed R, Matloubian M. 2007. Regulation of Homeostatic Chemokine Expression and Cell Trafficking During Immune Responses. Science 317:670–674.

91. Castellino F, Huang AY, Altan-Bonnet G, Stoll S, Scheinecker C, Germain RN. 2006. Chemokines enhance immunity by guiding naive CD8 + T cells to sites of CD4 + T cell–dendritic cell interaction. Nature 440:890–895.

92. Hickman HD, Li L, Reynoso GV, Rubin EJ, Skon CN, Mays JW, Gibbs J, Schwartz O, Bennink JR, Yewdell JW. 2011. Chemokines control naive CD8+ T cell selection of optimal lymph node antigen presenting cells. J Exp Med 208:2511–2524.

93. Groom JR, Richmond J, Murooka TT, Sorensen EW, Sung JH, Bankert K, von Andrian UH, Moon JJ, Mempel TR, Luster AD. 2012. CXCR3 Chemokine Receptor-Ligand Interactions in the Lymph Node Optimize CD4+ T Helper 1 Cell Differentiation. Immunity 37:1091–1103.

94. Guarda G, Hons M, Soriano SF, Huang AY, Polley R, Martín-Fontecha A, Stein JV, Germain RN, Lanzavecchia A, Sallusto F. 2007. L-selectin-negative CCR7− effector and memory CD8+ T cells enter reactive lymph nodes and kill dendritic cells. Nature Immunology 8:743–752.

95. Mescher MF, Curtsinger JM, Agarwal P, Casey KA, Gerner M, Hammerbeck CD, Popescu F, Xiao Z. 2006. Signals required for programming effector and memory development by CD8+ T cells. Immunological Reviews 211:81–92.

96. Jung YW, Rutishauser RL, Joshi NS, Haberman AM, Kaech SM. 2010. Differential Localization of Effector and Memory CD8 T Cell Subsets in Lymphoid Organs during Acute Viral Infection. The Journal of Immunology 185:5315–5325.

97. Seo Y-J, Jothikumar P, Suthar MS, Zhu C, Grakoui A. 2016. Local Cellular and Cytokine Cues in the Spleen Regulate In Situ T Cell Receptor Affinity, Function, and Fate of CD8+ T Cells. Immunity 45:988–998.

98. Dauner JG, Williams IR, Jacob J. 2008. Differential Microenvironment Localization of Effector and Memory CD8 T Cells. The Journal of Immunology 180:291–299.

99. Khanna KM, McNamara JT, Lefrançois L. 2007. In Situ Imaging of the Endogenous CD8 T Cell Response to Infection. Science 318:116–120.

100. Pircher H, Baenziger J, Schilham M, Sado T, Kamisaku H, Hengartner H, Zinkernagel RM. 1987. Characterization of virus-specific cytotoxic T cell clones from allogeneic bone marrow chimeras. European Journal of Immunology 17:159–166.

101. Pircher H, Michalopoulos EE, Iwamoto A, Ohashi PS, Baenziger J, Hengartner H, Zinkernagel RM, Mak TW. 1987. Molecular analysis of the antigen receptor of virus-specific cytotoxic T cells and identification of a new Vα family. European Journal of Immunology 17:1843–1846.

102. Wiesel M, Walton S, Richter K, Oxenius A. 2009. Virus-specific CD8 T cells: activation, differentiation and memory formation. APMIS 117:356–381.

103. Ahn E, Araki K, Hashimoto M, Li W, Riley JL, Cheung J, Sharpe AH, Freeman GJ, Irving BA, Ahmed R. 2018. Role of PD-1 during effector CD8 T cell differentiation. PNAS 115:4749–4754.

104. Chen Z, Ji Z, Ngiow SF, Manne S, Cai Z, Huang AC, Johnson J, Staupe RP, Bengsch B, Xu C, Yu S, Kurachi M, Herati RS, Vella LA, Baxter AE, Wu JE, Khan O, Beltra J-C, Giles JR, Stelekati E, McLane LM, Lau CW, Yang X, Berger SL, Vahedi G, Ji H, Wherry EJ. 2019. TCF-1-Centered Transcriptional Network Drives an Effector versus Exhausted CD8 T Cell-Fate Decision. Immunity https://doi.org/10.1016/j.immuni.2019.09.013.

105. Danilo M, Chennupati V, Silva JG, Siegert S, Held W. 2018. Suppression of Tcf1 by Inflammatory Cytokines Facilitates Effector CD8 T Cell Differentiation. Cell Reports 22:2107–2117.

106. Lin W-HW, Nish SA, Yen B, Chen Y-H, Adams WC, Kratchmarov R, Rothman NJ, Bhandoola A, Xue H-H, Reiner SL. 2016. CD8+ T Lymphocyte Self-Renewal during Effector Cell Determination. Cell Reports 17:1773–1782.

107. Wu T, Ji Y, Moseman EA, Xu HC, Manglani M, Kirby M, Anderson SM, Handon R, Kenyon E, Elkahloun A, Wu W, Lang PA, Gattinoni L, McGavern DB, Schwartzberg PL. 2016. The TCF1-Bcl6 axis counteracts type I interferon to repress exhaustion and maintain T cell stemness. Science Immunology 1:eaai8593.

108. Zhou X, Yu S, Zhao D-M, Harty JT, Badovinac VP, Xue H-H. 2010. Differentiation and Persistence of Memory CD8+ T Cells Depend on T Cell Factor 1. Immunity 33:229–240.

109. Buchholz VR, Schumacher TNM, Busch DH. 2016. T Cell Fate at the Single-Cell Level. Annual Review of Immunology 34:65–92.

110. Kakaradov B, Arsenio J, Widjaja CE, He Z, Aigner S, Metz PJ, Yu B, Wehrens EJ, Lopez J, Kim SH, Zuniga EI, Goldrath AW, Chang JT, Yeo GW. 2017. Early transcriptional and epigenetic regulation of CD8+ T cell differentiation revealed by single-cell RNA sequencing. Nat Immunol 18:422–432.

111. Arsenio J, Kakaradov B, Metz PJ, Kim SH, Yeo GW, Chang JT. 2014. Early specification of CD8+ T lymphocyte fates during adaptive immunity revealed by single-cell gene-expression analyses. Nature Immunology 15:365–372.

112. Shin H, Blackburn SD, Blattman JN, Wherry EJ. 2007. Viral antigen and extensive division maintain virus-specific CD8 T cells during chronic infection. The Journal of Experimental Medicine 204:941–949.

113. Zajac AJ, Blattman JN, Murali-Krishna K, Sourdive DJD, Suresh M, Altman JD, Ahmed R. 1998. Viral Immune Evasion Due to Persistence of Activated T Cells Without Effector Function. The Journal of Experimental Medicine 188:2205–2213.

114. Wherry EJ, Blattman JN, Murali-Krishna K, van der Most R, Ahmed R. 2003. Viral Persistence Alters CD8 T-Cell Immunodominance and Tissue Distribution and Results in Distinct Stages of Functional Impairment. Journal of Virology 77:4911–4927.

115. Fuller MJ, Khanolkar A, Tebo AE, Zajac AJ. 2004. Maintenance, loss, and resurgence of T cell responses during acute, protracted, and chronic viral infections. J Immunol 172:4204–4214.

116. Fuller MJ, Zajac AJ. 2003. Ablation of CD8 and CD4 T Cell Responses by High Viral Loads1. The Journal of Immunology 170:477–486.

117. Wherry EJ, Ha S-J, Kaech SM, Haining WN, Sarkar S, Kalia V, Subramaniam S, Blattman JN, Barber DL, Ahmed R. 2007. Molecular Signature of CD8+ T Cell Exhaustion during Chronic Viral Infection. Immunity 27:670–684.

118. Sen DR, Kaminski J, Barnitz RA, Kurachi M, Gerdemann U, Yates KB, Tsao H-W, Godec J, LaFleur MW, Brown FD, Tonnerre P, Chung RT, Tully DC, Allen TM, Frahm N, Lauer GM, Wherry EJ, Yosef N, Haining WN. 2016. The epigenetic landscape of T cell exhaustion 7.

119. Scott-Browne JP, López-Moyado IF, Trifari S, Wong V, Chavez L, Rao A, Pereira RM. 2016. Dynamic Changes in Chromatin Accessibility Occur in CD8+ T Cells Responding to Viral Infection. Immunity 45:1327–1340.

120. Scharer CD, Bally APR, Gandham B, Boss JM. 2017. Cutting Edge: Chromatin Accessibility Programs CD8 T Cell Memory. The Journal of Immunology 198:2238–2243.

121. Pauken KE, Sammons MA, Odorizzi PM, Manne S, Godec J, Khan O, Drake AM, Chen Z, Sen DR, Kurachi M, Barnitz RA, Bartman C, Bengsch B, Huang AC, Schenkel JM, Vahedi G, Haining WN, Berger SL, Wherry EJ. 2016. Epigenetic stability of exhausted T cells limits durability of reinvigoration by PD-1 blockade. Science 354:1160–1165.

122. Bengsch B, Johnson AL, Kurachi M, Odorizzi PM, Pauken KE, Attanasio J, Stelekati E, McLane LM, Paley MA, Delgoffe GM, Wherry EJ. 2016. Bioenergetic Insufficiencies Due to Metabolic Alterations Regulated by the Inhibitory Receptor PD-1 Are an Early Driver of CD8(+) T Cell Exhaustion. Immunity 45:358–373.

123. Shin H, Wherry EJ. 2007. CD8 T cell dysfunction during chronic viral infection. Current Opinion in Immunology 19:408–415.

124. Philip M, Schietinger A. 2019. Heterogeneity and fate choice: T cell exhaustion in cancer and chronic infections. Current Opinion in Immunology 58:98–103.

125. Paley MA, Kroy DC, Odorizzi PM, Johnnidis JB, Dolfi DV, Barnett BE, Bikoff EK, Robertson EJ, Lauer GM, Reiner SL, Wherry EJ. 2012. Progenitor and Terminal Subsets of CD8+ T Cells Cooperate to Contain Chronic Viral Infection. Science 338:1220–1225.

126. Utzschneider DT, Charmoy M, Chennupati V, Pousse L, Ferreira DP, Calderon-Copete S, Danilo M, Alfei F, Hofmann M, Wieland D, Pradervand S, Thimme R, Zehn D, Held W. 2016. T Cell Factor 1-Expressing Memory-like CD8+ T Cells Sustain the Immune Response to Chronic Viral Infections. Immunity 45:415–427.

127. Wieland D, Kemming J, Schuch A, Emmerich F, Knolle P, Neumann-Haefelin C, Held W, Zehn D, Hofmann M, Thimme R. 2017. TCF1+ hepatitis C virus-specific CD8+ T cells are maintained after cessation of chronic antigen stimulation. 1. Nat Commun 8:15050.

128. Leong YA, Chen Y, Ong HS, Wu D, Man K, Deleage C, Minnich M, Meckiff BJ, Wei Y, Hou Z, Zotos D, Fenix KA, Atnerkar A, Preston S, Chipman JG, Beilman GJ, Allison CC, Sun L, Wang P, Xu J, Toe JG, Lu HK, Tao Y, Palendira U, Dent AL, Landay AL, Pellegrini M, Comerford I, McColl SR, Schacker TW, Long HM, Estes JD, Busslinger M, Belz GT, Lewin SR, Kallies A, Yu D. 2016. CXCR5+ follicular cytotoxic T cells control viral infection in B cell follicles. 10. Nat Immunol 17:1187–1196.

129. Im SJ, Hashimoto M, Gerner MY, Lee J, Kissick HT, Burger MC, Shan Q, Hale JS, Lee J, Nasti TH, Sharpe AH, Freeman GJ, Germain RN, Nakaya HI, Xue H-H, Ahmed R. 2016. Defining CD8+ T cells that provide the proliferative burst after PD-1 therapy. Nature 537:417–421.

130. He R, Hou S, Liu C, Zhang A, Bai Q, Han M, Yang Y, Wei G, Shen T, Yang X, Xu L, Chen X, Hao Y, Wang P, Zhu C, Ou J, Liang H, Ni T, Zhang X, Zhou X, Deng K, Chen Y, Luo Y, Xu J, Qi H, Wu Y, Ye L. 2016. Follicular CXCR5-expressing CD8+ T cells curtail chronic viral infection. 7620. Nature 537:412–416.

131. Hashimoto M, Kamphorst AO, Im SJ, Kissick HT, Pillai RN, Ramalingam SS, Araki K, Ahmed R. 2018. CD8 T Cell Exhaustion in Chronic Infection and Cancer: Opportunities for Interventions. Annual Review of Medicine 69:301–318.

132. Zehn D, Thimme R, Lugli E, de Almeida GP, Oxenius A. 2022. 'Stem-like' precursors are the fount to sustain persistent CD8+ T cell responses. 6. Nat Immunol 23:836–847.

133. Jadhav RR, Im SJ, Hu B, Hashimoto M, Li P, Lin J-X, Leonard WJ, Greenleaf WJ, Ahmed R, Goronzy JJ. 2019. Epigenetic signature of PD-1+ TCF1+ CD8 T cells that act as resource cells during chronic viral infection and respond to PD-1 blockade. Proceedings of the National Academy of Sciences 116:14113–14118.

134. Im SJ, Konieczny BT, Hudson WH, Masopust D, Ahmed R. 2020. PD-1+ stemlike CD8 T cells are resident in lymphoid tissues during persistent LCMV infection. PNAS https://doi.org/10.1073/pnas.1917298117.

135. Dähling S, Mansilla AM, Knöpper K, Grafen A, Utzschneider DT, Ugur M, Whitney PG, Bachem A, Arampatzi P, Imdahl F, Kaisho T, Zehn D, Klauschen F, Garbi N, Kallies A, Saliba A-E, Gasteiger G, Bedoui S, Kastenmüller W. 2022. Type 1 conventional dendritic cells maintain and guide the differentiation of precursors of exhausted T cells in distinct cellular niches. Immunity https://doi.org/10.1016/j.immuni.2022.03.006.

136. Beltra J-C, Manne S, Abdel-Hakeem MS, Kurachi M, Giles JR, Chen Z, Casella V, Ngiow SF, Khan O, Huang YJ, Yan P, Nzingha K, Xu W, Amaravadi RK, Xu X, Karakousis GC, Mitchell TC, Schuchter LM, Huang AC, Wherry EJ. 2020. Developmental Relationships of Four Exhausted CD8+ T Cell Subsets Reveals Underlying Transcriptional and Epigenetic Landscape Control Mechanisms. Immunity https://doi.org/10.1016/j.immuni.2020.04.014.

137. Hudson WH, Gensheimer J, Hashimoto M, Wieland A, Valanparambil RM, Li P, Lin J-X, Konieczny BT, Im SJ, Freeman GJ, Leonard WJ, Kissick HT, Ahmed R. 2019. Proliferating Transitory T Cells with an Effector-like Transcriptional Signature Emerge from PD-1+ Stem-like CD8+ T Cells during Chronic Infection. Immunity 51:1043-1058.e4.

138. Chen Y, Zander RA, Wu X, Schauder DM, Kasmani MY, Shen J, Zheng S, Burns R, Taparowsky EJ, Cui W. 2021. BATF regulates progenitor to cytolytic effector CD8+ T cell transition during chronic viral infection. Nat Immunol 22:996–1007.

139. Zander R, Schauder D, Xin G, Nguyen C, Wu X, Zajac A, Cui W. 2019. CD4+ T Cell Help Is Required for the Formation of a Cytolytic CD8+ T Cell Subset that Protects against Chronic Infection and Cancer. Immunity 51:1028-1042.e4.

140. Schildberg FA, Klein SR, Freeman GJ, Sharpe AH. 2016. Coinhibitory Pathways in the B7-CD28 Ligand-Receptor Family. Immunity 44:955–972.

141. Chemnitz JM, Parry RV, Nichols KE, June CH, Riley JL. 2004. SHP-1 and SHP-2 Associate with Immunoreceptor Tyrosine-Based Switch Motif of Programmed Death 1 upon Primary Human T Cell Stimulation, but Only Receptor Ligation Prevents T Cell Activation. The Journal of Immunology 173:945–954.

142. Freeman GJ, Long AJ, Iwai Y, Bourque K, Chernova T, Nishimura H, Fitz LJ, Malenkovich N, Okazaki T, Byrne MC, Horton HF, Fouser L, Carter L, Ling V, Bowman MR, Carreno BM, Collins M, Wood CR, Honjo T. 2000. Engagement of the Pd-1 Immunoinhibitory Receptor by a Novel B7 Family Member Leads to Negative Regulation of Lymphocyte Activation. Journal of Experimental Medicine 192:1027–1034.

143. Hui E, Cheung J, Zhu J, Su X, Taylor MJ, Wallweber HA, Sasmal DK, Huang J, Kim JM, Mellman I, Vale RD. 2017. T cell costimulatory receptor CD28 is a primary target for PD-1–mediated inhibition. Science 355:1428–1433.

144. Parry RV, Chemnitz JM, Frauwirth KA, Lanfranco AR, Braunstein I, Kobayashi SV, Linsley PS, Thompson CB, Riley JL. 2005. CTLA-4 and PD-1 Receptors Inhibit T-Cell Activation by Distinct Mechanisms. Molecular and Cellular Biology 25:9543–9553.

145. Yokosuka T, Takamatsu M, Kobayashi-Imanishi W, Hashimoto-Tane A, Azuma M, Saito T. 2012. Programmed cell death 1 forms negative costimulatory microclusters that directly inhibit T cell receptor signaling by recruiting phosphatase SHP2. Journal of Experimental Medicine 209:1201–1217.

146. Garcia-Diaz A, Shin DS, Moreno BH, Saco J, Escuin-Ordinas H, Rodriguez GA, Zaretsky JM, Sun L, Hugo W, Wang X, Parisi G, Saus CP, Torrejon DY, Graeber TG, Comin-Anduix B, Hu-Lieskovan S, Damoiseaux R, Lo RS, Ribas A. 2017. Interferon Receptor Signaling Pathways Regulating PD-L1 and PD-L2 Expression. Cell Reports 19:1189–1201.

147. Cha J-H, Chan L-C, Li C-W, Hsu JL, Hung M-C. 2019. Mechanisms Controlling PD-L1 Expression in Cancer. Molecular Cell 76:359–370.

148. Patsoukis N, Bardhan K, Chatterjee P, Sari D, Liu B, Bell LN, Karoly ED, Freeman GJ, Petkova V, Seth P, Li L, Boussiotis VA. 2015. PD-1 alters T-cell metabolic reprogramming by inhibiting glycolysis and promoting lipolysis and fatty acid oxidation. 1. Nat Commun 6:6692.

149. Frebel H, Nindl V, Schuepbach RA, Braunschweiler T, Richter K, Vogel J, Wagner CA, Loffing-Cueni D, Kurrer M, Ludewig B, Oxenius A. 2012. Programmed death 1 protects from fatal circulatory failure during systemic virus infection of mice. Journal of Experimental Medicine 209:2485–2499.

150. Odorizzi PM, Pauken KE, Paley MA, Sharpe A, Wherry EJ. 2015. Genetic absence of PD-1 promotes accumulation of terminally differentiated exhausted CD8+ T cells. Journal of Experimental Medicine 212:1125–1137.

151. Barber DL, Wherry EJ, Masopust D, Zhu B, Allison JP, Sharpe AH, Freeman GJ, Ahmed R. 2006. Restoring function in exhausted CD8 T cells during chronic viral infection. Nature 439:682–687.

152. Velu V, Titanji K, Zhu B, Husain S, Pladevega A, Lai L, Vanderford TH, Chennareddi L, Silvestri G, Freeman GJ, Ahmed R, Amara RR. 2009. Enhancing SIV-specific immunity in vivo by PD-1 blockade. Nature 458:206–210.

153. Fuller MJ, Callendret B, Zhu B, Freeman GJ, Hasselschwert DL, Satterfield W, Sharpe AH, Dustin LB, Rice CM, Grakoui A, Ahmed R, Walker CM. 2013. Immunotherapy of chronic hepatitis C virus infection with antibodies against programmed cell death-1 (PD-1). Proceedings of the National Academy of Sciences 110:15001–15006.

154. Murciano-Goroff YR, Warner AB, Wolchok JD. 2020. The future of cancer immunotherapy: microenvironment-targeting combinations. 6. Cell Res 30:507–519.

155. Gardiner D, Lalezari J, Lawitz E, DiMicco M, Ghalib R, Reddy KR, Chang K-M, Sulkowski M, Marro SO, Anderson J, He B, Kansra V, McPhee F, Wind-Rotolo M, Grasela D, Selby M, Korman AJ, Lowy I. 2013. A Randomized, Double-Blind, Placebo-Controlled Assessment of BMS-936558, a Fully Human Monoclonal Antibody to Programmed Death-1 (PD-1), in Patients with Chronic Hepatitis C Virus Infection. PLOS ONE 8:e63818.

156. Porichis F, Hart MG, Zupkosky J, Barblu L, Kwon DS, McMullen A, Brennan T, Ahmed R, Freeman GJ, Kavanagh DG, Kaufmann DE. 2014. Differential Impact of PD-1 and/or

Interleukin-10 Blockade on HIV-1-Specific CD4 T Cell and Antigen-Presenting Cell Functions. Journal of Virology 88:2508–2518.

157. Scully EP, Rutishauser RL, Simoneau CR, Delagrèverie H, Euler Z, Thanh C, Li JZ, Hartig H, Bakkour S, Busch M, Alter G, Marty FM, Wang C-C, Deeks SG, Lorch J, Henrich TJ. 2018. Inconsistent HIV reservoir dynamics and immune responses following anti-PD-1 therapy in cancer patients with HIV infection. Annals of Oncology 29:2141–2142.

158. Guihot A, Marcelin A-G, Massiani M-A, Samri A, Soulié C, Autran B, Spano J-P. 2018. Drastic decrease of the HIV reservoir in a patient treated with nivolumab for lung cancer. Annals of Oncology 29:517–518.

159. Gay CL, Bosch RJ, Ritz J, Hataye JM, Aga E, Tressler RL, Mason SW, Hwang CK, Grasela DM, Ray N, Cyktor JC, Coffin JM, Acosta EP, Koup RA, Mellors JW, Eron JJ, for the AIDS Clinical Trials 5326 Study Team. 2017. Clinical Trial of the Anti-PD-L1 Antibody BMS-936559 in HIV-1 Infected Participants on Suppressive Antiretroviral Therapy. The Journal of Infectious Diseases 215:1725–1733.

160. Nowicki TS, Hu-Lieskovan S, Ribas A. 2018. Mechanisms of Resistance to PD-1 and PD-L1 blockade. Cancer J 24:47–53.

161. Kamphorst AO, Pillai RN, Yang S, Nasti TH, Akondy RS, Wieland A, Sica GL, Yu K, Koenig L, Patel NT, Behera M, Wu H, McCausland M, Chen Z, Zhang C, Khuri FR, Owonikoko TK, Ahmed R, Ramalingam SS. 2017. Proliferation of PD-1+ CD8 T cells in peripheral blood after PD-1–targeted therapy in lung cancer patients. Proceedings of the National Academy of Sciences 114:4993–4998.

162. Kamphorst AO, Wieland A, Nasti T, Yang S, Zhang R, Barber DL, Konieczny BT, Daugherty CZ, Koenig L, Yu K, Sica GL, Sharpe AH, Freeman GJ, Blazar BR, Turka LA, Owonikoko TK, Pillai RN, Ramalingam SS, Araki K, Ahmed R. 2017. Rescue of exhausted CD8 T cells by PD-1–targeted therapies is CD28-dependent. Science 355:1423–1427.

163. Kim KH, Kim HK, Kim H-D, Kim CG, Lee H, Han JW, Choi SJ, Jeong S, Jeon M, Kim H, Koh J, Ku BM, Park S-H, Ahn M-J, Shin E-C. 2021. PD-1 blockade-unresponsive human tumor-infiltrating CD8+ T cells are marked by loss of CD28 expression and rescued by IL-15. 2. Cell Mol Immunol 18:385–397.

164. Dutton RW, Bradley LM, Swain SL. 1998. T Cell Memory. Annual Review of Immunology 16:201.

165. Kaech SM, Cui W. 2012. Transcriptional control of effector and memory CD8 + T cell differentiation. Nat Rev Immunol 12:749–761.

166. Homann D, Teyton L, Oldstone MBA. 2001. Differential regulation of antiviral T-cell immunity results in stable CD8+ but declining CD4+ T-cell memory. 8. Nat Med 7:913–919.

167. Martin MD, Badovinac VP. 2018. Defining Memory CD8 T Cell. Front Immunol 9:2692.

168. Mueller SN, Zaid A, Carbone FR. 2014. Tissue-resident T cells: dynamic players in skin immunity. Front Immunol 5:332.

169. Potsch C, Vöhringer D, Pircher H. 1999. Distinct migration patterns of naive and effector CD8 T cells in the spleen: correlation with CCR7 receptor expression and chemokine reactivity. European Journal of Immunology 29:3562–3570.

170. Mackay LK, Stock AT, Ma JZ, Jones CM, Kent SJ, Mueller SN, Heath WR, Carbone FR, Gebhardt T. 2012. Long-lived epithelial immunity by tissue-resident memory T (TRM) cells in the absence of persisting local antigen presentation. Proceedings of the National Academy of Sciences 109:7037–7042.

171. Sarkar S, Teichgraber V, Kalia V, Polley A, Masopust D, Harrington LE, Ahmed R, Wherry EJ. 2007. Strength of Stimulus and Clonal Competition Impact the Rate of Memory CD8 T Cell Differentiation. The Journal of Immunology 179:6704–6714.

172. Martin MD, Kim MT, Shan Q, Sompallae R, Xue H-H, Harty JT, Badovinac VP. 2015. Phenotypic and Functional Alterations in Circulating Memory CD8 T Cells with Time after Primary Infection. PLOS Pathogens 11:e1005219.

173. Escobar G, Mangani D, Anderson AC. 2020. T cell factor 1: A master regulator of the T cell response in disease. Science Immunology 5.

174. Kratchmarov R, Magun AM, Reiner SL. 2018. TCF1 expression marks self-renewing human CD8+ T cells. Blood Adv 2:1685–1690.

175. Willinger T, Freeman T, Herbert M, Hasegawa H, McMichael AJ, Callan MFC. 2006. Human Naive CD8 T Cells Down-Regulate Expression of the WNT Pathway Transcription Factors Lymphoid Enhancer Binding Factor 1 and Transcription Factor 7 (T Cell Factor-1) following Antigen Encounter In Vitro and In Vivo. The Journal of Immunology 176:1439–1446.

176. Zhao D-M, Yu S, Zhou X, Haring JS, Held W, Badovinac VP, Harty JT, Xue H-H. 2010. Constitutive Activation of Wnt Signaling Favors Generation of Memory CD8 T Cells. The Journal of Immunology 184:1191–1199.

177. Linsley PS, Ledbetter JA. 1993. The role of the CD28 receptor during T cell responses to antigen. Annu Rev Immunol 11:191–212.

178. Esensten JH, Helou YA, Chopra G, Weiss A, Bluestone JA. 2016. CD28 Costimulation: From Mechanism to Therapy. Immunity 44:973–988.

179. Groom JR, Luster AD. 2011. CXCR3 in T cell function. Experimental Cell Research 317:620–631.

180. Hu JK, Kagari T, Clingan JM, Matloubian M. 2011. Expression of chemokine receptor CXCR3 on T cells affects the balance between effector and memory CD8 T-cell generation. PNAS 108:E118–E127.

181. Kurachi M, Kurachi J, Suenaga F, Tsukui T, Abe J, Ueha S, Tomura M, Sugihara K, Takamura S, Kakimi K, Matsushima K. 2011. Chemokine receptor CXCR3 facilitates CD8+ T cell differentiation into short-lived effector cells leading to memory degeneration. J Exp Med 208:1605–1620.

182. Böttcher JP, Beyer M, Meissner F, Abdullah Z, Sander J, Höchst B, Eickhoff S, Rieckmann JC, Russo C, Bauer T, Flecken T, Giesen D, Engel D, Jung S, Busch DH, Protzer U, Thimme R, Mann M, Kurts C, Schultze JL, Kastenmüller W, Knolle PA. 2015. Functional classification of memory CD8+ T cells by CX3CR1 expression. Nature Communications 6:8306.

183. Gerlach C, Moseman EA, Loughhead SM, Alvarez D, Zwijnenburg AJ, Waanders L, Garg R, de la Torre JC, von Andrian UH. 2016. The Chemokine Receptor CX3CR1 Defines Three Antigen-Experienced CD8 T Cell Subsets with Distinct Roles in Immune Surveillance and Homeostasis. Immunity 45:1270–1284.

184. Most RG van der, Sette A, Oseroff C, Alexander J, Murali-Krishna K, Lau LL, Southwood S, Sidney J, Chesnut RW, Matloubian M, Ahmed R. 1996. Analysis of cytotoxic T cell responses to dominant and subdominant epitopes during acute and chronic lymphocytic choriomeningitis virus infection. The Journal of Immunology 157:5543–5554.

185. van der Most RG, Murali-Krishna K, Whitton JL, Oseroff C, Alexander J, Southwood S, Sidney J, Chesnut RW, Sette A, Ahmed R. 1998. Identification of Db- and Kb-Restricted Subdominant Cytotoxic T-Cell Responses in Lymphocytic Choriomeningitis Virus-Infected Mice. Virology 240:158–167.

186. Blattman JN, Wherry EJ, Ha S-J, van der Most RG, Ahmed R. 2009. Impact of Epitope Escape on PD-1 Expression and CD8 T-Cell Exhaustion during Chronic Infection. Journal of Virology 83:4386–4394.

187. Boesteanu AC, Katsikis PD. 2009. Memory T cells need CD28 costimulation to remember. Seminars in Immunology 21:69–77.

188. Borowski AB, Boesteanu AC, Mueller YM, Carafides C, Topham DJ, Altman JD, Jennings SR, Katsikis PD. 2007. Memory CD8+ T Cells Require CD28 Costimulation. The Journal of Immunology 179:6494–6503.

189. Fuse S, Zhang W, Usherwood EJ. 2008. Control of Memory CD8+ T Cell Differentiation by CD80/CD86-CD28 Costimulation and Restoration by IL-2 during the Recall Response. The Journal of Immunology 180:1148–1157.

190. Suresh M, Whitmire JK, Harrington LE, Larsen CP, Pearson TC, Altman JD, Ahmed R. 2001. Role of CD28-B7 Interactions in Generation and Maintenance of CD8 T Cell Memory. The Journal of Immunology 167:5565–5573.

191. Altman JD, Moss PAH, Goulder PJR, Barouch DH, McHeyzer-Williams MG, Bell JI, McMichael AJ, Davis MM. 1996. Phenotypic Analysis of Antigen-Specific T Lymphocytes. Science 274:94–96.

192. Cunningham F, Allen JE, Allen J, Alvarez-Jarreta J, Amode MR, Armean IM, Austine-Orimoloye O, Azov AG, Barnes I, Bennett R, Berry A, Bhai J, Bignell A, Billis K, Boddu S, Brooks L, Charkhchi M, Cummins C, Da Rin Fioretto L, Davidson C, Dodiya K, Donaldson S, El Houdaigui B, El Naboulsi T, Fatima R, Giron CG, Genez T, Martinez JG, Guijarro-Clarke C, Gymer A, Hardy M, Hollis Z, Hourlier T, Hunt T, Juettemann T, Kaikala V, Kay M, Lavidas I, Le T, Lemos D, Marugán JC, Mohanan S, Mushtaq A, Naven M, Ogeh DN, Parker A, Parton A, Perry M, Piližota I, Prosovetskaia I, Sakthivel MP, Salam AIA, Schmitt BM, Schuilenburg H, Sheppard D, Pérez-Silva JG, Stark W, Steed E, Sutinen K, Sukumaran R, Sumathipala D, Suner M-M, Szpak M, Thormann A, Tricomi FF, Urbina-Gómez D, Veidenberg A, Walsh TA, Walts B, Willhoft N, Winterbottom A, Wass E, Chakiachvili M, Flint B, Frankish A, Giorgetti S, Haggerty L, Hunt SE, IIsley GR, Loveland JE, Martin FJ, Moore B, Mudge JM, Muffato M, Perry E, Ruffier M, Tate J, Thybert D, Trevanion SJ, Dyer S, Harrison PW, Howe KL, Yates AD, Zerbino DR, Flicek P. 2022. Ensembl 2022. Nucleic Acids Res 50:D988–D995.

193. Quezada LK, Jin W, Liu YC, Kim ES, He Z, Indralingam CS, Tysl T, Labarta-Bajo L, Wehrens EJ, Jo Y, Kazane KR, Hattori C, Zuniga EI, Yeo GW, Chang JT. 2023. Early transcriptional and epigenetic divergence of CD8+ T cells responding to acute versus chronic infection. PLOS Biology 21:e3001983.

194. Hao Y, Hao S, Andersen-Nissen E, Mauck WM, Zheng S, Butler A, Lee MJ, Wilk AJ, Darby C, Zager M, Hoffman P, Stoeckius M, Papalexi E, Mimitou EP, Jain J, Srivastava A, Stuart T, Fleming LM, Yeung B, Rogers AJ, McElrath JM, Blish CA, Gottardo R, Smibert P, Satija R. 2021. Integrated analysis of multimodal single-cell data. Cell 184:3573-3587.e29.

195. Trapnell C, Cacchiarelli D, Grimsby J, Pokharel P, Li S, Morse M, Lennon NJ, Livak KJ, Mikkelsen TS, Rinn JL. 2014. The dynamics and regulators of cell fate decisions are revealed by pseudotemporal ordering of single cells. 4. Nat Biotechnol 32:381–386.

196. Araki K, Morita M, Bederman AG, Konieczny BT, Kissick HT, Sonenberg N, Ahmed R. 2017. Translation is actively regulated during the differentiation of CD8+ effector T cells. 9. Nat Immunol 18:1046–1057.

197. Howden AJM, Hukelmann JL, Brenes A, Spinelli L, Sinclair LV, Lamond AI, Cantrell DA. 2019. Quantitative analysis of T cell proteomes and environmental sensors during T cell differentiation. 11. Nat Immunol 20:1542–1554.

198. Hukelmann JL, Anderson KE, Sinclair LV, Grzes KM, Murillo AB, Hawkins PT, Stephens LR, Lamond AI, Cantrell DA. 2016. The cytotoxic T cell proteome and its shaping by the kinase mTOR. 1. Nat Immunol 17:104–112.

199. Piccirillo CA, Bjur E, Topisirovic I, Sonenberg N, Larsson O. 2014. Translational control of immune responses: from transcripts to translatomes. 6. Nat Immunol 15:503–511.

200. Cebrián M, Yagüe E, Rincón M, López-Botet M, de Landázuri MO, Sánchez-Madrid F. 1988. Triggering of T cell proliferation through AIM, an activation inducer molecule expressed on activated human lymphocytes. Journal of Experimental Medicine 168:1621–1637.

201. Hara T, Jung LK, Bjorndahl JM, Fu SM. 1986. Human T cell activation. III. Rapid induction of a phosphorylated 28 kD/32 kD disulfide-linked early activation antigen (EA 1) by 12-o-tetradecanoyl phorbol-13-acetate, mitogens, and antigens. Journal of Experimental Medicine 164:1988–2005.

202. Radulovic K, Manta C, Rossini V, Holzmann K, Kestler HA, Wegenka UM, Nakayama T, Niess JH. 2012. CD69 Regulates Type I IFN-Induced Tolerogenic Signals to Mucosal CD4 T Cells That Attenuate Their Colitogenic Potential. The Journal of Immunology 188:2001–2013.

203. Sánchez-Mateos P, Cebrián M, Acevedo A, López-Botet M, De Landázuri MO, Sánchez-Madrid F. 1989. Expression of a gp33/27,000 MW activation inducer molecule (AIM) on human lymphoid tissues. Induction of cell proliferation on thymocytes and B lymphocytes by anti-AIM antibodies. Immunology 68:72–79.

204. Shiow LR, Rosen DB, Brdičková N, Xu Y, An J, Lanier LL, Cyster JG, Matloubian M. 2006. CD69 acts downstream of interferon-α/β to inhibit S1P1 and lymphocyte egress from lymphoid organs. 7083. Nature 440:540–544.

205. Castellanos MC, Muñoz C, Montoya MC, Lara-Pezzi E, López-Cabrera M, Landázuri MO de. 1997. Expression of the leukocyte early activation antigen CD69 is regulated by the transcription factor AP-1. The Journal of Immunology 159:5463–5473.

206. López-Cabrera M, Muñoz E, Blázquez MV, Ursa MA, Santis AG, Sánchez-Madrid F. 1995. Transcriptional Regulation of the Gene Encoding the Human C-type Lectin Leukocyte Receptor AIM/CD69 and Functional Characterization of Its Tumor Necrosis Factor-α-responsive Elements (∗). Journal of Biological Chemistry 270:21545–21551.

207. Risso A, Smilovich D, Capra MC, Baldissarro I, Yan G, Bargellesi A, Cosulich ME. 1991. CD69 in resting and activated T lymphocytes. Its association with a GTP binding protein and biochemical requirements for its expression. The Journal of Immunology 146:4105–4114.

208. Mackay LK, Braun A, Macleod BL, Collins N, Tebartz C, Bedoui S, Carbone FR, Gebhardt T. 2015. Cutting Edge: CD69 Interference with Sphingosine-1-Phosphate Receptor Function Regulates Peripheral T Cell Retention. The Journal of Immunology 194:2059–2063.

209. de la Fuente H, Cruz-Adalia A, Martinez del Hoyo G, Cibrián-Vera D, Bonay P, Pérez-Hernández D, Vázquez J, Navarro P, Gutierrez-Gallego R, Ramirez-Huesca M, Martín P, Sánchez-Madrid F. 2014. The Leukocyte Activation Receptor CD69 Controls T Cell Differentiation through Its Interaction with Galectin-1. Molecular and Cellular Biology 34:2479–2487.

210. Hamann J, Fiebig H, Strauss M. 1993. Expression cloning of the early activation antigen CD69, a type II integral membrane protein with a C-type lectin domain. The Journal of Immunology 150:4920–4927.

211. Lin C-R, Wei T-YW, Tsai H-Y, Wu Y-T, Wu P-Y, Chen S-T. 2015. Glycosylation-dependent interaction between CD69 and S100A8/S100A9 complex is required for regulatory T-cell differentiation. The FASEB Journal 29:5006–5017.

212. López-Cabrera M, Santis AG, Fernández-Ruiz E, Blacher R, Esch F, Sánchez-Mateos P, Sánchez-Madrid F. 1993. Molecular cloning, expression, and chromosomal localization of the human earliest lymphocyte activation antigen AIM/CD69, a new member of the C-type animal lectin superfamily of signal-transmitting receptors. Journal of Experimental Medicine 178:537–547.

213. Cibrian D, Saiz ML, de la Fuente H, Sánchez-Díaz R, Moreno-Gonzalo O, Jorge I, Ferrarini A, Vázquez J, Punzón C, Fresno M, Vicente-Manzanares M, Daudén E, Fernández-Salguero PM, Martín P, Sánchez-Madrid F. 2016. CD69 controls the uptake of L-tryptophan through LAT1-CD98 and AhR-dependent secretion of IL-22 in psoriasis. 8. Nat Immunol 17:985–996.

214. Bankovich AJ, Shiow LR, Cyster JG. 2010. CD69 Suppresses Sphingosine 1-Phosophate Receptor-1 (S1P1) Function through Interaction with Membrane Helix 4*. Journal of Biological Chemistry 285:22328–22337.

215. Hunter MC, Teijeira A, Halin C. 2016. T Cell Trafficking through Lymphatic Vessels. Frontiers in Immunology 7.

216. Nakamura S, Sung SS, Bjorndahl JM, Fu SM. 1989. Human T cell activation. IV. T cell activation and proliferation via the early activation antigen EA 1. Journal of Experimental Medicine 169:677–689.

217. Santis AG, Campanero MR, Alonso JL, Tugores A, Alonso MA, Yagüe E, Pivel JP, Sánchez-Madrid F. 1992. Tumor necrosis factor-α production induced in T lymphocytes through the AIM/CD69 activation pathway. European Journal of Immunology 22:1253–1259.

218. Testi R, Phillips JH, Lanier LL. 1989. T cell activation via Leu-23 (CD69). The Journal of Immunology 143:1123–1128.

219. Tugores A, Alonso MA, Sánchez-Madrid F, Landázuri MO de. 1992. Human T cell activation through the activation-inducer molecule/CD69 enhances the activity of transcription factor AP-1. The Journal of Immunology 148:2300–2306.

220. Matloubian M, Lo CG, Cinamon G, Lesneski MJ, Xu Y, Brinkmann V, Allende ML, Proia RL, Cyster JG. 2004. Lymphocyte egress from thymus and peripheral lymphoid organs is dependent on S1P receptor 1. Nature 427:355–360.

221. Paessler S, Walker DH. 2013. Pathogenesis of the viral hemorrhagic fevers. Annu Rev Pathol 8:411–440.

222. Yun NE, Linde NS, Dziuba N, Zacks MA, Smith JN, Smith JK, Aronson JF, Chumakova OV, Lander HM, Peters CJ, Paessler S. 2008. Pathogenesis of XJ and Romero Strains of Junin Virus in Two Strains of Guinea Pigs. Am J Trop Med Hyg 79:275–282.

223. Guo Z, Zhang Z, Prajapati M, Li Y. 2021. Lymphopenia Caused by Virus Infections and the Mechanisms Beyond. 9. Viruses 13:1876.

224. Kim T-S, Shin E-C. 2019. The activation of bystander CD8+ T cells and their roles in viral infection. 12. Exp Mol Med 51:1–9.

225. Puglielli MT, Zajac AJ, van der Most RG, Dzuris JL, Sette A, Altman JD, Ahmed R. 2001. In Vivo Selection of a Lymphocytic Choriomeningitis Virus Variant That Affects Recognition of the GP33-43 Epitope by H-2Db but Not H-2Kb. Journal of Virology 75:5099–5107.

226. Müller U, Steinhoff U, Reis LFL, Hemmi S, Pavlovic J, Zinkernagel RM, Aguet M. 1994. Functional Role of Type I and Type II Interferons in Antiviral Defense. Science 264:1918–1921.

227. Colina R, Costa-Mattioli M, Dowling RJO, Jaramillo M, Tai L-H, Breitbach CJ, Martineau Y, Larsson O, Rong L, Svitkin YV, Makrigiannis AP, Bell JC, Sonenberg N. 2008. Translational control of the innate immune response through IRF-7. 7185. Nature 452:323–328.

228. Thoreen CC, Chantranupong L, Keys HR, Wang T, Gray NS, Sabatini DM. 2012. A unifying model for mTORC1-mediated regulation of mRNA translation. 7396. Nature 485:109–113.

229. Brummelman J, Mazza EMC, Alvisi G, Colombo FS, Grilli A, Mikulak J, Mavilio D, Alloisio M, Ferrari F, Lopci E, Novellis P, Veronesi G, Lugli E. 2018. High-dimensional single cell analysis identifies stem-like cytotoxic CD8+ T cells infiltrating human tumors. Journal of Experimental Medicine 215:2520–2535.

230. Eberhardt CS, Kissick HT, Patel MR, Cardenas MA, Prokhnevska N, Obeng RC, Nasti TH, Griffith CC, Im SJ, Wang X, Shin DM, Carrington M, Chen ZG, Sidney J, Sette A, Saba NF, Wieland A, Ahmed R. 2021. Functional HPV-specific PD-1+ stem-like CD8 T cells in head and neck cancer. 7875. Nature 597:279–284.

231. Jansen CS, Prokhnevska N, Master VA, Sanda MG, Carlisle JW, Bilen MA, Cardenas M, Wilkinson S, Lake R, Sowalsky AG, Valanparambil RM, Hudson WH, McGuire D, Melnick K, Khan AI, Kim K, Chang YM, Kim A, Filson CP, Alemozaffar M, Osunkoya AO, Mullane P, Ellis C, Akondy R, Im SJ, Kamphorst AO, Reyes A, Liu Y, Kissick H. 2019. An intra-tumoral niche maintains and differentiates stem-like CD8 T cells. 7787. Nature 576:465–470.

232. Siddiqui I, Schaeuble K, Chennupati V, Fuertes Marraco SA, Calderon-Copete S, Pais Ferreira D, Carmona SJ, Scarpellino L, Gfeller D, Pradervand S, Luther SA, Speiser DE, Held W. 2019. Intratumoral Tcf1+PD-1+CD8+ T Cells with Stem-like Properties Promote

Tumor Control in Response to Vaccination and Checkpoint Blockade Immunotherapy. Immunity 50:195-211.e10.

233. Jadhav RR, Im SJ, Hu B, Hashimoto M, Li P, Lin J-X, Leonard WJ, Greenleaf WJ, Ahmed R, Goronzy JJ. 2019. Epigenetic signature of PD-1+ TCF1+ CD8 T cells that act as resource cells during chronic viral infection and respond to PD-1 blockade. PNAS 201903520.

234. Utzschneider DT, Charmoy M, Chennupati V, Pousse L, Ferreira DP, Calderon-Copete S, Danilo M, Alfei F, Hofmann M, Wieland D, Pradervand S, Thimme R, Zehn D, Held W. 2016. T Cell Factor 1-Expressing Memory-like CD8+ T Cells Sustain the Immune Response to Chronic Viral Infections. Immunity 45:415–427.

235. Wang PH, Washburn R, Maniar R, Mu M, Ringham O, Kratchmarov R, Henick BS, Reiner SL. 2022. Cutting Edge: Promoting T Cell Factor 1+ T Cell Self-Renewal to Improve Programmed Cell Death Protein 1 Blockade. The Journal of Immunology https://doi.org/10.4049/jimmunol.2200317.

236. M. Hashimoto, K. Araki, M. Cardenas, P. Li, R. R. Jadhav, H. T. Kissick, W. H. Hudson, D. J. McGuire, R. C. Obeng, A. Wieland, J. Lee, D. T. McManus, J. L. Ross, S. J. Im, J. Lee, J. X. Lin, B. Hu, E. E. West, C. D. Scharer, G. J. Freeman, A. H. Sharpe, S. S. Ramalingam, A. Pellerin, V. Teichgräber, W. J. Greenleaf, C. Klein, J. J. Goronzy, P. Umana, W. J. Leonard, K. A. Smith, R. Ahmed. 2022. PD-1 combination therapy with IL-2 modifies CD8+ T cell exhaustion program. Nature In press.

237. Codarri Deak L, Nicolini V, Hashimoto M, Karagianni M, Schwalie PC, Lauener L, Varypataki EM, Richard M, Bommer E, Sam J, Joller S, Perro M, Cremasco F, Kunz L, Yanguez E, Hüsser T, Schlenker R, Mariani M, Tosevski V, Herter S, Bacac M, Waldhauer I, Colombetti S, Gueripel X, Wullschleger S, Tichet M, Hanahan D, Kissick HT, Leclair S, Freimoser-Grundschober A, Seeber S, Teichgräber V, Ahmed R, Klein C, Umaña P. 2022. PD-1-cis IL-2R agonism yields better effectors from stem-like CD8+ T cells. 7930. Nature 610:161–172.

238. Ribas A, Wolchok JD. 2018. Cancer immunotherapy using checkpoint blockade. Science 359:1350–1355.

239. Brahmer JR, Tykodi SS, Chow LQM, Hwu W-J, Topalian SL, Hwu P, Drake CG, Camacho LH, Kauh J, Odunsi K, Pitot HC, Hamid O, Bhatia S, Martins R, Eaton K, Chen S, Salay TM, Alaparthy S, Grosso JF, Korman AJ, Parker SM, Agrawal S, Goldberg SM, Pardoll DM, Gupta A, Wigginton JM. 2012. Safety and Activity of Anti–PD-L1 Antibody in Patients with Advanced Cancer. New England Journal of Medicine 366:2455–2465.

240. Hodi FS, O'Day SJ, McDermott DF, Weber RW, Sosman JA, Haanen JB, Gonzalez R, Robert C, Schadendorf D, Hassel JC, Akerley W, van den Eertwegh AJM, Lutzky J, Lorigan P, Vaubel JM, Linette GP, Hogg D, Ottensmeier CH, Lebbé C, Peschel C, Quirt I, Clark JI, Wolchok JD, Weber JS, Tian J, Yellin MJ, Nichol GM, Hoos A, Urba WJ. 2010. Improved Survival with Ipilimumab in Patients with Metastatic Melanoma. N Engl J Med 363:711–723.

241. Powles T, Eder JP, Fine GD, Braiteh FS, Loriot Y, Cruz C, Bellmunt J, Burris HA, Petrylak DP, Teng S, Shen X, Boyd Z, Hegde PS, Chen DS, Vogelzang NJ. 2014. MPDL3280A (anti-PD-L1) treatment leads to clinical activity in metastatic bladder cancer. Nature 515:558–562.

242. Garon EB, Rizvi NA, Hui R, Leighl N, Balmanoukian AS, Eder JP, Patnaik A, Aggarwal C, Gubens M, Horn L, Carcereny E, Ahn M-J, Felip E, Lee J-S, Hellmann MD, Hamid O, Goldman JW, Soria J-C, Dolled-Filhart M, Rutledge RZ, Zhang J, Lunceford JK, Rangwala R, Lubiniecki GM, Roach C, Emancipator K, Gandhi L. 2015. Pembrolizumab for the Treatment of Non–Small-Cell Lung Cancer. N Engl J Med 372:2018–2028.

243. Hamid O, Robert C, Daud A, Hodi FS, Hwu W-J, Kefford R, Wolchok JD, Hersey P, Joseph RW, Weber JS, Dronca R, Gangadhar TC, Patnaik A, Zarour H, Joshua AM, Gergich K, Elassaiss-Schaap J, Algazi A, Mateus C, Boasberg P, Tumeh PC, Chmielowski B, Ebbinghaus SW, Li XN, Kang SP, Ribas A. 2013. Safety and Tumor Responses with Lambrolizumab (Anti–PD-1) in Melanoma. N Engl J Med 369:134–144.

244. Gallimore A, Glithero A, Godkin A, Tissot AC, Plückthun A, Elliott T, Hengartner H, Zinkernagel R. 1998. Induction and Exhaustion of Lymphocytic Choriomeningitis Virus–specific Cytotoxic T Lymphocytes Visualized Using Soluble Tetrameric Major Histocompatibility Complex Class I–Peptide Complexes. The Journal of Experimental Medicine 187:1383–1393.

245. Sen DR, Kaminski J, Barnitz RA, Kurachi M, Gerdemann U, Yates KB, Tsao H-W, Godec J, LaFleur MW, Brown FD, Tonnerre P, Chung RT, Tully DC, Allen TM, Frahm N, Lauer GM, Wherry EJ, Yosef N, Haining WN. 2016. The epigenetic landscape of T cell exhaustion. Science 354:1165–1169.

246. Butler A, Hoffman P, Smibert P, Papalexi E, Satija R. 2018. Integrating single-cell transcriptomic data across different conditions, technologies, and species. 5. Nat Biotechnol 36:411–420.

247. Hao Y, Hao S, Andersen-Nissen E, Mauck WM, Zheng S, Butler A, Lee MJ, Wilk AJ, Darby C, Zager M, Hoffman P, Stoeckius M, Papalexi E, Mimitou EP, Jain J, Srivastava A, Stuart T, Fleming LM, Yeung B, Rogers AJ, McElrath JM, Blish CA, Gottardo R, Smibert P, Satija R. 2021. Integrated analysis of multimodal single-cell data. Cell 184:3573-3587.e29.

248. Stuart T, Butler A, Hoffman P, Hafemeister C, Papalexi E, Mauck WM, Hao Y, Stoeckius M, Smibert P, Satija R. 2019. Comprehensive Integration of Single-Cell Data. Cell 177:1888-1902.e21.

249. Satija R, Farrell JA, Gennert D, Schier AF, Regev A. 2015. Spatial reconstruction of single-cell gene expression data. 5. Nat Biotechnol 33:495–502.

250. Dammeijer F, van Gulijk M, Mulder EE, Lukkes M, Klaase L, van den Bosch T, van Nimwegen M, Lau SP, Latupeirissa K, Schetters S, van Kooyk Y, Boon L, Moyaart A, Mueller YM, Katsikis PD, Eggermont AM, Vroman H, Stadhouders R, Hendriks RW, Thüsen J von der, Grünhagen DJ, Verhoef C, van Hall T, Aerts JG. 2020. The PD-1/PD-L1-

Checkpoint Restrains T cell Immunity in Tumor-Draining Lymph Nodes. Cancer Cell 38:685-700.e8.

251. Hsu FJ, Benike C, Fagnoni F, Liles TM, Czerwinski D, Taidi B, Engleman EG, Levy R. 1996. Vaccination of patients with B–cell lymphoma using autologous antigen–pulsed dendritic cells. 1. Nat Med 2:52–58.

252. Lichtenegger FS, Rothe M, Schnorfeil FM, Deiser K, Krupka C, Augsberger C, Schlüter M, Neitz J, Subklewe M. 2018. Targeting LAG-3 and PD-1 to Enhance T Cell Activation by Antigen-Presenting Cells. Frontiers in Immunology 9.

253. Nestle FO, Alijagic S, Gilliet M, Sun Y, Grabbe S, Dummer R, Burg G, Schadendorf D. 1998. Vaccination of melanoma patients with peptide- or tumorlysate-pulsed dendritic cells. 3. Nat Med 4:328–332.

254. Lee AH, Sun L, Mochizuki AY, Reynoso JG, Orpilla J, Chow F, Kienzler JC, Everson RG, Nathanson DA, Bensinger SJ, Liau LM, Cloughesy T, Hugo W, Prins RM. 2021. Neoadjuvant PD-1 blockade induces T cell and cDC1 activation but fails to overcome the immunosuppressive tumor associated macrophages in recurrent glioblastoma. 1. Nat Commun 12:6938.

255. Rao G, Latha K, Ott M, Sabbagh A, Marisetty A, Ling X, Zamler D, Doucette TA, Yang Y, Kong L-Y, Wei J, Fuller GN, Benavides F, Sonabend AM, Long J, Li S, Curran M, Heimberger AB. 2020. Anti-PD-1 induces M1 polarization in the glioma microenvironment and exerts therapeutic efficacy in the absence of CD8 cytotoxic T cells. Clin Cancer Res 26:4699–4712.

256. Rahman SA, Yagnik B, Bally AP, Morrow KN, Wang S, Vanderford TH, Freeman GJ, Ahmed R, Amara RR. 2021. PD-1 blockade and vaccination provide therapeutic benefit against SIV by inducing broad and functional CD8+ T cells in lymphoid tissue. Science Immunology 6:eabh3034.